S-N Curves and Fracture Mechanics Based Fatigue Assessment of Offshore Floating Wind Turbines

Junyi Wu

B.Sc., M.Sc

A thesis submitted for the degree of

Doctor of Philosophy

March 2020

School of Engineering

Newcastle University

United Kingdom

ABSTRACT

With increasing water depth in offshore applications, the traditional fixed wind turbines have a higher cost in design safety and energy production. Therefore, several concepts of offshore floating wind turbines (FWTs) have been proposed. However, these kinds of structures are prone to fatigue damage due to harsh environmental conditions. The objective of this thesis is not only to quantify the fatigue damage predicted by different methods but also to provide a basis for the currently immature procedure of fatigue assessment of FWTs.

The traditional S-N curves and fracture mechanics (FM) based fatigue assessment approaches are widely used in offshore fixed wind turbine systems. However, hydro-elastic loads and coupled loads between floating platform and mooring system cannot be ignored in FWT system. The wave and wind induced loads are highly related to the structural motions and responses and the instantaneous position should be updated with the changes of hydrodynamic and aerodynamic forces all the time. Moreover, the structure response amplitude increases at the nature frequency and nature eigen-frequency. These factors bring a lot of challenges in the fatigue assessment of offshore FWTs.

Due to a lot of non-linearities in FWT systems, the fully coupled aero-hydro-servo-elastic analysis is conducted with use of FAST software to obtain the time history of structural dynamic response. Then the fatigue life is calculated by Rainflow counting method with related S-N curves and Miner's rule. A simplified lumping approach combined with joint probability of wind and waves is utilized to reduce large amount of computational time. Only 498 load cases have a probability of 0.1 ‰ and higher which makes the time-domain analysis more efficient and accurate. The total probability of occurrence is 98.2% and it is feasible to use these load cases to conduct fatigue calculation. The results calculated by the simplified lumping approach show a good agreement with only 0.91% discrepancy. Although the non-linearities for the entire FWT structure and dynamic control system are taken into account by time-domain analysis, the analysis may end up due to the complicated and time-consuming process. Thus, the spectral fatigue analysis can be regarded as an alternative to the time-domain analysis for the quick fatigue assessment of FWTs. A narrow-band solution and six wide-band solutions are presented and compared. The results show the big discrepancy in fatigue lives compared to the results predicted by time-domain analysis when use different spectral fatigue models. However, the solution proposed by Tunna has only two parameters which can be considered as the best quick spectral prediction model for FWTs even though the result

is not superior.

FM based analysis is an alternative to predict remaining fatigue lives. It is advanced compared to S-N curves based approaches since it can provide detailed crack growth description. Parametric studies of initial crack sizes, critical crack depths, stress concentration factors (SCFs) and mathematical load sequences are investigated with use of Paris' equation. Nevertheless, it is found that FWTs are more prone to physical load sequence effect due to the noticeable increases and decreases in mean stress. Therefore, two overload (OL) retardation models are explained and compared based on experimental data. Afterwards, a modified Space-state model is proposed with consideration of threshold stress intensity factor range and fracture toughness which has been applied in the fatigue assessment of a spar-type FWT successfully.

As a summary, S-N curves based approaches can be applied in the design phase of FTWs with consideration of SCFs. But it is not reliable for the reassessment after some years in operation e.g. due to corrosion effect, change of geometry or the variations of material constants which are not described in S-N curves. FM based approach with Paris' equation gives the details of crack propagation process but does not take load sequence effect into account which results in a more conservative fatigue life. Thus, the modified Space-state model with consideration of threshold stress intensity factor range and fracture toughness is recommended herein to perform fatigue assessment for offshore FWTs.

Keywords: Offshore floating wind turbine, fatigue assessment, coupled aero-hydro-servo-elastic analysis, S-N curve, fracture mechanics, load sequence

Dedication

I dedicate this thesis to my family.

Acknowledgement

Table of contents

List of Figures

List of Tables

List of Symbols

A = fatigue strength coefficient

A_r = fatigue strength coefficient

a_c = critical crack depth

α_k = the constraint factor

α_t = the angle of attack

a_x = the axial induction factor

a' = the tangential induction factor

a_0 = initial crack size

B = scale parameter of Weibull distribution

C = crack growth rate coefficient

C_d = the drag coefficient

C_l = the lift coefficient

D = total fatigue damage

D_{narrow} = fatigue damage calculated by narrow-band

solution

$D_{i,j}^*$ = unit fatigue damage for sea state (i,j)

$d_{i,j}$ = real fatigue damage for sea state (i,j)

dT = the elemental thrust

dQ = the elemental torque

E = the modulus of elasticity

$\overrightarrow{F_{AM}}$ = total added mass force

$\overrightarrow{F_{AMF}}$	= the added mass force due to ballasted fluid
$\overrightarrow{F_{AMM}}$	= the added mass force of the structure
$\overrightarrow{F_{AMMG}}$	= the added mass force due to marine growth
$\overrightarrow{F_B}$	= the buoyance force
$\overrightarrow{F_D}$	= drag force
$\overrightarrow{F_{FB}}$	= the force due to fluid ballasting
$\overrightarrow{F_{HS}}$	= hydrostatic force
$\overrightarrow{F_I}$	= inertial force
$\overrightarrow{F_{MG}}$	= marine growth-related force
$\overrightarrow{F_{RD}}$	= radiation memory-effect force
$\overrightarrow{F_W}$	= incident-wave excitation force
f	= crack opening ratio
f_p	= peak occurrence frequency
g	= acceleration of gravity
H_s	= significant wave height
I_x	= sectional moment of area
I_y	= sectional moment of area
K_{max}	= the maximum of stress intensity factor.
K_{IC}	= fracture toughness
k_t	= stress concentration factor
M_k	= the correction factor
M_x	= flapwise bending moment

M_y	= Edgewise bending moment
m	= material constant
m_0	= the 0th spectral moment of power spectral density
N	= cycles to failure
N_z	= axial force
n	= number of stress cycles
p	= probability of occurrence of wind and waves
R	= load ratio
S_y	= yield stress
S^o	= crack opening stress
T_d	= the time length that the stress occurs
T_i	= turbulence intensity
T_p	= wave peak period
t	= tower base thickness
U	= mean wind speed
U_{10}	= mean wind speed at 10 m height
U_∞	= the free-stream wind speed
V_{rel}	= induced relative velocity
V_∞	= the free-stream velocity
W	= the width of plate
z	= hub height

α	= the spectral parameter
α_{WL}	= the correction factor
β	= the form parameter
β_x	= the local twist angle
γ	= shape parameter of Weibull distribution
γ_p	= peak enhancement factor
δ	= wind spectral parameter
ρ	= air density
σ	= the applied stress
σ_s	= spectral width parameter
ω	= wave frequency
ω_p	= peak wave-frequency
η	= retardation factor
$\emptyset$	= crack arrest factor
Γ	= gamma function,
ΔK	= stress intensity factor range
ΔK_{eff}	= the effective stress intensity factor range
ΔK_{th}	= threshold stress intensity factor range
ΔK_0	= the threshold value at R=0
ΔS	= stress range
Δt	= time step

List of abbreviations

ABS	American Bureau of Shipping
BEM	Beam Element Momentum
BS	British Standard
CA	Constant Amplitude
DNV	Det Norske Veritas
FEA	Finite Element Analysis
FFT	Fast Fourier Transform
FLS	Fatigue Limit State
FM	Fracture Mechanics
FWT	FWT
GDW	Generalized Dynamic Wake
IEC	International Electrotechnique Commission
OL	Overload
SCF	Stress Concentration Factor
UL	Underload
VA	Variable Amplitude

List of publications

1. Wu, J. , & Chen, N. Z. . (2017). Fracture Mechanics Based Fatigue Assessment for a Spar-Type Floating Wind Turbine. ASME International Conference on Ocean, Offshore and Arctic Engineering

2. Wu, J. , & Chen, N. Z. . (2017). An improved lumping approach for fatigue analysis of a spar-type wind turbine. Proceedings of 6th International Conference on Marine Structure

Chapter 1. Introduction

1.1 Background for Offshore Wind Energy

Fossil fuels, such as oil, coal, and gas, supply the world with primary energy in the past decades. The research (Conti and Holtberg, 2011) indicated that the consumption of world's total crude oil, coal and natural gas would increase by 1%, 1.5% and 1.6% per year on average from 2008 to 2035 respectively. Despite the increased demand of fossil fuels, the reserves are still enough to sustain humans for more decades, and unexplored resources may even outpace the demand.

Nevertheless, human beings never cease discovering renewable energies. The main reason is that the burning of fossil flues will release significant amounts of carbon dioxide which can cause the phenomenon of global warming. Moreover, considering human health, the research (Smith et. al, 1999) revealed that between 25% and 33% of the global burden of diseases is brought by environmental factors.

The sustainable energies have shown great potential to overcome the challenges of environmental issues, for instance, global warming and human health problems. Generally, wind, wave and tidal are the main types of offshore renewable energies. Offshore wind energy is one of the sustainable sources that is currently well supported by the public. Therefore, the wind energies received much attention from many offshore industries and offshore wind energy is expected to play an indispensable role in the future power generation.

Wind power deployment has a substantial increase from 2008, approaching 300GW of cumulative installed capacities. China takes the leading position by 75GW, followed by USA 60GW and Germany 31GW. Now wind power provides 2.5% of total global electricity demand, up to 30%

in Denmark, 20% in Portugal and 18% in Spain (Karimirad, 2014). With the incentive policies, the utilization of wind energy has seen a tremendous growth. Land-based wind turbines are installed all over the world with cost-effective designs where wind resources are strong and financing conditions are good. This onshore wind turbines have been already recognized as a mature form of reliable renewable energy infrastructure.

Offshore sites with abundant wind resources seem to be more appropriate to install the wind turbines. However, high capital cost, operating and maintenance challenges, severer environmental conditions delay the development of offshore wind turbines. The majority of the costs are related to design, which highlights the importance of having an optimized design based on verified concepts. As can be seen from Figure 1.1, there is a clear pattern that most offshore fixed wind farms are located in sites within an average water depth of 40 meters and are not far away from shore at least by 2012. Hence, possibility is sought to move these projects to a greater water depth with floating bases to obtain maximum wind energy in the future.

FWTs have recently appeared in the wind market but there is no real application in wind farms based on this concept. However, the global market potential of FWTs is huge and it is the only realistic option for many locations with vast wind resources and deep waters. A comparison has been made between fixed wind turbines and FWTs in terms of the cost drivers, as shown in Table 1.1. It likely that a highly competitive tariff of energy can be reached for FWTs when the industry has matured.
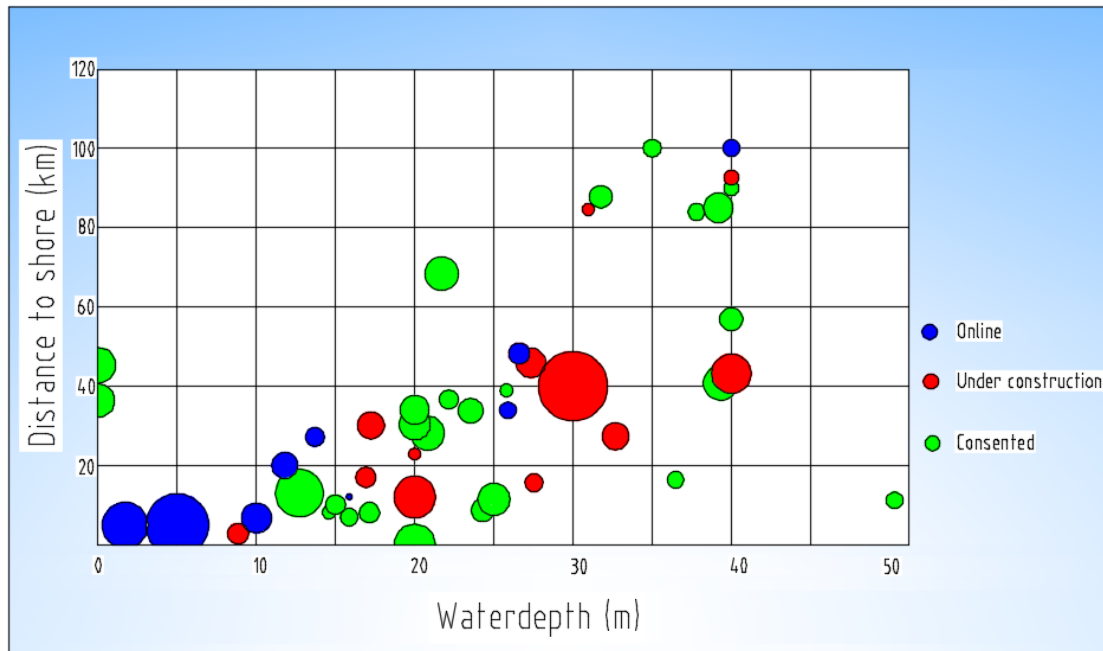
Figure 1.1 Average size, distance to shore and water depth. (EWEA, 2012)

In summary, the information indicates that there is more potential with FWTs than it is for fixed wind turbines, but there are challenges in popularizing the FWT technology.

Table 1.1 Qualitative comparisons between fixed and FWTs

Fixed wind turbines		FWTs
Generally lower mass	**Substructure**	Site independent, high potential for mass production
Does not need mooring and anchors	**Moorings & Anchors**	\
\	**Transportation**	Easier removal, tug back to shore
\	**Installation**	Simple installation
\	**Energy**	Not limited to shallow waters
\	**Maintenance Costs**	Enable major repair inshore (but difficult offshore)
Good track record, more predicTable reliability	**Proven Technology**	\

1.2 Offshore Fixed Wind Turbines

This section is primarily focused on the introduction of traditional types of offshore fixed wind turbines. The different application concepts for fixed offshore wind turbines are given. Their characteristics, advantages and disadvantages are briefly discussed.

1.2.1 Monopile Wind Turbine

Monopile wind turbine is one of the earliest concepts utilized in the shallow waters, within 30 m water depth, as shown in Figure 1.2. There are many wind farms based on this concept, like Lely, Belwind and London Array.

The design is quite simple as it consists of a tubular structure which extends to the seabed. The wind turbine is usually connected with pile by a transition part. The transition part is made of cement and seawater with a water/cement weight ratio of 39%. This part is prone to the fatigue due to the aerodynamic thrust and the complicated material behavior. However, monopile type is used widely for offshore wind projects and more than 65% such projects are based on this concept (Karimirad, 2014).
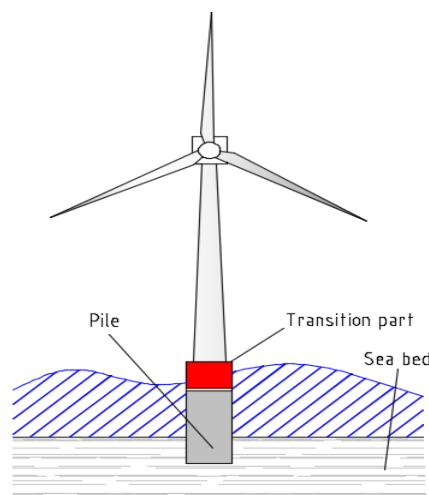
Figure 1.2 Monopile wind turbine (Karimirad, 2014)

The monopile support structure, with approximate 700 t in weight and 150 mm in thickness, is relatively light compared to that of other concepts. The diameters of the pile are between 3 to 6 m and the length of the pile is about 60 m (DNV, 2010; Lorc, 2011). The transition part is slightly larger than the monopile thus it can be easily mounted on the monopile. The limitation of this concept is the overall deflection and vibration due to the long slender shape. However, it is still the first choice for the offshore wind markets due to its low cost and ease of installation.

1.2.2 Jacket Wind Turbine

With the increasing water depth, the cost of monopile wind turbine becomes higher. Thus, the jacket concept has been proposed to the market, as shown in Figure 1.3. This concept was deployed for the oil and gas business over 50 years and wasapplied in a wide range of water depths, from 30 m to 200 m. The jacket platforms are connected to frames and the support legs. Normally, this concept has three to four inclined legs, which is practical and sufficient to keep the entire structure sTable. Similarly, the transition piece is adopted to connect the tower and jackets, which is also prone to the fatigue due to bending moments induced by wind and wave loads.

The cost of construction is highly dependent on location, resources available, production cost and owner preference, and the design of transition part also affects the overall cost because of its weight. Thus, more researches are needed to come up with practical solutions and construction methods. Many jacket wind turbine farms have already been established, e.g., Ormonde in the UK, Suizhong Demonstration in China and Alpha Ventus in German.
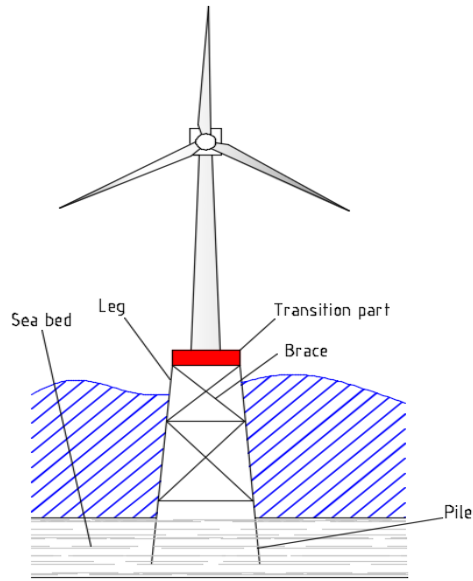
Figure 1.3 Jacket wind turbine (Karimirad, 2014)

1.2.3 Tripile Wind Turbine

The monopile wind turbine becomes unsTable in deeper water due to the large bending moment induced by wind and waves. Thus, the concept of using several piles has been proposed to make the whole system more sTable and reliable. The Figure 1.4 shows the wind turbine supported by a tripile structure.

Three piles are used to support the wind turbine, which makes the structure more sTable compared to the monopile concept. Higher stiffness ensures better suitability for the deeper water, e.g., 30 m to 50 m. The diameter of each pile is about 3 m and the weight up to 400 t. However, high cost is caused by the large amount of steel and more complicated manufacturing, e.g., three piles, support structures and the transition piece.
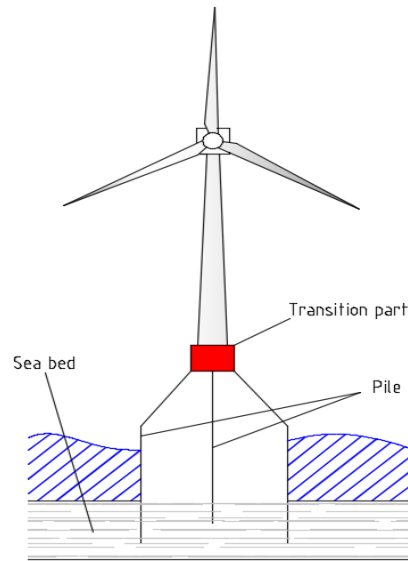
Figure 1.4 Tripile wind turbine (Karimirad, 2014)

1.2.4 Tripod Wind Turbine

The tripod wind turbine is a quite popular concept in the offshore wind market. Compared with the tripile type, it has a relatively light weight with good stability and stiffness. Similar structures like tripile make it rigid in deep water up to50 m. However, the tripod structure is more complicated than the monopile type due to the large number of welding joints which increase the risk of fatigue failure.

One of the main differences between tripod concept and tripile concept is the wave loads. The support structure of tripile is above sea surface while tripods have a big central column connecting braces and foundation below the sea surface. This entails a great diameter of central column, consequently increasing the wave loads. The layout of tripod wind turbine is illustrated in Figure 1.5.

7
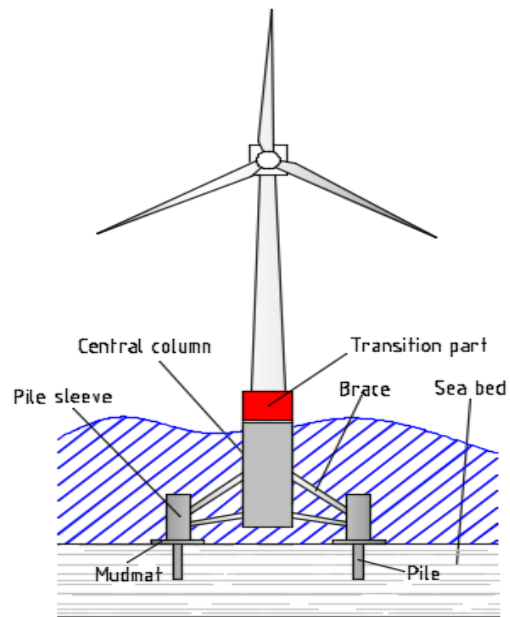
Figure 1.5 Tripod wind turbine (Karimirad, 2014)

1.2.5 Gravity-based Wind Turbine
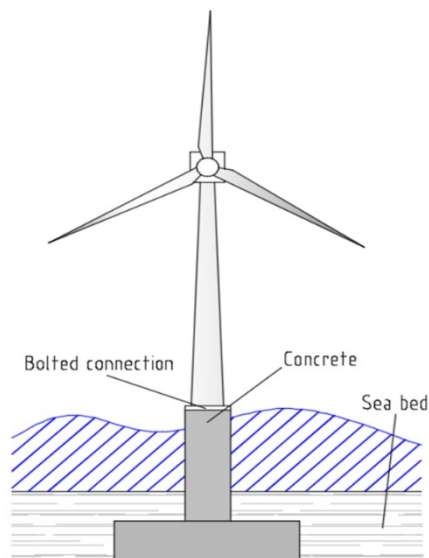
Figure 1.6 Gravity-based wind turbine (Karimirad, 2014)

The first offshore wind farm was built in Denmark with 11 large gravity-based wind turbines in the

year 1991. A layout of a gravity-based wind turbine is shown in Figure 1.6. It is clear that a large heavy concrete foundation is installed on the seabed and no drilling and hammering is needed due to the large amount of weight. Unlike the concepts mentioned above, there is no transition part in this structure and the tower can be mounted on the top of cylindrical part by means of bolts. The gravity-based wind turbine can be transported from one site to another. However, it also becomes more expensive in deeper waters.

1.3 Offshore FWTs

The cost of fixed-bottom wind turbines grows rapidly with the increase of water depth. In addition, some concepts like monopile and gravity-based wind turbines are more readily influenced by increase of water depth. Thus, the new concept of FWTs has been proposed and many researches have been conducted to explore its feasibility. In this section, an overview of various kinds of offshore FWTs is given.

1.3.1 Semisubmersible Wind Turbine

The semisubmersible wind turbine usually includes three or four columns connected by pontoons and braces, as shown in Figure 1.7. The columns provide flotation stability and ballast for the structure with low draft. The restoring moments highly depends on the surface area of columns and distance between each column. Large water surface makes the structure more sTable. Several mooring lines are linked to the platform to keep the system erect while allowing some freedom for slowly varying motions. The selection of anchors is usually based on the soil conditions. Horizontal distance between fairlead and anchor is about 4 to 6 times of the water depth. The structure should

be designed properly to reduce the response with heave, roll or pitch eigenperiods considering the effects caused by extreme loads. This type of wind turbine can be installed near shore and then pulled to the working site by the traditional tugs. Some wind projects were built based on this concept, e.g., DeepCWind and WindFloat in USA, HiPR Wind in Spain.
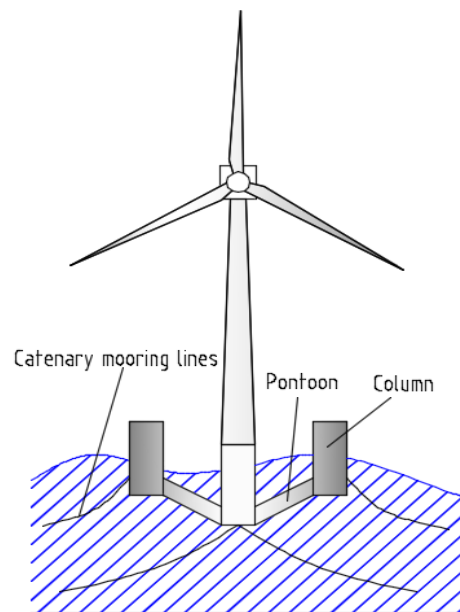
Figure 1.7 Semisubmersible wind turbine (Karimirad, 2014)

1.3.2 Tension-leg Wind Turbine

The layout of tension-leg wind turbine is shown in Figure 1.8. It normally has one large central column and three arms attached with tendons. The structure is simple and highly sTable because the tension legs compensates the force difference between total weight and buoyancy. Tension-leg wind turbines are typically flexible in surge and sway but stiff in the rotation modes. This concept is more complex compared to other types of wind turbines since tendons are pre-tensioned. One method is to ballast the system prior to transport and de-ballast it before the installing the tension legs.

The central column with a slender shape can reduce the hydrodynamic loads. Three arms

should keep the distance from central column to ensure enough restoring moments. The tendons are fixed by suction or gravity anchors on the seabed.

1.3.3 Spar-type Wind Turbine

Spar-type wind turbine consists of a buoyant part, stiff bars, a concrete ballast and mooring lines, as illustrated in Figure 1.9. The concrete cylinder with low water plane area, ballasted with solid or water, keeps the center of buoyancy above the center of gravity. This concept has the capacity to work in moderate water depths if the system is coupled with properly designedmooring lines and masses. The high metacentric height makes sTable the whole structure and there is no wave excitation for yaw motion thus reducing the number of mooring lines. Due to the slender shape of the structure, two kinds of mooring line connection methods are used in the project to guarantee enough restoring ability. One is attaching mooring lines on the stiff bars and another one is using delta lines. Similarly, Horizontal distance between fairlead and anchor is about 4 to 6 times of the water depth. The Hywind project located near shore of Norway has adopted the most sophisticated technology and a small array of Hywind turbines will be deployed in 2020 in the Nordic country.

Figure 1.8 Tension-leg wind turbine (Karimirad, 2014)

Figure 1.9 Spar wind turbine (Karimirad, 2014)

1.4 Wind Turbine Components
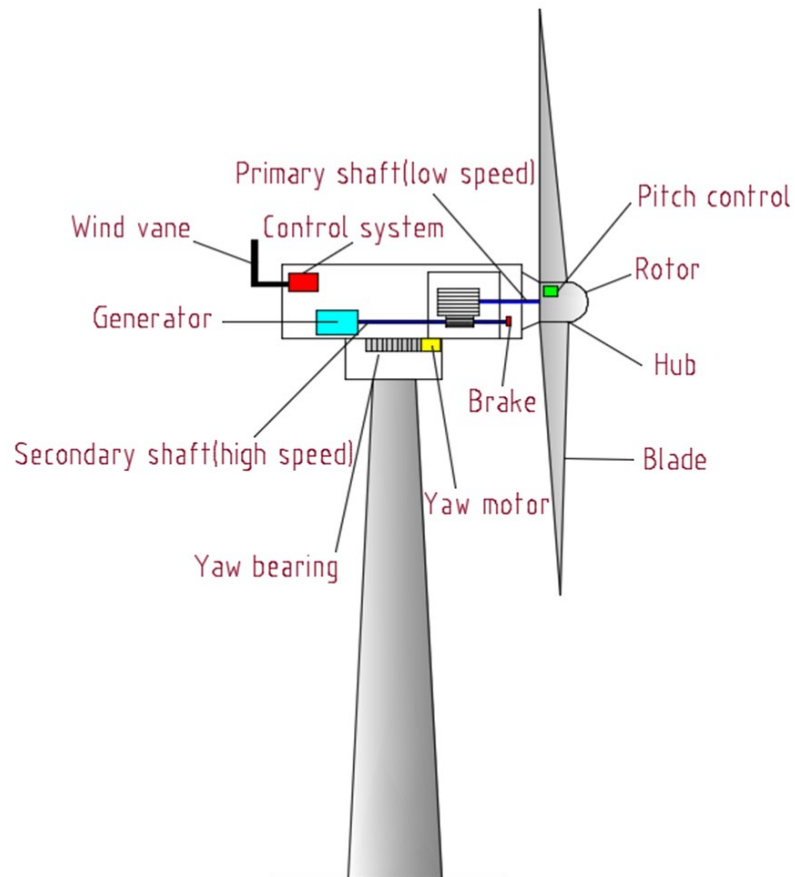
Figure 1.10 Wind turbine components configuration (Karimirad, 2014)

Components of an offshore wind turbine transform wind energy into electricity. The wind forces the

blades to rotate around the rotor. The main shaft and low-speed shaft are connected by the rotor.

Then the drive train accelerates the rotation speed. At last, the generator connected with high-speed

shaft generates electricity. In this section, a brief introduction about the components of a typical

wind turbine is given. Figure 1.10 shows the layout of a wind turbine components.

1.4.1 Wind Turbine Tower

A wind turbine tower is usually constructed by connecting tubular sections by means of bolted flanges. Every ring is made of steel plate manufactured with rolling processes. The rings are connected by the longitudinal welding and circumferential welding which is subject to the fatigue failure (Khatri, 2009). The wind becomes stronger as height increase, thus taller towers can capture more wind energy to produce electricity. However, tall height means larger bending moment and higher cost of construction. Therefore, proper design details should be investigated to balance the cost and efficiency.

1.4.2 Hub

A hub is a part connecting wind turbine blades and nacelle. Also, it is a part of pitch control system that regulates the pitch angle of the blades all the time to optimize the utilization of wind energy. The blades are mounted on the hub with special bearings which allow the blade to vary the pitch angel to suit for different environmental conditions.

1.4.3 Nacelle

The nacelle is the main part of the wind turbine where conversion of the wind energy to electricity is achieved. It is composed of a low speed shaft, gear box, high speed shaft, yaw system, generator and controller. The nacelle is located on the top of wind turbine tower and sometimes it is large enough to allow a helicopter to land on.

In the nacelle, the low speed shaft is connected to the blades and slow-rotating side of the gearbox. The gearbox increases the rotational speed to a high level. Also, a disc brake is installed in

the front of gearbox to put the wind turbine in a parked status in emergency. At the back of the gearbox, there is a high-speed shaft connecting the generator that creates electricity using wind energy. Finally, the power cables transfer electricity from generator to the grids.

1.4.4 Blades

Currently, the wind turbine solution usually uses three blades as the basic design. However, two blades design is also used in the downwind wind turbines. Every blade has an airfoil shape which affects the airflow streamlines and pressure differences. The lift force caused by pressure differences determines the torque on the rotor. Normally, more blades over the same swept area will produce more power, however, the research indicated that profits decrease with the increased number of blades (Lorc, 2011).

1.4.5 Pitch Control System

Originally, blades are directly connected to the hub and a fixed angel of attack is adopted. There was no pitch control system, leading to lower efficiency in converting wind energy. Later, scientists realized that the angel between incoming wind and the blade chord should be controlled by a system, which applies the controller's commands and feathers the blades (Jonkman et al., 2015). Pitch control system is created for this purpose and used to determine how much the angle need to turn the blades. For various velocities of incoming wind, there is an optimal angel of attack to deliver the maximum power to the main shaft. Thus, the wind turbine should continually adjust the pitch to obtain the maximum energy power (Muljadi and Butterfield, 1999).

Apart from the function mentioned above, the pitch control system also works in possible

shutdown or fault conditions. The angle of attack can be set rapidly to zero to neutralize the wind force. In current designs, all the blades are in the same pitch angel. However, some researches proposed that a blade can be separated in several sections and each section has its own pitch system to improve the maximum capacity to convert the wind energy.

1.5 Challenges in Offshore FWT

The technical route of offshore FWT will see both technical and economic issues in that safety and profit should be both guaranteed during the development. The main challenges are listed below:

Environmental challenge:

-The wind source is not characterized well, which increases the uncertainty in the design phase

-The offshore site specification and metocean data cannot be predicted well

-Extreme weather conditions

Structural challenges:

-Dynamic response induced by severe wind and waves is quite different from that of onshore wind turbines or offshore fixed wind turbine

-Fatigue problems caused by dynamic loadings

-Corrosion

Cost drivers:

-The management of cost driver should be optimized in the stage of development, manufacture, installation and operation

-Application for regulatory approvals for offshore wind farm is an uncertain and lengthy process

(Minguez et al., 2011)

Human:

-Lack of qualified staff

-High risk in the installation, operation and maintenance

One of the crucial aspects is the fatigue problem among these challenges due to highly random large loads on the FWTs. In offshore industries, fatigue limit state (FLS) is determined to guide fatigue design and prediction of fatigue lives of offshore structures. For offshore FWTs, the fatigue life is highly dependent on the accumulated fatigue damage which caused by start-up, shut-down, normal operation, parked conditions, fault conditions and extreme conditions. Hence, such parameters should be carefully considered during assessment of fatigue lives.

1.6 Aims and Objectives of the Thesis

This thesis aims to provide a basis for performing fatigue assessment of offshore FWTs due to the fact that the fatigue analysis procedure of this kind of structures is still immature.

Offshore FWTs usually have low frequency responses and are highly sensitive to the wind and waves. For land-based wind turbine, 10-min simulation length is adequate to catch the effects of wind loads. For offshore fixed wind turbines, the length should be increased to 30 min. Unlike land-based and offshore fixed wind turbines, 3-hour analysis is needed to capture nonlinearities to build proper design load. This means thousands of load cases with large amount of long-time simulations should be done for fatigue analysis, which is a time-consuming process. Thus, a proper method is proposed to improve the efficiency of computation and accuracy of quantification.

Also, FWTs have many non-linear contributing factors such as mooring line forces, viscous and aerodynamic forces and large motions which mandate calculating loads at an updated position.

This means that wind and wave loads cannot not be treated separately because of these non-linearities. The traditional frequency-domain analysis cannot capture nonlinear dynamic characteristics of FWTs and some researches suggested that motions of floating platforms had a substantial effect on the loads which was not seen in offshore fixed wind turbines (Henderson and Patel, 2003; Fulton et al., 2006). Therefore, a fully coupled aero-hydro-servo-elastic analysis is adopted to obtain the dynamic response of FWTs.

The traditional S-N curves with Palmgren Miner's rule-based fatigue assessment approaches are widely used in offshore FWTs. However, S-N curves based approaches cannot give details of crack propagation and fail to capture the impacts of load sequence which is crucial to FWTs. Moreover, S-N curves based approaches do not distinguish between steel grades as they assume similar behaviors for all steel structures while FM based approaches are sensitive to the variation of material constants. Thus, FM based approaches are adopted herein to explore the applicability in fatigue analysis because load sequence is considered.

Therefore, the main objectives of the thesis are:

- To propose a simplified lumping approach for offshore FWTs, which reduces the computationally demand to a big extent and still keeps a good accuracy level.

- To conduct the fully coupled aero-hydro-servo-elastic analysis of FWTs.

- To perform a comparison among different S-N curves based fatigue models. This research is not only to quantify the discrepancy of models but also provide a basis for the evaluation and selection of fatigue prediction models for offshore FWTs.

- To conduct fatigue analysis with FM based approaches and investigate the parametric effects.

- To develop a novel FM based model which can be applied to the FWTs with consideration of

the load sequence effect, threshold stress intensity factor range and fracture toughness.

1.7 Organizations and Scopes of the Thesis

The thesis is organized as follow:

Chapter 1 briefly discusses the development history of wind turbines and the current performance of offshore wind turbines. Various types of wind turbines are reviewed including the advantages and disadvantages. Also, this chapter establishes the aims and objectives of the research.

Chapter 2 summarizes the state-of-the-art of fatigue analysis of offshore wind turbines. The advantages and disadvantages of time-domain analysis and frequency-domain analysis have been reviewed. A coupled aero-hydro-servo-elastic tool, FAST, is introduced. The S-N curves and FM based fatigue assessment approaches have been compared and discussed. Load sequence effects on FWTs are detailed, which cannot be ignored during fatigue assessment.

Chapter 3 proposes a simplified lumping approach combined with S-N curves to calculate fatigue life of a spar-type wind turbine. Joint probability of wind and waves has been built for each sea state and fatigue damage has been assessed under every sea state. This chapter also presents narrow-band solution and wide-band solution for fatigue analysis. Six wide-band models are detailed and compared.

Chapter 4 deals with FM based fatigue analysis. Comparisons have been made with S-N curves based approaches and parametric study has been conducted to investigate the sensitivity of initial crack size, critical crack depth and stress concentration factor. Two retardation models have been presented and validated. Also, parametric study of retardation impacts has been done. Then, a modified Space-state model has been proposed and applicated in the fatigue assessment of an

offshore FWT with consideration of threshold stress intensity factor range and fracture toughness.

Finally, Chapter 5 draws conclusions from this research. It also gives an outlook for further research on the basis of this study.

Chapter 2. State-of-the-Art of Fatigue Analysis of Wind Turbines

2.1 Introduction

There is a pressing need to explore renewable energy resources. Offshore wind turbines received much attention from the energy industry and considerable researches have been conducted on land-based wind turbines (Mandell et. al., 1992; Laino et al., 1997; Sutherland and Mandell, 2004; Robertson and Jonkman, 2011), shallow water bottom-fixed wind turbines (Kensche, 2006; Long and Moe, 2012; Dong et al., 2012; Nejad et al., 2014; Yeter et al. 2015), and offshore FWTs (Skaare et al., 2007; Kvittem et al., 2011; Bachynski et al., 2014; Kvittem and Moan, 2015; Nejad et al. 2015).

Wind turbines, especially FWTs, are exposed to dynamic and cyclic environmental loadings during their service lives. Robertson and Jonkman (2011) made a comparison on fatigue equivalent loadings acting on six types of FWTs and one land-based wind turbine and the results showed that the loadings on the components of FWTs were greater than those on the land-based wind turbine. FWTs are normally subjected to the combined dynamic environmental loadings induced by wind and waves. The researchers noted that repeated loadings would propagate the initial crack on the structure and finally lead to rupture. This phenomenon is called fatigue.

The IEC61400 (2009) for wind turbine design requirements states that fatigue problem should be taken into account during the design phase. Fatigue life is usually defined in terms of cycles to failure, which is the number of cycles of a specified character that a specimen sustains before structural failure. Normally, offshore wind turbines need a long service life such as more than 20 years based on the design code (BS7910, 2015). Thus, the design of fatigue lives and the prediction

of remaining fatigue lives are essential. Fatigue Demand is explained in terms of stress ranges that are produced by the variable loadings acting on the structure. It is usually accomplished by an appropriate structure analysis considering aspects like structural modeling, boundary conditions and load combinations based on the published rules and guidance. Moreover, the influence of stress concentrations and how they modify the values of acting stress ranges should be considered as well. This issue is dealt with by applying a Stress Concentration Factor (SCF) in the fatigue analysis, and this factor sensitively relies on the geometry of the structure and welding quality.

The linear fatigue damage cumulative rule was first proposed by Miner (1945) and many kinds of fatigue assessment approaches are proposed based on this rule. ABS (2003) recommends three common methods to assess fatigue damage: namely the Simplified Method, the Spectral Method and the Deterministic Method.

The Simplified Method is linked to permissible stress range or allowable stress range which does not need the specific value of fatigue damage. Only a 'pass/fail' is used to convey whether the acting stress range is above or below the value of permissible stress range. The Spectral Method is a direct method to assess results in terms of fatigue damage or fatigue life. ABS guide (2003) states that the fundamental task of this method is to determine the stress transfer function, which clarifies the relationship between stress at a particular structural location per unit wave height and wave frequency and heading. This method is the most appropriate when there is a linear relationship between wave height and wave induced loadings. However, it hardly addresses the nonlinear effects since the structure response to a sea state is not always linear. The Deterministic Method is a simplified version of the Spectral Method. The difference between these two methods is that a sea state is simply characterized using a deterministic wave height and wave period in the Deterministic

Method. This method cannot calculate structure dynamic response directly since it does not represent the energy content of the sea state. It highly depends on experience to select proper discrete deterministic wave parameters that are sufficient to establish the fatigue model.

Currently, the design of offshore wind turbines, with respect to fatigue, is based on time-domain analysis. For this analysis, a fully coupled aero-hydro-servo-elastic analysis is adopted to obtain structural stress history, and the stress ranges and corresponding cycle numbers are achieved through Rainflow counting technique. A comparison was made by Jonkman and Buhl (2007) for response of the floating system and the response of the turbine installed on land to quantify the impact on dynamic couplings between the turbine and floating barge combined with wind and wave loading. The coupling between the wind turbine response and the barge pitch motion, in particular, was found to produce larger extreme loads in the FWT, especially in wind turbine tower. The offshore fixed wind turbine can be assumed as a beam with elastic boundary conditions at sea bed. And the rotor-nacelle can be regarded as a mass at the tower top. There are no motions occurring in the system. Unlike offshore fixed wind turbines, hydro-elastic loads and coupled loads between floating platform and mooring system cannot be ignored in FWT system. The wave and wind induced loads are highly related to the structural motions and responses and the instantaneous position should be updated with the changes of hydrodynamic and aerodynamic forces all along. Moreover, the structure response amplitude increases at the nature frequency and nature eigen-frequency. Figure 2.1 shows the spectral density functions of the tower base axial stress with three load cases for a FWT. The simulation adopts wind speed of 24 m/s for wind only condition, significant wave height and peak period of 8 m and 12 s for wave only condition and the combination for wind and wave condition (Kvittem et. al, 2011). It illustrates three main frequency zones which

are pitch nature frequency, wave frequency and 1st tower bending mode. The wave decreases the

resonant impact of wind and vice versa, which again indicates the nonlinearities in the system and

tells the importance of conducting coupled aero-hydro-servo-elastic analysis.
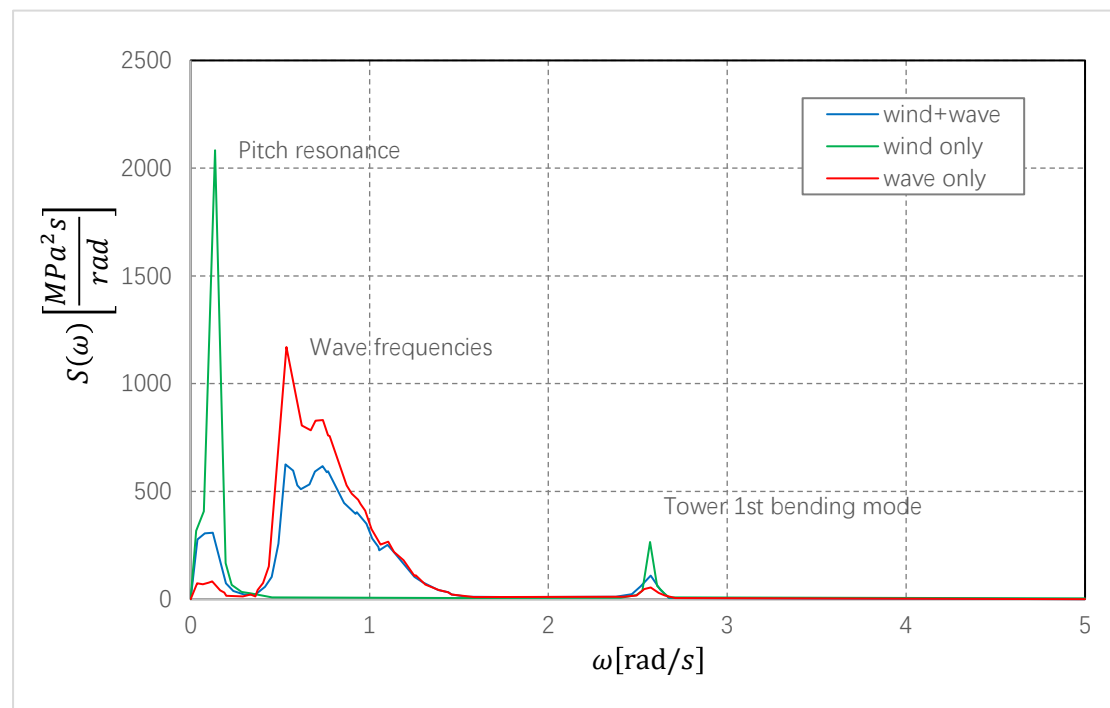
Figure 2.1 Spectral density functions of the tower base's axial stress

Thus, the fully coupled aero-hydro-servo-elastic analysis is recommended herein to obtain the

dynamic response of FWTs. However, this fully coupled dynamic analysis is really complicated and

needs to be conducted for every sea state within wave scatter diagrams.

Therefore, to improve the efficiency of time-domain analysis, lumping several sea states into

a smaller number of manageable blocks is recommended by industry codes (DNV, 2005). The

standard specifies that a wave scatter diagram is subdivided into a number of representative blocks

and then a single sea state is selected within each block, along with lumping the probabilities of

occurrence for all sea states to the selected sea state. The DNV (2005) also indicated that the selected

sea state should give equal or greater fatigue damage than other original sea states. For offshore FWTs, the wind should be considered in every sea state and simulation length should be long enough to capture all nonlinearities which makes lumping approach more complicated and time-consuming.

Seidel (2014) proposed a new approach for lumping of a scatter diagram and site-specified fatigue loads had been worked out based on frequency-domain method. This method allowed rapidly calculation of wave induced fatigue loadings for monopile offshore wind turbines. To improve accuracy, Passon and Branner (2015) proposed a concept of damage equivalent lumping which could preserve the distribution of hydrodynamic fatigue damage of wind turbines, whereas this method did not reflect the influence of coupled wind and wave climates, and also indicated that lumping approach had a significant effect on the calculation of hydrodynamic fatigue loads. In addition, this approach was rather complicated and time consuming. Passon (2015) illustrated a new lumping method which took wind-wave correlation into account and verified the damage equivalency criterions at different locations within the monopile wind turbine system, but it did not give any details to calculate the probability for each sea state. Hence, lumping sea states into several blocks properly is essential as it not only largely reduces the number of simulation requirements and computational time but also has sound accuracy.

The spectral fatigue analysis, based on frequency-domain, can be considered as an alternative to the time-domain analysis owning to its complexity and high computational demand. It has been a very common practice for offshore industries for some time. However, the spectral approach on fatigue damage calculation in the field of offshore FWT does not go a long way. Tempel (2006) proposed a method for fatigue design of offshore fixed wind turbine which considered both wind and wave induced response and also aerodynamic damping. Long and Moe (2012) proposed a

redesign method of three and four-legged offshore wind turbine tower with consideration for the FLS. The frequency-domain analysis was used, and two load combinations were considered. It is concluded that fatigue is the major issue in offshore wind turbine support structures. The ultimate limit state cannot meet the requirements of fatigue, especially for the joints. Yeter et al. (2014) performed a spectral fatigue assessment for a tripod wind turbine with consideration of wind and wave combination. A finite element method was adopted for the coupled dynamic analysis in frequency-domain analysis.

Both time-domain analysis and frequency-domain analysis are all combined with S-N curves and Palmgren-Miner's equation to calculate fatigue damage. It is assumed that the cumulative fatigue damage caused by various stress ranges is a linear summation of the individual fatigue damage from all the considered stress ranges (Miner, 1945). The individual fatigue damage can be calculated through related S-N curves, which is the relationship between the CA stress ranges and the numbers of cycles to failure. S-N curves based fatigue assessment approaches are popular and accepTable in offshore industries. Many researches already have been conducted on fatigue assessment of offshore wind turbines using S-N curves based approaches.

Mandell et. al., (1997) published a report related to the fatigue problem of wind turbine blade materials. The report has shown a variety fatigue behavior of materials which were used in the manufacture of wind turbine blades. Laino et al. (1997) did some early work to perform a fatigue analysis for the steel blade root of a land-based wind turbine using Palmgren Miner's rule and S-N curves. Sutherland and Mandell (2004) investigated the effect of mean stress on the fatigue damage of wind turbine blades with the S-N curves based fatigue analysis. A comparison of fatigue assessment with a detailed Goodman diagram, a power law, a linear Goodman diagram and a bi-

linear Goodman diagram was given. The comparison indicated that the power law formulation was the most conservative among these four formulations. Kensche (2006) conducted fatigue experiments on different blade structures of an offshore bottom-fixed wind turbine and the S-N curves based approach was applied to predict fatigue life. It also explored the fact that the relevant S-N curves could be applied to both 0 degree orientated fibres and ±45 degree lay-ups in shear web and shell. Moreover, a review was given in terms of the influence of fibre content, architecture and environmental factors. Marin et al. (2008) also did a study on fatigue damage in wind turbine blades combined with S-N curves based approach. The research revealed that the damage on the wind turbine blades was due to a fatigue mechanism and the reason was studied and verified by means of the simplified evaluation procedure of Germanischer Lloyd (GL) standard. Kvittem et al. (2011) performed a short-term fatigue analysis for the wind turbine tower of a semi-submersible FWT with a S-N curves based approach. 13 load cases were simulated with time-domain analysis, including cases of wind only, wave only and different misalignment angles of wind and waves. The load response of FWTs could be regarded as a wide band Gaussian process, thus the result calculated by narrow band process may be more conservative. The results showed that narrow band method overestimated fatigue damage by 20%-50% with wave only conditions while 350%-1200% for the wind only conditions. Bachynski et al. (2014) examined short-term fatigue damage of tower base and tower top of the wind turbine using a S-N curves based approach and made a comparison of fatigue lives and motions of several types of FWTs with consideration for the misalignments of wind and waves. Kvittem and Moan (2015) conducted a fatigue assessment for the tower and platform members of a semi-submersible wind turbine using a S-N curves based approach and fatigue loading was estimated by a time-domain aerodynamic and hydrodynamic analysis. In this

study, effects of simulation length, the number of necessary realizations of wind and wave loadings, bin size and wind-wave misalignment were discussed. It also observed the fatigue damage was unexpectedly high for the wind turbine tower due to resonant motion in the first bending frequency.

The drivetrain system is an important part in the offshore wind turbines and the current design is based on IEC 61400-4 rules (2012), which is more suiTable for offshore fixed bottomed wind turbines. The gearbox in drivetrain system is a sophisticated technology with monopoly market share over 85% in one company (Kaldellis and Zafirakis, 2012). Some researchers conducted investigations on the fatigue problems of gear contact, gear tooth root and bearing contact, respectively (Nejad et al., 2014; Jiang et al., 2015). Nejad et al. (2014) performed a long-term fatigue analysis of gear tooth root bending in drivetrains. A simplified approach and a Multi-body Simulation method were adopted to obtain dynamic loadings on the gear. A good agreement was reached by using these two methods. Then the short-term fatigue damage and long-term fatigue damage were calculated using S-N curves based approaches. The research indicated that wind speeds around the rated speed resulted in a higher fatigue damage. Finally, fatigue reliability analysis was conducted by the first-order reliability method. It should be pointed out that the reliability level was site-specific and is only applicable to gear tooth root stress. The fatigue limit state-based design code for all wind turbine gears should be investigated in the future. Nejad et al. (2015) investigated the fatigue damage of drivetrains in land-based, tension-leg, spar and semi-submersible wind turbines using a Spectral Method. The dynamic loadings acting on the drivetrain were achieved from a de-coupled analysis. Fatigue damage was estimated for various environmental conditions and suggested that the fatigue damage of drivetrains in FWTs were higher than that in land-based wind turbines, especially for spar-type wind turbine due to the axial force induced by big waves on

the main shaft.

Additionally, wind turbine status, control strategies and different wind and wave models also have impacts on the fatigue lives. Skaare et al. (2007) made a comparison of different FWT pitch control strategies based on the fatigue lives of tower base and blade root calculated with the S-N curves based approach. It is reported that estimator control strategy could extend the fatigue life to 5 times compared with the conventional control strategy. Meanwhile, the standard deviations of nacelle motion, thrust force and pitch angle also decreased with the estimator control strategy. Marino et. al. (2017) investigated the difference of fatigue lives between linear and fully nonlinear wave models, as well as various mean wind speeds and turbulence intensities. The outcome of the study suggested that the wind turbine in the parked condition with fully nonlinear wave kinematics suffered significant fatigue damage at all mean wind speeds. Ziegler and Muskulus (2015) proposed a simplified method to assess fatigue damage for a jacket-type wind turbine with simulated load cases reduced from 21 to 3. The main idea is to predict the total fatigue damage using piecewise linear regression and multivariate linear statistical models. The research indicated accepTable results with a maximum error of 6% compared to total fatigue assessment.

However, S-N curves based approaches are mainly used in fatigue design phase of offshore wind turbines. Only a single curve presents three stages of crack propagations which neither offer detailed crack growth process nor give the description of load sequence effects. The load sequence effects highly depend on the stress pattern that structures experienced. Figure 2.2 shows stress data of a ship, a bridge and an offshore FWT (Dragt et al., 2016). It can be easily found that the wave loading variations around a general steady mean value for the deck girder of the ship while the stress on bridge also shows a steady mean value caused by traffic. As for the measurement from the

offshore FWT, there are noticeable increases and decreases in mean stress which may be affected by the changing directions of wind and waves and its own unique structure. Thus, it can be concluded that the FWTs are more prone to load sequence effects.
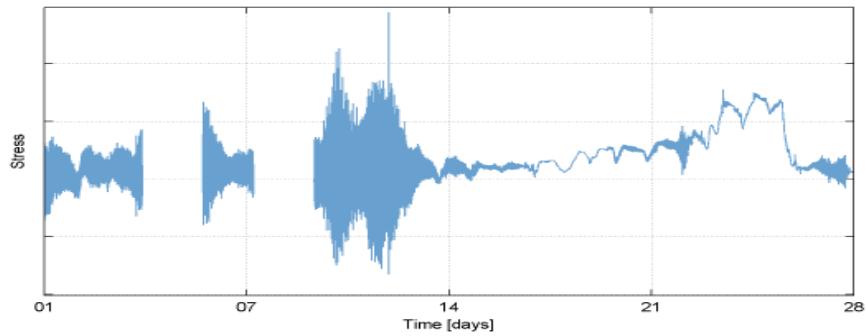
(a)
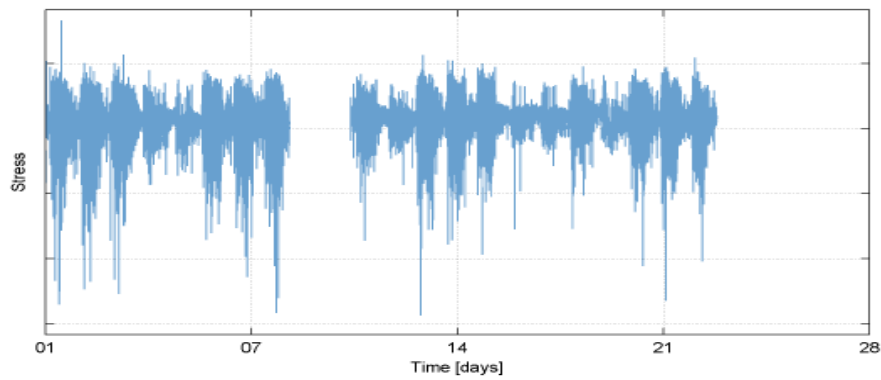
(b)
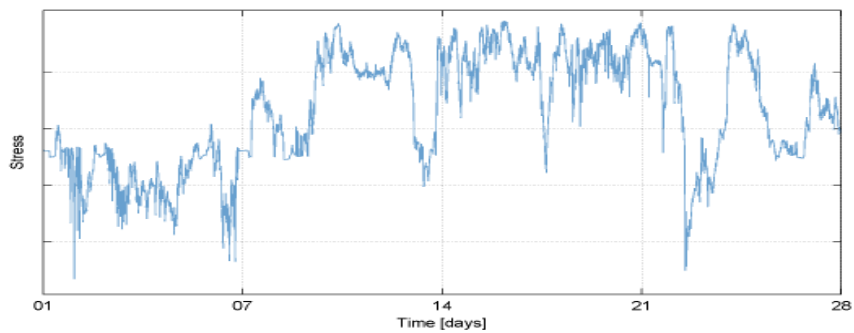
(c)

Figure 2.2 Stress history of a) a ship, b) a bridge and c) a FWT (Dragt et al., 2016)

FM analysis is an alternative to predict remaining fatigue lives. It is advanced compared to S-

N curves based approaches since it can provide detailed crack growth description. However, practical problems such as model complexity and uncertain material constants also limit the application of this method. The most frequently applied model is Paris' law (Paris and Erdogan, 1963) which can only be used for calculation in the sTable crack propagation period. It cannot describe the regions near threshold stress intensity factor range and fracture toughness and also ignore the effects on retardation and acceleration cause by OLs and underloads (ULs), respectively. Very few researches related to the fatigue assessment using FM based approaches on FWTs or even on fixed wind turbines have been done. Dong et al. (2012) carried out a fatigue reliability analysis of a jacket-type wind turbine while considering the corrosion impact. A hot spot location was selected to perform fatigue reliability analysis with FM propagation models calibrated by S-N data because of the uncertainties in the initiation phase of the crack. The research indicated that at least 5 to 6 simulations for each short-term environmental condition should be performed to ensure the accuracy of results. Furthermore, the effects of repair and inspection with and without corrosion impact were compared. Sensitivity study was also performed to investigate the effects of random variables. Eder and Bitsche (2015) found that one adhesive joint at the trailing edge was prone to fatigue failure. Thus, a fracture analysis of adhesive joint was carried out to examine the fracture process. The results showed that the process of crack propagation at the trailing edge was highly complex even under simplified crack extension assumptions. Mehmanparast et al (2017) conducted an experimental and numerical study to investigate fatigue crack initiation and fatigue crack growth rates at weldments of a monopile wind turbine in both air and seawater environments. A FM analysis was carried out and the results compared with experimental data showed that BS7910 (2013) provided accepTable estimations of fatigue crack growth behavior of base metal in air or seawater.

Nevertheless, all researches reviewed above ignored the load sequence effects of wind turbines.

To determine the remaining life of a FWT is one important aspect in the maintenances and inspections. Therefore, a mature fatigue assessment procedure and proper FM based models are essential for offshore FWTs.

2.2 Stress Analysis

The challenge in structural damage estimation is that the offshore FWTs are under complex loadings, for instance, aerodynamic loadings, inertial loadings and operational loadings. Among these loadings, the aerodynamic loadings are significant since the spectrum of wind speed is in high frequency and amplitude. Steel tubular welded structures are widely adopted in the offshore industries because of the high strength and low drag coefficient. The stress acting on the tubular welded structures can be classified in three categories, shown in Figure 2.3.

1) Nominal stress: The stress acts on the cross section away from welded spot. There is no effect caused by geometry or welding.

2) Hot spot stress: The stress is derived through superposition of nominal stress which is weighted with a SCF.

3) Notch stress: The total stress acts on the weld toe region caused by the extra stiffening effect of the weld.
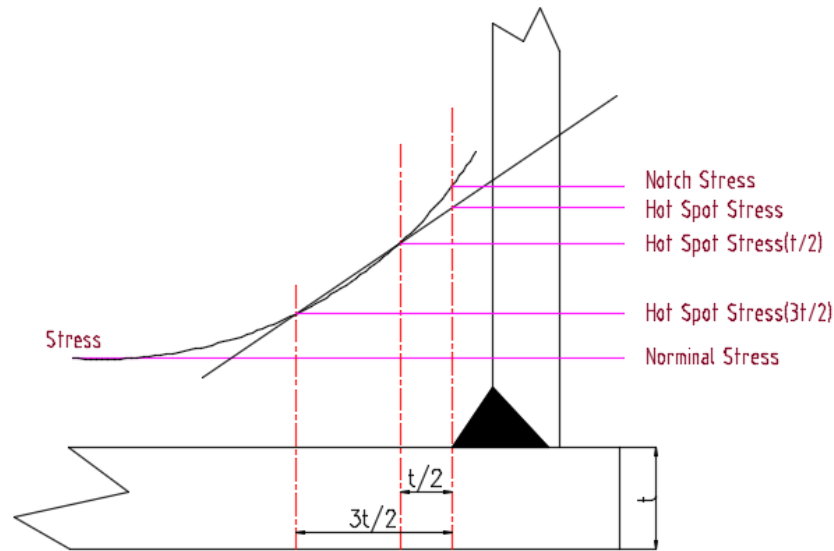
Figure 2.3 Stress categories

The Figure 2.3 shows the stress increasing curve near awelding toe. It is an accepTable method which can obtain the hot spot stress at the welding toe. The 'reference' stress at t/2 and 3t/2 are used to calculate the hot spot stress and the use of ABS Offshore S-N Curve-Joint Class 'T' curve is recommended. The hot spot stress has already been adopted in most offshore structure design guidance since the notch stress is not easy to obtain directly by means of strain guage.

2.2.1 Dynamic Analysis Tool

FAST is an aero-hydro-servo-elastic tool which is developed and verified by National Renewable Energy Laboratory (NREL). It is used to predict dynamic response of wind turbines by fully coupled analysis in time-domain. In this thesis, FAST is applied to achieve dynamic response from offshore wind turbines. There are several subroutines in FAST, e.g., AeroDyn (Moriarty and Hansen, 2005), TurbSim (Jonkman and Kilcher, 2012), HydroDyn (Jonkman, et al., 2014) and BeamDyn (Wang et al., 2016).

AeroDyn is a series of routines used for the calculation of aerodynamic for horizontal axis wind turbines. It gives the results of aerodynamic lift, drag, and pitching moment of blades. Additionally, AeroDyn provides several aerodynamic models for different purposes and two wake models, Blade Element Momentum theory and Generalized Dynamic Wake theory, are most important. TurbSim is a stochastic inflow turbulence code which provides numerical simulation of full-filed flow. In the design of advanced wind turbines, TurbSim can be used to simulate inflow turbulence environments which affect aerodynamic response and loadings. The HydroDyn is used to calculate hydrodynamic loadings based on the potential theory and Morrison's equation. HydroDyn generates waves for finite water depth with use of first order or first order plus second order wave theory (Sharma and Dean, 1981) with wave directions included. The viscous drag forces are estimated by means of the drag term of Morrisons' equation and second-order wave forces are negligible since there are very small impacts compared with the first order wave forces for spar-type wind turbines (Roald et al., 2013).

2.2.2 Frequency-domain Analysis

The spectrum gives the statistical information of the process in terms of the frequency. It is convenient and useful to obtain enough information and to transform time-domain results to frequency-domain spectra, thus easily illustrating the crucial components of frequency and physical phenomenon.

In experiments or numerical simulations, a time series can provide useful information such as the mean value, maximum and minimum value and standard deviation value. In offshore industries, it is common sense to repeat simulations several times to modify the predicted parameters to ensure

the desired level of accuracy. The results can be averaged to stand for more realistic data. In other words, time-domain simulations are post-processed to define statistical characteristics, and Fast Fourier transform (FFT) can be used to transform time-domain results to frequency-domain results.

2.2.3 Time-domain Analysis

One main limitation of frequency-domain method is that the procedure can only be applied for linear systems and Gaussian processes. Thus, time-domain analysis is recommended to be used in the stochastic analysis of systems including nonlinearity. However, time-domain analysis is a time-consuming process, especially for offshore floating structures with low-frequency components. To get an accurate dynamic response of structures, large numbers of simulations and long simulation lengths should be executed. Kvittem and Moan (2015) indicated that 7 seeds of 3-hour simulations of offshore FWTs are enough to meet the requirements of accuracy. Moreover, time step also has a significant effect on the accuracy of results and large time step is not recommended. The proper selection of time step is highly dependent on the different variables, i.e. simulation tools, environmental conditions or system status. One method is to conduct a convergence study to find the suiTable value of time step.

2.2.4 Definition of Stress Concentration Factor (SCF)

The hot spot stress concentration factor is defined as the ratio of the hot spot stress to the nominal stress (ABS, 2003). The changes of the shape near the intersection cause significant increase of the stress, where structures may fail easily. The hot spot SCF can be obtained from semi-empirical equations or by means of Finite Element Analysis (FEA).

The FEA needs to be conducted at critical locations on the structure to obtain the hot spot stress. Several literature references have given successful examples and proper approaches to get the distribution of hot spot stress (Kwon and Frangopol, 2010; Nejad et al., 2014). In general, element type, element size, aspect ratio and gradation of the mesh should be considered during the establishment of the FEA model.

2.3 Fatigue Analysis Methods

As mentioned above, offshore FWTs are subjected to wear, fracture and fatigue problems. The design life of wind turbine components is highly dependent on the accumulated fatigue damage. Unlike other traditional offshore structures, offshore wind turbines not only have normal operation conditions but also other harsh conditions, i.e. start-up, shut-down, parking, fault or extreme conditions. These cases should be considered while performing the fatigue analysis. Meanwhile, the possible environmental conditions with high probability of occurrences should be estimated in advance. As it is clarified before, thousands of simulations are needed to obtain a convergence result, which is a computationally demanding process. Therefore, proper sensitivity study is also required to reduce the number of simulations.

2.3.1 S-N Curves Based Approaches

S-N curves are generated from the test of material specimen which are usually clarified as piecewise-linear curves with one or two segments. S-N curves are distinguished by environmental conditions and the type of welding connection. DNV rules (2014) stated that these curves normally refer to mean-minus-two-standard-deviation curves from experiments with 97.7% probability of survival. The fatigue life of the FWT is calculated according to the S-N curves published in the ABS guide for fatigue assessment of offshore structures (ABS, 2014). These S-N curves are two-segment

curves and can be expressed as:

$$N\Delta S^m = A \qquad\qquad when\, N \leq 10^7 \qquad\qquad (2.1)$$

$$N\Delta S^r = A_r \qquad\qquad when\, N > 10^7 \qquad\qquad (2.2)$$

where N is cycles to failure, ΔS is the stress range, m and r are the fatigue strength exponent, and A and A_r are the fatigue strength coefficients, as shown in Figure 2.4.

ABS (2014) recommends long-term fatigue stress range of offshore structures is fitted by a two-parameter Weibull distribution (Guedes and Moan, 1991), and the probability density function and the cumulative distribution function of the stress range are expressed below:

$$f(S) = \frac{\gamma}{B}\left(\frac{\Delta S}{B}\right)^{\gamma-1} exp\left[-\left(\frac{\Delta S}{B}\right)^{\gamma}\right] \qquad\qquad (2.3)$$

and

$$F(S) = 1 - exp\left[-\left(\frac{\Delta S}{B}\right)^{\gamma}\right] \qquad\qquad (2.4)$$

where B and γ are the scale and shape parameters of Weibull distribution.

For each sea state (i,j), the fatigue damage of the structure can be estimated using the Palmgren-Miner's rule, which states that where there are Q different stress magnitudes in a spectrum, ΔS_k $(1 \leq k \leq Q)$, each contributing $n_k(\Delta S_k)$ cycles, then if $K_k(\Delta S_k)$ is the number of cycles to failure of a constant stress reversal ΔS_k, fatigue damage is given by

$$D_{ij} = \sum_{k=1}^{Q} \frac{n_k}{N_k} \qquad\qquad (2.5)$$

If the probability of occurrence of this combination of wind and waves is $p_{i,j}$, then the fatigue damage can be expressed as

$$D_{i,j}^* = p_{i,j} \cdot D_{i,j} \qquad\qquad (2.6)$$

The total fatigue damage D of the structure can be then derived as

$$D = \sum D_{i,j}^* \qquad\qquad (2.7)$$

Bendat (1964) proposed a method to calculate fatigue damage by using the power spectral

density of stress ranges based on the assumption that the stress ranges followed a Rayleigh distribution. (Kvittem et. al, 2011) indicated that the stress ranges of FWTs could be described by a Rayleigh distribution, as validated by the stress ranges of a spar-type FWT in Figure 2.5, which is true for narrow-banded Gaussian process, and the fatigue damage can be estimated by:

$$D = \frac{f_0 T}{A}\left(2\sqrt{2}S\right)^m \Gamma\left(1 + \frac{m}{2}\right) \tag{2.8}$$

where f_0 is long-term average zero-up-crossing frequency expressed as $\sqrt{m_2/m_0}$ and $\Gamma(.)$ is gamma function and m is the material constant .

However, the response of a FWT approximately follows a wide-band Gaussian process and Rayleigh approximation is conservative for a wide-band process (Benasciutti, 2004).
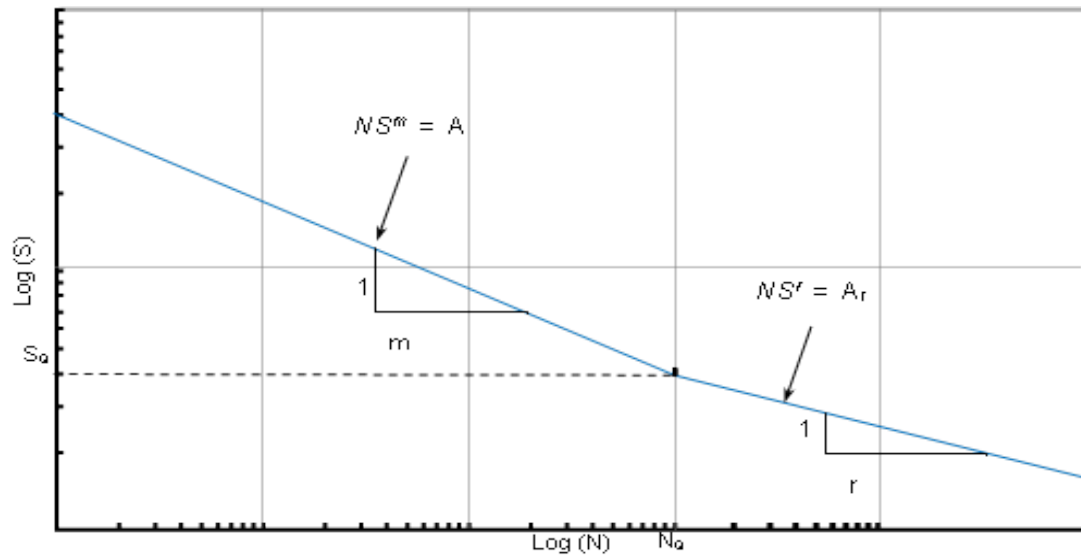
Figure 2.4 Two-Segment S-N curve
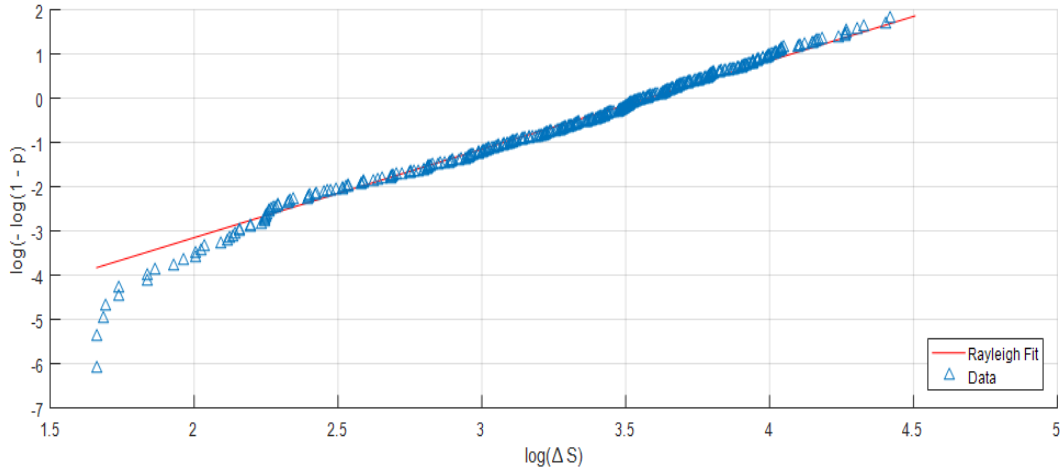
Figure 2.5 Rayleigh distribution curve fitting for a spar-type FWT

2.3.2 Linear Elastic FM Based Approaches

FM based approach has been widely adopted in the fatigue assessment of offshore structures. The procedure for estimating remaining service life is combined with Paris' law, which is expressed as:

$$\frac{da}{dN} = C(\Delta K)^m \tag{2.9}$$

where C is the crack growth rate coefficient and m is material constant, and ΔK is the stress intensity factor range in terms of a stress cycle.

The calculation for the stress intensity factor K is defined by BS 7910 (2013) shown below:

$$K = Y\sigma\sqrt{\pi a} \tag{2.10}$$

where σ is the applied stress on the structural component and

$$Y = M f_w M_m k_t M_k \tag{2.11}$$

where the parameters M, f_w, M_m and M_k are given as:

$$M = 1 \tag{2.12}$$

$$f_w = \left\{ sec\left[(\frac{\pi c}{W}) \left(\frac{a}{t}\right)^{0.5} \right] \right\}^{0.5} \tag{2.13}$$

$$M_m = \frac{\left[M_1 + M_2 \left(\frac{a}{t}\right)^2 + M_3 \left(\frac{a}{t}\right)^4\right] g_0 f_\theta}{\varphi} \qquad (2.14)$$

$$M_k = f_1 + f_2 + f_3 \qquad (2.15)$$

where W is the width of plate along the direction of surface flaw, M_k is the correction factor, which is a function of crack size, geometry and loadings and k_t is the stress concentration factor. The initial crack in this thesis was assumed to be a surface crack so that the geometry of surface flaw on plate can be seen below in Figure 2.6.

Typically, there is a minimum threshold stress intensity factor ΔK_{th}, below which the stress ranges can be neglected. Hence, offshore standard DNV-OS-J101 (2014) recommends the crack propagation equation, which leads to less conservative results for identical material parameters. The recommendation of this value is $\Delta K_{th} = 79.1 MPa\sqrt{mm}$.

$$\frac{da}{dN} = C(\Delta K^m - \Delta K_{th}{}^m) \qquad (2.16)$$

The equation above results in a smaller crack growth rate especially for if a large number of stress intensity factors near the threshold value exist. However, BS 7910 (2013) recommends a modified version which has a less conservative result. R is the stress ratio defined as ratio of minimum to maximum absolute stress level.

$$\frac{da}{dN} = C\left(\frac{\Delta K - \Delta K_{th}}{1-R}\right)^m \qquad (2.17)$$

Based on DNV GL (2014), the fatigue life estimated by FM based approaches is shorter than that estimated by S-N curves based approaches. The reason is that crack initiation period is included in S-N curves but not in FM models.

With the formulations above, crack growth increments Δa and Δc can be calculated for one

stress cycle. Repeat this step for crack height $a + \Delta a$ and continue until the limit to crack growth

or the specified design life is reached.
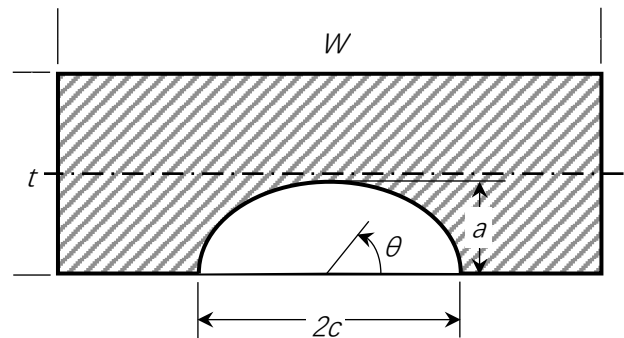
Figure 2.6 Surface flaw

2.3.3 Comparisons between S-N Curves and FM Based Approaches

Normally, there is not enough information to obtain material constants, thus the parameters in Paris'

Law are determined by calibration of the FM model to S-N curve model. In this case, fatigue life

predicted by these two methods should be the same but there may some discrepancies due to the

different assumptions used in the models.:

1) The fatigue life predicted by FM based approach is sensitive to the variation of material

    constants.

2) The FM based approach cannot be applied to the fatigue design since the stress intensity factor

    applies only if the crack length is larger than zero. Moreover, Paris' Law can only be used in

    the period of sTable crack propagation.

3) S-N curves are obtained with a CA of stress range with stress ratio R equal to 0 or -1. For FM

    based approach, however, it is usually derived at a stress ratio R of 0 or close to 0 due to

    compression loadings leading to closure of cracks.

2.3.4 Load Sequence Impacts on Fatigue Life

In real offshore wind turbine structures, it is not sufficient to predict fatigue lives using traditional S-N curves based approaches or linear elastic FM based approaches since variable amplitude (VA) loadings result in acceleration and retardation due to UL and OL. And these two methods cannot capture the impacts from load sequence when estimating the fatigue crack growth.

The mechanism of retardation influence caused by OLs is widely researched than acceleration influence caused by ULs because the acceleration effect due to ULs is significantly weaker than the retardation effect due to OLs (Ding et al., 2017). A summary provided by Anderson (2015) illustrated three basically different physical concepts and explained the crack retardation after a single OL in constant amplitude (CA) loadings.

The first concept is based on the existence of residual compressive stress in the plastic zone in front of the crack tip. See Figure 2.5(a). The retardation occurs due to residual compressive stress in the primary plastic zone caused by the OLs. It reduces the range of the effective stress intensity and therefore decreases the crack growth rate. Then the crack growth rate recovers until the subsequent crack extension and the secondary plastic zone has passed the primary plastic zone. The Generalized Willenborg model is based on this concept (Willenborg et al., 1971).

The second concept considers the plastic wake zone at crack flanks, and this is called strip-yield model, see Figure 2.5(b). The large plastic wake zone caused by OLs requires increasing stress to open the crack thus it results in the drop of the crack growth rate of subsequent smaller cycles. With the propagation of the crack, the influence of plastic wake zone reduces the distance between crack tip and plastic wake zone. Finally, the crack opening stress returns to the normal level of CA load values. Some models are developed under this theory (Ray and Patankar, 2001; Newman, 1981).

The third concept mainly describes the crack tip re-initiation. See Figure 2.5(c). The OLs blunt the crack tip and the cracking process needs to be re-initiated. The initiation period is supposed to be equal to the retardation.

Great efforts have been made on modeling the OLs and ULs based on the aforementioned concepts. Wheeler (1972) proposed the concept that OL caused a larger plastic zone ahead of crack tip and then some researchers (Yuen and Taheri, 2006; Zhao et al., 2008) made it applicable for different materials under VA loadings. The modified Wheeler's model has also been utilized to estimate the fatigue lives of 7075-T651 aluminum alloy successfully. Elber (1971) firstly created the crack closure model in the wake of the crack and some experiments had been conducted to explain the effects of OLs and ULs on the crack growth rate based on this theory (Codrington and Kotousov, 2009; Espinosa et al., 2013).

However, all the three concepts and their simplified models have their inherent drawbacks. The Generalized Willenborg model can only predict the retardation effects of single OL following the CA loadings but cannot predict the effects due to the UL. Some researches (Ding et al., 2017; Anderson, 2015) indicated that an instantaneous crack growth acceleration after OL was observed before retardation which was not predicted by the first and the third concepts. The strip-yield models cannot be applied in some cases due to the limitations of crack shapes, stress conditions and geometry, for instance, semi-elliptical cracks, which are more relevant for thick-walled welded structures but the parameters provided in the strip-yield models are related to the through-thickness crack and plane stress conditions.

Since OLs have significant effects on the fatigue lives, and some reviews have been performed to discuss the root cause of the retardation phenomenon. The results of experimental research in

fatigue crack growth over the past several decades provide a knowledge base to explore the possibility of modeling the crack opening stress S^o as a state variable (Ray and Patankar, 2001). Schijve (1988) conducted an experiment to predict fatigue crack growth rate under VA loadings and found that when the experiments were repeated with the same CA loadings with one single OL added, the crack propagated slower than that CA loadings without OL. After that, Yisheng and Schijve (1995) observed from experimental data that there was a sudden decrease for the S^o followed by a rapid increase and a subsequent slow decrease. However, it happened in a few cycles, which had no huge impacts on the overall crack growth rate. This phenomenon is in line with the Paris equation modified for the crack-closure concept which is further illustrated below.

The abrupt OL causes immediate increase in $S^{max} - S^o$, which results in the significant increase of crack growth rate in the present cycle. As S^{max} returns to the original CA value, the consequence of increased S^o is a shape decrease in $S^{max} - S^o$, which causes the drop of the crack growth rate. Subsequently, with the S^o decreases to its original CA value, crack growth rate bounces back to its higher value. See Figure 2.6. Consequently, the fast rise and subsequent slow decay of S^o is the dominant factor for the retardation phenomenon (Newman, 1992). However, some other researchers attributed it to the plastic zone ahead of crack tip. The plastic zone delays the propagation of the crack until the it grows out of the plastic zone. Although this model can capture the effect of a single-cycle OL, it cannot adequately explain the sequence effects like the initial acceleration after applying OL. Hence, treating S^o as a state variable is preferable.
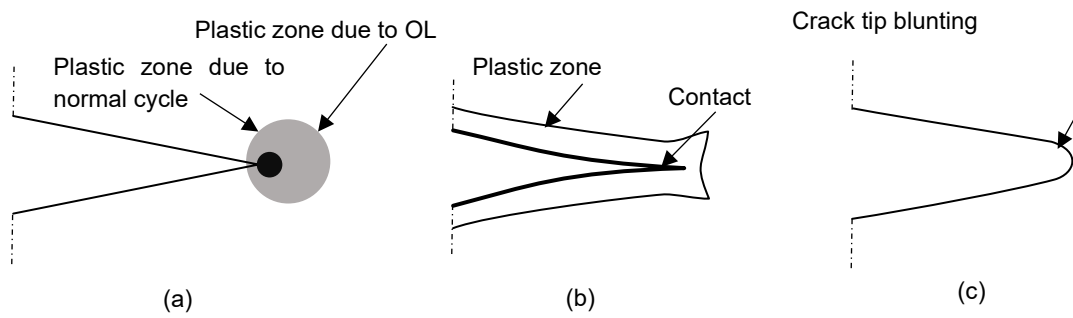
Figure 2.7 Schematic presentation of three retardation concepts. (a) Plastic zone ahead of crack tip

(b) Plastic zone at crack flanks (c) Crack tip blunting (Maljaars et al., 2015)
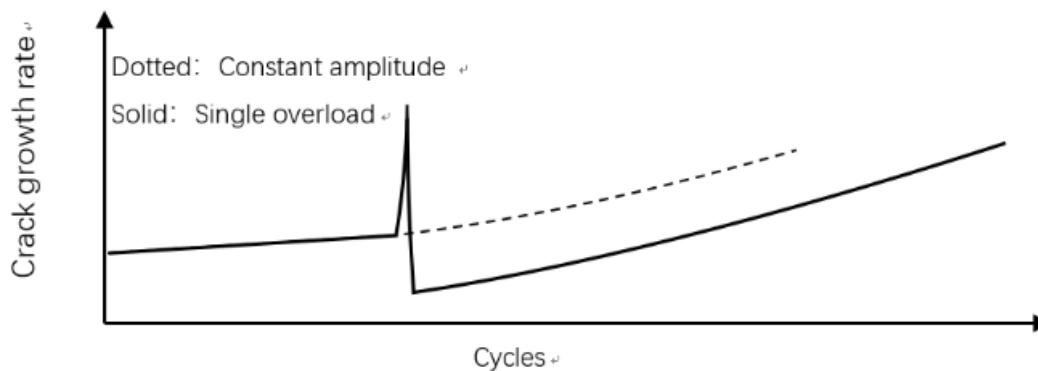
Figure 2.8 Crack growth rate with applying a single OL

2.4 Summary

In this chapter, the advantages and disadvantages of time-domain analysis and frequency-domain analysis have been reviewed. The aerodynamic and hydrodynamic loadings of FWTs are obtained through a coupled aero-hydro-servo-elastic tool, FAST. The S-N curves and FM based fatigue assessment approaches have been compared and discussed. OL and UL effects on FWTs are detailed and they cannot be ignored during fatigue assessment. Due to the unique structural characteristics of FWTs, a mature fatigue assessment procedure and proper FM based models should be developed.

Chapter 3. S-N Curves Based Fatigue Analysis of FWTs

3.1 Introduction

As outlined in the first chapter, the S-N curves based approaches are used in the design phase. This chapter will give a detailed introduction and application of various fatigue assessment methods based on the theory of S-N curves. Three types of FWTs are utilized: spar-type, tension-leg type and semi-submersible type. A simplified lumping approach is used together with joint probability of wind and waves. Then the narrow-band method and wide-band methods (Wirsching-Light method, Dirlik method, Tunna method, Zhao-Baker method, Tovo and Benasciutti method and the Rice formula) are used to analysis fatigue lives of the tower base of FWT. Finally, a comparison of fatigue lives predicted with the methods mentioned above is performed. The S-N curves based fatigue assessment procedure is shown in Figure 3.1.

3.2 FWT Models

The NREL 5MW wind turbine is taken as a benchmark for this study. The diameter of rotor is 126 m and the tower height is 77.6 m; the rated wind speed is 12m/s, the cut-in speed is 3 m/s and the cut-out speed is 23m/s. The hull is modelled as a rigid body, while the tower, blades and mooring lines were consisted of flexible components. The wind turbine dimensions are listed in Table 3.1. More details can be found in Jonkman et al. (2009) and Jonkman (2010).

Figure 3.1 S-N curves based fatigue assessment procedure

Table 3.1. The properties of 5MW NREL wind turbine

Parameter	Value
Tower height	77.6 m
Tower base diameter	6.5 m
Tower base thickness	0.027 m
Tower top diameter	3.87 m
Tower top thickness	0.019 m
Hub height	90 m
Cut-in wind speed	3 m/s
Cut-out wind speed	23 m/s

3.2.1 Spar-type Wind Turbine

The spar buoy is a platform that was developed within the Offshore Code Comparison Collaboration (OC3) (Jonkman and Musial, 2010). Heavy ballast in the hull maintains stability for the wind turbine. The spar platform is characterized by large draft and small waterline area. For the hydrodynamic forces, the first order and viscous forces are applied together with Newman's equation to predict the wave excitation. The delta lines and clumps consist of mooring lines which are modelled as bar elements.

3.2.2 Tension Leg Platform Wind Turbine

The tension-leg wind turbine has one large central column and three arms are attached with tendons (Karimirad, 2014). The structure is simple and highly sTable because the tension legs compensates the force difference between total weight and buoyancy. Tension-leg wind turbines are typically flexible in surge and sway but stiff in the rotation modes. As shown in Table 3.2, the tension-leg has lower natural periods than other types.

3.2.3 Semi-submersible Wind Turbine

The semi-submersible wind turbine adopts the design of WindFloat (Roddier et al., 2011). The

natural periods of semi-platform are longer than the first order wave periods. As stated in the design, the wind turbine is installed on one of the offset columns. The columns and plates are recognized as rigid bodies and the braces are modelled as flexible beams. The details of these three concepts can be found in Table 3.3 and Table 3.4.

Table 3.3 Nature periods of three types of wind turbines

	Spar-type	Tension-leg	Semi-submersible
Surge period	129.5 s	41.9 s	107.0 s
Sway period	129.5 s	41.9 s	124.8 s
Heave period	31.7 s	0.6 s	19.9 s
Roll period	29.7 s	2.8 s	35.6 s
Pitch period	29.7 s	2.8 s	37.4 s
Yaw period	8.2 s	18.0 s	68.5 s

Table 3.4 Properties of the floating platforms (Robertson and Jonkman, 2011)

	Tension-leg	Spar-type	Semi-submersible
Water depth (m)	200	320	200
Diameter or width×length (m)	18	6.5 to 9.4 (tapered)	50 (column spacing) 6.5 (main column) 12 (offset column)
Draft (m)	47.89	120	20
Water displacement (m^3)	12,180	8,029	13,990
Numbers of mooring lines	8	3	3
Depth to fairleads, anchors (m)	47.89;200	70;320	14;200

3.2.4 Axial Stress Calculation

The wind turbine tower is simplified as a thin-walled cylinder as shown in Figure 3.2. 12 locations at the tower base section are selected for the fatigue assessment in this thesis. No welding effect is considered thus the stress concentration factor of 1 is applied in the calculation. The tower base is subjected to axial force, shear force, torsional and bending moments. Bachynski et al. (2014) indicated that fatigue damage caused by shear stress could be ignored and the fatigue damage was

primarily induced by axial stresses. According to Bachynski et al. (2014), the axial stresses can be estimated as

$$\sigma = \frac{N_z}{A} + \frac{M_x}{I_x} r \cos \theta + \frac{M_y}{I_y} r \sin \theta \qquad (3.1)$$

where N_z is the axial force, A is the area of cross section, M_x and M_y are bending moments, which are calculated by means of FAST software. I_x and I_y are the sectional moments of area, r is the cross section radius and θ is the angle from Location 1 to the calculated point   The maximum stress occurs around the locations of 0 and 180 degree which indicates that the locations 0 and 180 degree are two critical locations of the FWT tower base.
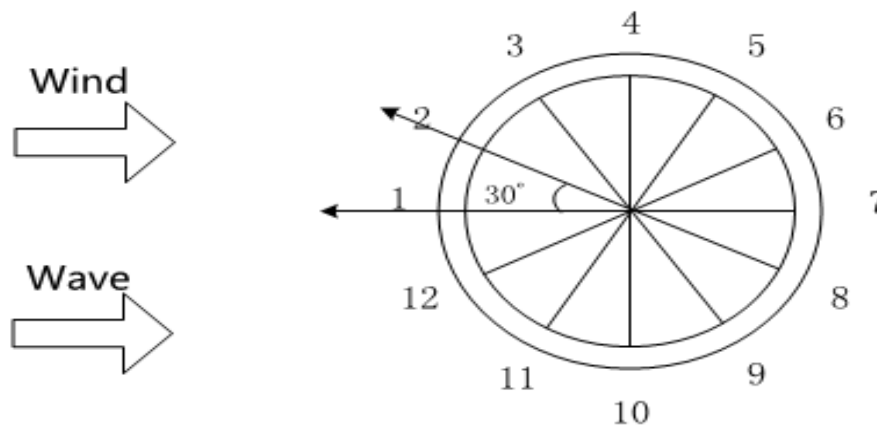
Figure 3.2 Layout of 12 locations on the tower base section

where N_z is the axial force, A is the area of cross section, M_x and M_y are bending moments, which are calculated by means of FAST software. I_x and I_y are the sectional moments of area, r is the cross section radius and θ is the angle from Location 1 to the calculated point. The maximum stress occurs around location 0 and 180 degree which indicates that the two locations are critical ones in the FWT tower base

3.2.5 Rainflow Counting Method

In the time-domain analysis, the dynamic response of structures is represented by stress or strain time history and the most important aspect is to achieve the stress ranges and related cycles. Rainflow counting is one of the most widely used cycle counting methods and was proposed by Matsuishi and Endo (1968). The peak-finding algorithm begins with adding the first time-series data to the peak list. The entire time-series is then traversed, and a peak is identified by a change in sign of the time-series derivative. If a peak value occurs multiple, consecutive times, only the last point of the group is added to the peaks list. Finally, the last data point in the time-series is added to the peaks list. The extreme values are estimated based on 3-point surrounding each local extreme value. Meanwhile, a racetrack filter is used to eliminate small stress ranges which do not contribute to fatigue damage significantly. The algorithm filters out all potential peaks around their adjacent peaks withamplitudes less than a threshold percentage of the maximum range. The details of cycle-counting methods can be found in ASTM E 1049-85 (2011).

3.3 Simplified Lumping Approach

As seen from literature review, it is clearly observed that the lumping approach has a wide applicability and good performance in the fatigue assessment of offshore structures except for offshore FWTs, because the traditional lumping approach does not take wind into account and wind climate is a quite vital component in the fatigue design of offshore FWTs.

To solve this problem, a simplified joint wind and wave probability -based lumping approach is used in the present thesis. With this approach, the joint probability distribution of wind and waves for a specific site is combined with the traditional lumping approach for fatigue damage prediction.

3.3.1 Wind Distribution

Wind is characterized by 1-hour mean wind speed at 10m above the average sea level and a two-parameter Weibull distribution is followed. The probability density function (PDF) of the wind distribution is thus given as:

$$f_{U_w}(u) = \frac{\alpha_U}{\beta_U} \left(\frac{u}{\beta_U}\right)^{\alpha_U - 1} exp\left[-\left(\frac{u}{\beta_U}\right)^{\alpha_U}\right] \qquad (3.2)$$

where α_U and β_U are the shape and scale parameters, respectively.

The mean wind speed U at hub height can be obtained by the wind speed profile as:

$$U(z) = U_{10}\left(\frac{z}{10}\right)^{\alpha} \qquad (3.3)$$

where z is the height (e.g. the hub height, from hub to the tower base) and U_{10} means the reference mean wind speed at 10 m. The wind speed is therefore extrapolated to hub height using a power law of 0.14 in the thesis in accordance with IEC61400-3 guidance (2009).

3.3.2 Wave Distribution

Under the condition of mean wind speed, the conditional PDF of significant wave height H_s can be also described as a two-parameter Weibull distribution as:

$$(H_s|u) = \frac{\alpha_{HC}}{\beta_{HC}} \left(\frac{H_s}{\beta_{HC}}\right)^{\alpha_{HC} - 1} exp\left[-\left(\frac{H_s}{\beta_{HC}}\right)^{\alpha_{HC}}\right] \qquad (3.4)$$

α_{HC} and β_{HC} are the shape and scale parameters, respectively. Then the two parameters are fitted to power functions to achieve the conditionality below:

$$\alpha_{HC} = a_1 + a_2 u^{a_3} \qquad (3.5)$$

$$\beta_{HC} = b_1 + b_2 u^{b_3} \qquad (3.6)$$

where a_1, a_2, a_3, b_1, b_2 and b_3 are the parameters obtained from the curve fitting of the raw data.

With the given conditions of H_s and U_w, the peak periods of waves are indicated as a lognormal distribution, which is defined as:

$$f_{Tp|Uw,Hs}(t|u,h) = \frac{1}{\sqrt{2\pi}\sigma_{\ln(Tp)}t} exp\left(-\frac{1}{2}\left(\frac{\ln(t) - \mu_{\ln(Tp)}}{\sigma_{\ln(Tp)}}\right)^2\right) \tag{3.7}$$

where $\mu_{\ln(Tp)}$ and $\sigma_{\ln(Tp)}$ can be achieved by:

$$\mu_{\ln(Tp)} = ln\left[\frac{\mu_{T_p}}{\sqrt{1+v_{T_p}^2}}\right] \tag{3.8}$$

$$\sigma_{\ln(Tp)}{}^2 = ln\left[v_{T_p}^2 + 1\right] \tag{3.9}$$

$$v_{T_p} = \frac{\sigma_{T_p}}{\mu_{T_p}} \tag{3.10}$$

where μ_{T_p} and σ_{T_p} correspond to the mean value and standard deviation of T_p. v_{T_p} is the coefficient of variance.

According to the suggestion of Johannessen et al. (2001), the mean value of T_p is given by

$$\mu_{T_p} = \overline{T_p}(u,h) = \overline{T_p}(h) \cdot \left[1 + \theta\left(\frac{u - \bar{u}(h)}{\bar{u}(h)}\right)^\gamma\right] \tag{3.11}$$

where $\overline{T_p}(h)$ and $\bar{u}(h)$ are the expected spectral peak period and mean wind speed for the given value of H_s. The two parameters can be estimated by:

$$\overline{T_p}(h) = e_1 + e_2 \cdot h^{e_3} \tag{3.12}$$

$$\bar{u}(h) = f_1 + f_2 \cdot h^{f_3} \tag{3.13}$$

where e_1, e_2, e_3, f_1, f_2 and f_3 are the parameters estimated from the raw data.

In addition, v_{T_p} is supposed to be a simplified function which is only related to H_s

$$v_{T_p}(h) = k_1 + k_2 \cdot exp(hk_3) \tag{3.14}$$

where k_1, k_2 and k_3 are also the parameters extracted from the raw data.

3.3.3 Joint Distribution of Wind and Waves

According to equations above, the joint distribution of U_W, H_s and T_p can be derived as

$$f_{Uw,Hs,Tp}(u,h,t) = f_{Uw}(u) \cdot f_{Hs|Uw}(h|u) \cdot f_{Tp|Uw,Hs}(t|u,h) \tag{3.15}$$

As suggested by Li et al. (2013), the distribution of mean wind speed has limited influence on the distribution parameters of T_p, the equation 3.15 is thus simplified as:

$$f_{Uw,Hs,Tp}(u,h,t) \approx f_{Uw}(u) \cdot f_{Hs|Uw}(h|u) \cdot f_{Tp|Hs}(t|h) \tag{3.16}$$

The probability of each combination of U_w, H_s and T_p can be then expressed as

$$P(U_w, H_s, T_p) = \int_{H_s-\Delta H}^{H_s+\Delta H} \int_{T_p-\Delta T}^{T_p+\Delta T} \int_{U_w-\Delta U}^{U_w+\Delta U} f_{Uw,Hs,Tp}(U_w, H_s, T_p)\, dH_s dT_p dU_w \tag{3.17}$$

And then a representative joint sea state (u,h,t) should be selected within each block for fatigue analysis.

The simplified lumping approach procedure is briefly summarized in Figure 3.3(a)-3.3(c).

For the fatigue assessment of individual block, dynamic response can be obtained from time-domain or frequency-domain approaches. For convenience, the time-domain-based approach is illustrated in this thesis. The simulation results obtained from FAST code give the time history of loadings. According to the time history of stress, the Rainflow counting technique is utilized to calculate the number of cycles at different stress levels. Eventually, the damage $D_{i,j}$ for a specific simulation length was determined by Palmgren-Mine's rule and S-N curves. Following the fatigue calculation of each block, real fatigue damage $d_{i,j}$ for each block is scaled by the joint probability of each combined sea state $p_{i,j}$.

$$d_{i,j} = p_{i,j} \cdot D_{i,j} \tag{3.18}$$

As for the total fatigue damage D of the structure, it can be derived as below:

$$D = \sum d_{i,j} \tag{3.19}$$

In summary, the simplified lumping approach can be illustrated by following steps:

- Step 1. Calculate unit fatigue damage of each block $D_{i,j}$.

- Step 2. Determine the joint probability of each block $p_{i,j}$.

- Step 3. Scale the unit fatigue damage with corresponding probability to obtain real damage $d_{i,j}$ for each sea state.

- Step 4. Sum the real damage $d_{i,j}$ of all possible sea states to achieve total damage.

		Hs[m]	0.0-1.0	1.0-2.0	…	10.0-11.0
Step 1						
	Hs,i[m]	0.5	1.5	…	10.5
Tp[s]	Tp,j[s]				

0.0-1.0	0.5	P(1,1)	P(2,1)	…	P(11,1)
1.0-2.0	1.5	P(1,2)	P(2,2)	…	P(11,2)
2.0-3.0	2.5	P(1,3)	P(2,3)	…	P(11,3)
…	…	…	…	…	…
19.0-20.0	19.5	P(1,20)	P(2,20)	…	P(11,20)
20.0-21.0	20.5	P(1,21)	P(2,21)	…	P(11,21)

Figure 3.3(a) Joint probability of each sea state $p_{i,j}$ under a particular wind speed U_w

Step 2	Hs[m]	0.0-1.0	1.0-2.0	…	10.0-11.0
	Hs,i[m]	0.5	1.5	…	10.5
Tp[s]	Tp,j[s]				
0.0-1.0	0.5	D(1,1)	D(2,1)	…	D(11,1)
1.0-2.0	1.5	D(1,2)	D(2,2)	…	D(11,2)
2.0-3.0	2.5	D(1,3)	D(2,3)	…	D(11,3)
…	…	…	…	…	…
19.0-20.0	19.5	D(1,20)	D(2,20)	…	D(11,20)
20.0-21.0	20.5	D(1,21)	D(2,21)	…	D(11,21)

Figure 3.3(b) Unit damage $D_{i,j}$ for each U_w, H_s and T_p combination

Step 3	Hs[m]	0.0-1.0	1.0-2.0	…	10.0-11.0
	Hs,i[m]	0.5	1.5	…	10.5
Tp[s]	Tp,j[s]				

0.0-1.0	0.5	d(1,1)	d(2,1)	…	d(11,1)
1.0-2.0	1.5	d(1,2)	d(2,2)	…	d(11,2)
2.0-3.0	2.5	d(1,3)	d(2,3)	…	d(11,3)
…	…	…	…	…	…
19.0-20.0	19.5	d(1,20)	d(2,20)	…	d(11,20)
20.0-21.0	20.5	d(1,21)	d(2,21)	…	d(11,21)

Figure 3.3(c) Real damage $d_{i,j}$ under a particular wind speed U_w

3.4 Theories of FAST Software

The coupled aero-hydro-servo-elastic tool, FAST(version 8) (NREL, 2019) is employed to calculate the dynamic response of the FWTs. The theories of the software are detailed in this section.

3.4.1 Wind and Wave Models

The data of environmental conditions are obtained from the Marina Platform project executed by National and Kapodistrian University of Athens (Martinez and Pavn, 2011) and the distribution parameters of the joint distribution of wind and waves refer to that of site No. 14 in North Sea Li et al. (2013). Only aligned wind and wave conditions are considered in this thesis and the positive direction of the global X axis (surge) is aligned with the wind and waves.

The irregular wave history is generated by the JONSWAP wave model with the time step $\Delta t = 0.2\ s$.

$$S(\omega) = \frac{\alpha g^2}{\omega^5} exp\left(-\beta \left(\frac{\omega_p}{\omega}\right)^4\right) \gamma_p^{exp\left(-\frac{1}{2}\left(\frac{\omega-\omega_p}{\sigma_s\omega}\right)^2\right)} \tag{3.20}$$

where α is the spectral parameter, g is the acceleration of gravity, β is the form parameter, ω_p is the peak wave-frequency, ω is the wave frequency, γ_p is the peak enhancement factor and σ_s is the spectral width parameter.

The full-field wind file is produced according to the Kaimal spectrum in TurbSim (Jonkman, 2009) with 32×32 grid points:

$$S_{Kaimal}(f) = 4\sigma_u^2 \cdot \frac{L_k}{U_m} \cdot \frac{1}{\left(1 + 6f \cdot \frac{L_k}{U_m}\right)^{\frac{5}{3}}} \tag{3.21}$$

$$\sigma_u = T_i \cdot (U_m \cdot 0.75 + 5.6) \tag{3.22}$$

$$L_k = 8.1 \cdot \delta \tag{3.23}$$

where T_i is the turbulence intensity, U_m is the mean wind speed, and δ is the spectral parameter. The normal turbulence model is obtained from IEC61400-3 guidance (IEC, 2009).

3.4.2 Hydrodynamic and Aerodynamic Analysis

A FWT is mainly subjected to the aerodynamic loading, hydrodynamic loading and their interaction. The time-domain dynamic responses of the FWT are obtained by using the linear potential-flow theory and the Morison equation.

According to the linear potential-flow theory, the total load at the reference point $\overrightarrow{F_{WRP}}$ is given by:

$$\overrightarrow{F_{WRP}} = \overrightarrow{F_W} + \overrightarrow{F_{HS}} + \overrightarrow{F_{AM}} + \overrightarrow{F_{RD}} \tag{3.24}$$

where $\overrightarrow{F_W}$ is the incident-wave excitation force, $\overrightarrow{F_{HS}}$ is the hydrostatic force, $\overrightarrow{F_{AM}}$ is the total added mass force and $\overrightarrow{F_{RD}}$ is the radiation memory-effect force.

In terms of the Morison equation, the hydrodynamic load is computed from:

$$\vec{F} = \vec{F_I} + \vec{F_D} + \vec{F_B} + \vec{F_{MG}} + \vec{F_{FB}} + \vec{F_{AMMG}} + \vec{F_{AMM}} + \vec{F_{AMF}} \tag{3.25}$$

where $\vec{F_I}$ is the inertial force, $\vec{F_D}$ is the drag force, $\vec{F_B}$ is the buoyance force, $\vec{F_{MG}}$ is marine growth-related force, $\vec{F_{FB}}$ is the force due to fluid ballasting, $\vec{F_{AMMG}}$ is the added mass force due to marine growth, $\vec{F_{AMM}}$ is the added mass force of the structure and $\vec{F_{AMF}}$ is the added mass force due to ballasted fluid.

For the combination of the potential-flow theory and Morison's equation, equation (3.25) can be simplified as:

$$\vec{F} = \vec{F_D} + \vec{F_{FB}} + \vec{F_{AM}} \tag{3.26}$$

The current model evaluating aerodynamic loading on wind turbines is based on the Beam Element Momentum (BEM) theory or Generalized Dynamic Wake (GDW) theory (Moriarty and Hasen, 2005). The BEM theory is a traditional method to calculate induced velocities on wind blades. It is assumed that blades can be divided into small elements that act independently of surrounding elements and can be calculated according to the local flow conditions.

Assuming a one-dimensional flow, the induced relative velocity, V_{rel}, and angle of attack, α_t, at an arbitrary blade element can be derived from:

$$V_{rel} = \sqrt{\left(\omega r(1 + a')\right)^2 + \left(V_\infty(1 - \alpha_t)\right)^2} \tag{3.27}$$

$$\alpha = \tan^{-1}\left(\frac{V_\infty(1 - \alpha_t)}{\omega r(1 + a')}\right) - \beta \tag{3.28}$$

where ω is the turbine rotational speed, r is the blade element radius, a' is the tangential induction factor, V_∞ is the free-stream velocity, a is the axial induction factor, and β is the local

twist angle.

Then the elemental thrust dT and torque dQ can be solved from:

$$dT = \rho U^2 4a(1-a)\pi r dr \tag{3.29}$$

$$dQ = 4a'(1-a)\rho U \pi r^3 \omega dr \tag{3.30}$$

where ρ is the air density and U is the mean flow velocity.

According to the BEM theory, the equations (3.29-3.30) can be also expressed as

$$dT = \sigma'\pi\rho \frac{U^2(1-a)^2}{sin^2\emptyset}(C_l cos\emptyset + C_d sin\emptyset)r dr \tag{3.31}$$

$$dQ = \sigma'\pi\rho \frac{U^2(1-a)^2}{sin^2\emptyset}(C_l sin\emptyset - C_d cos\emptyset)r^2 dr \tag{3.32}$$

where σ' is the local solidity, $\emptyset$ is the angle of relative wind, C_l and C_d are the lift and drag

coefficients, respectively.

GDW solves the Laplace equation for calculating pressure distributions over the rotor plane.

Assuming that the induced velocities are small perturbations relative to the free-stream inflow, the

conservation of momentum is simplified as

$$\frac{\partial u_i}{\partial t} + U_{\infty j}\frac{\partial u_i}{\partial x_j} = -\frac{1}{\rho}\frac{\partial p}{\partial x_i} \tag{3.33}$$

where u_i is the induced velocity in the ith direction, U_∞ is the free-stream wind speed, x_i is

the displacement in the ith direction, x_j is the displacement in the jth direction and p is the

pressure. Due to the conservation of mass, it follows that

$$\frac{\partial u_i}{\partial x_i} = 0 \tag{3.34}$$

Finally, it leads to the Laplace's equation for the pressure distribution

$$\nabla^2 p = 0 \tag{3.35}$$

However, GDW is not sTable at low wind speeds when the turbulent wake state is approached (Laino and Hansen, 2004). In a comparison between a simulation with BEM and GDW, without the unsTable behavior, GDW provided significantly less fatigue for wind speed which is under 9 m/s (Kvittem and Moan, 2015). Therefore, the BEM theory is adopted for wind speeds lower than 8 m/s, otherwise the GDW is applied (Moriarty and Hansen, 2005).

3.5 Application

Fatigue assessment was performed for the tower base of a spar-type FWT using the simplified lumping approach and the configuration of the spar-type FWT is shown in Figure 3.4. The total draft of platform is 120 m and the tower base is located at 10 m above still water line. More details can be found in reference (Jonkman, 2010). The Location 1 on the tower base section was selected as simulation point. The work applied the FAST code to have a coupled nonlinear aero-hydro-servo-elastic analysis in time-domain.

Figure 3.4 Configuration of spar-type FWT (Jonkman, 2010)

The 'NREL offshore 5-MW baseline wind turbine' supported by a spar platform was used. Representative S-N curves were chosen from guidance (ABS, 2003), as shown in Table 3.5. The tower base section is simplified as a thin-walled cylinder structure without considering welding effects. Therefore, a stress concentration factor of 1.0 is applied in this study.

Table 3.5 Parameters of S-N curve for the wind turbine

S-N Curve	A		m	C		r
	For MPa Units			For MPa Units		
T(Air)	1.46×10^{12}		3.0	4.05×10^{15}		5.0

The data of environmental conditions are obtained from the Marina Platform project executed

by National and Kapodistrian University of Athens (Martinez and Pavn, 2011) and the distribution

parameters of the joint distribution of wind and waves refer to that of site No. 14 in North Sea (Li

et al., 2013). Based on the equation (3.17), the joint probabilities of this site can be predicted as the

following Figure 3.5.
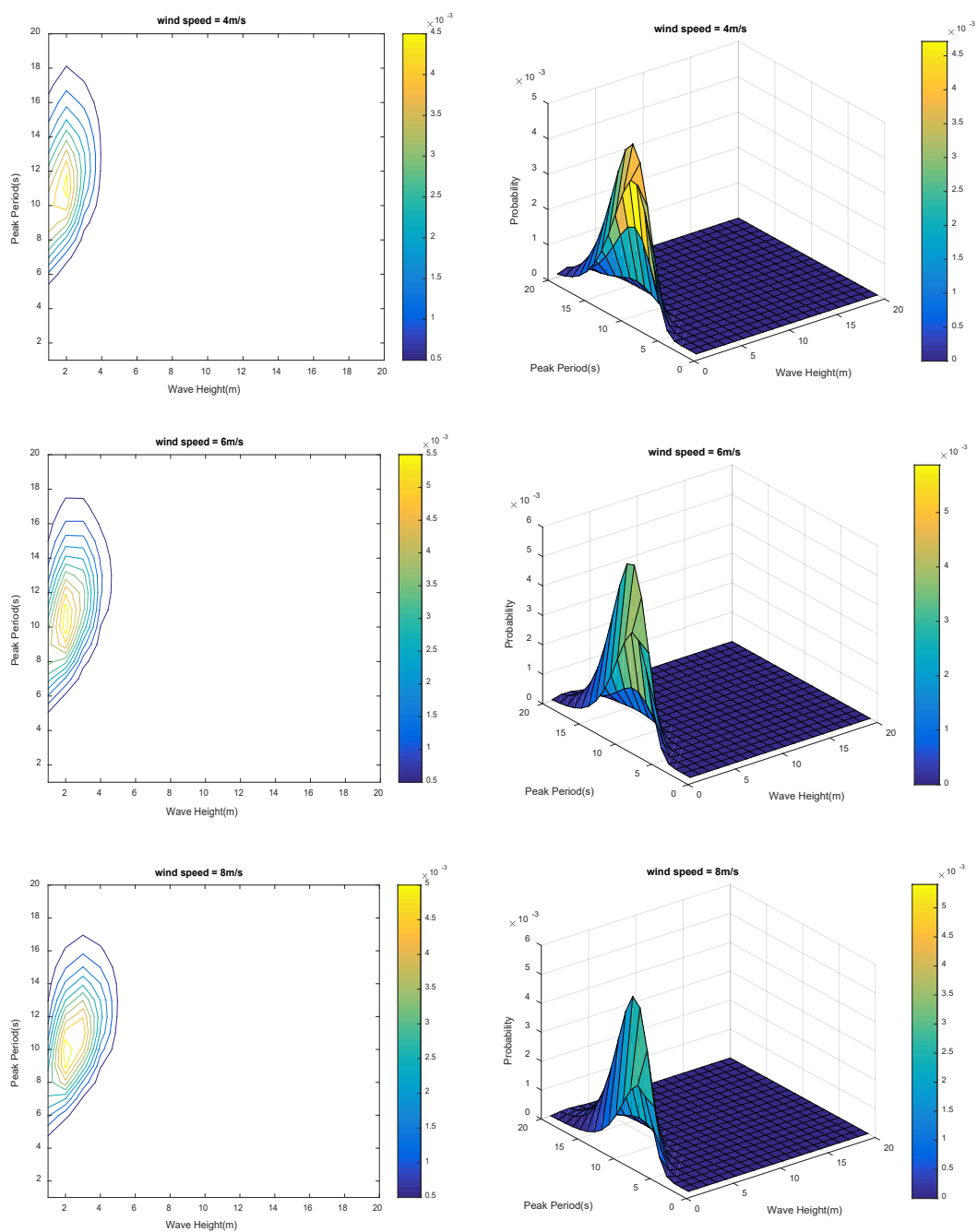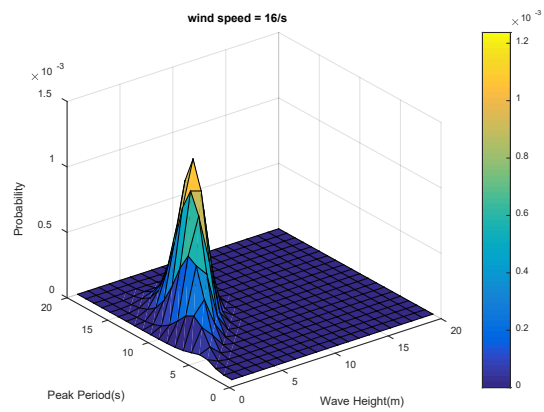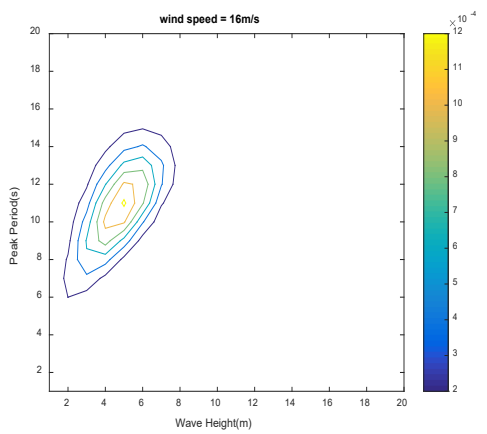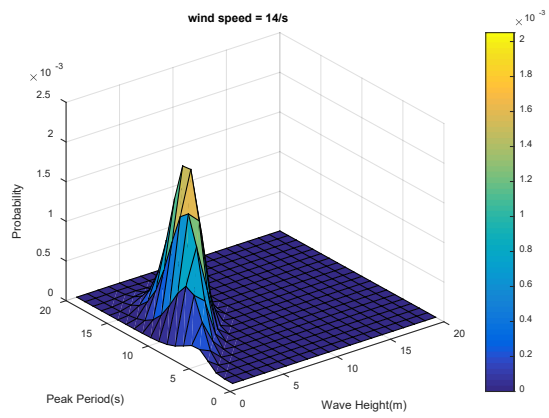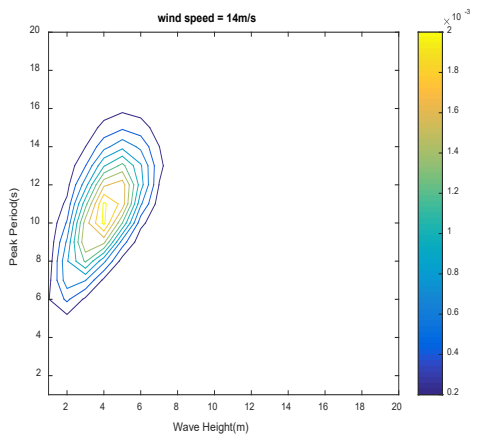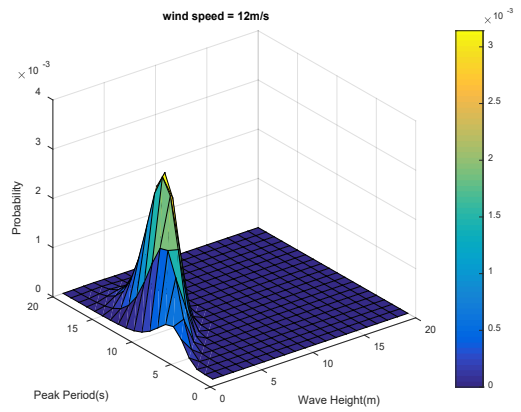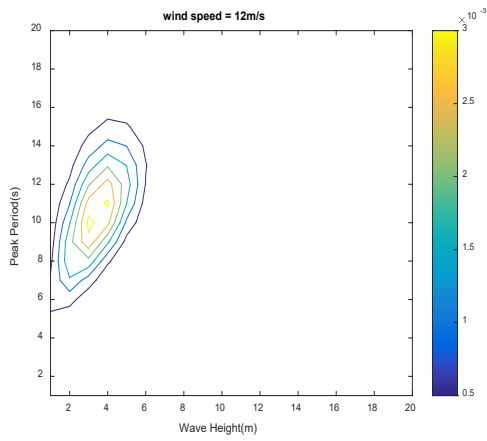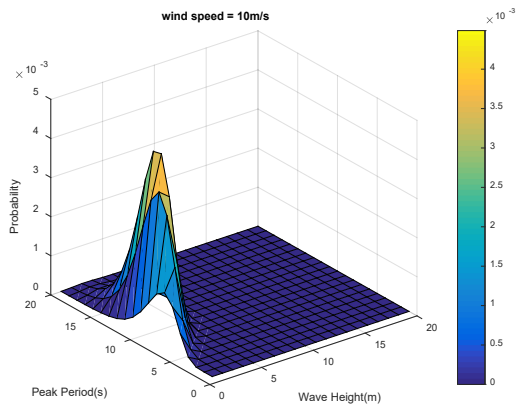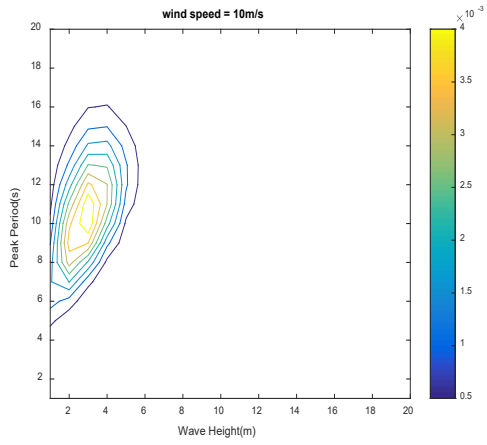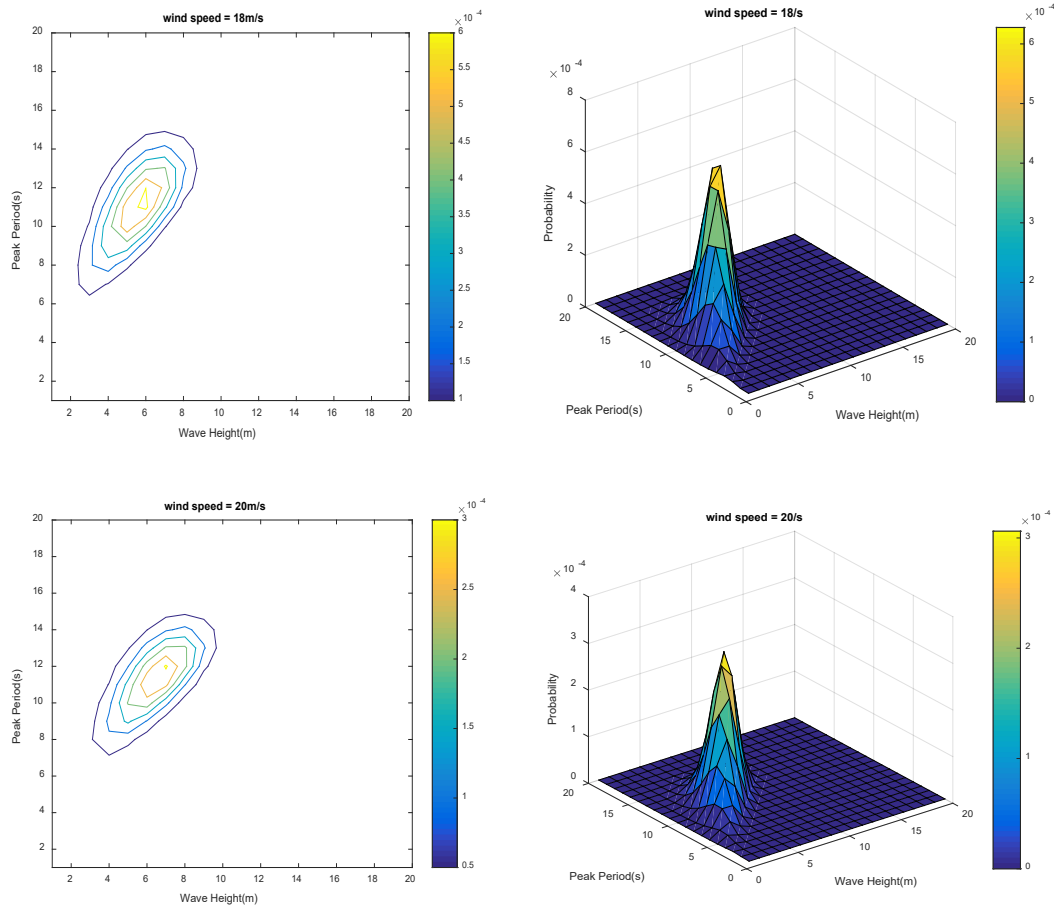
Figure 3.5 Joint probabilities of wind and waves of site No. 14 in North Sea

The normal operation condition of FWTs for fatigue analysis is considered, the range of 1-hour mean wind speed U_w is 4-20 m/s with an increment of 2 m/s; the range of significant wave heights H_s is 1-11 m with an increment of 1m/s; the range of spectral peak period T_p is 4-17 s with an increment of 1 s. Since 11 wave heights, 14 wave periods and 9 wind speed classes are considered, there are 1386 combinations of wind and waves. To improve the computational efficiency but maintain a reasonable numerical accuracy, 498 load cases with the probability of occurrence more than 0.1‰ (DnV-GL, 2015) are selected for calculation where the probability of occurrence of each combination is determined from the joint distribution of wind and waves. Table 3.6 shows a part of joint probabilities for mean wind speed at 18m/s to illustrate this approach.

Table 3.6 An example of joint probabilities for mean wind speed at 18m/s

	Hs[m]	0-1	1-2	2-3	3-4	4-5	5-6	6-7	7-8	8-9	9-10
	Hs,i[m]	0.5	1.5	2.5	3.5	4.5	5.5	6.5	7.5	8.5	9.5
Tp[s]	Tp,j[s]										
0-1	0.5										
1-2	1.5										
2-3	2.5										
3-4	3.5										
4-5	4.5										
5-6	5.5		0.015%	0.016%							
6-7	6.5		0.012%	0.036%	0.022%						
7-8	7.5			0.047%	0.061%	0.028%					
8-9	8.5			0.042%	0.095%	0.084%	0.029%				
9-10	9.5			0.028%	0.098%	0.143%	0.093%	0.023%			
10-11	10.5			0.016%	0.076%	0.157%	0.161%	0.076%	0.013%		
11-12	11.5				0.046%	0.123%	0.175%	0.128%	0.042%		
12-13	12.5				0.024%	0.075%	0.132%	0.129%	0.064%	0.014%	
13-14	13.5				0.011%	0.038%	0.075%	0.087%	0.056%	0.018%	
14-15	14.5					0.016%	0.034%	0.043%	0.031%	0.012%	
15-16	15.5						0.013%	0.016%	0.012%		
16-17	16.5										
17-18	17.5										

After determining the joint probabilities of each block, the coupled aero-hydro-servo-elastic analysis is performed with FAST. The relative parameters are set in the input files of HydroDyn and AeroDyn, and these parameters include wave height, wave period and wind speed. The time step is set to $\Delta t = 0.2\ s$ to ensure that the analysis can capture all nonlinearities; other essential input

parameters have been shown in Figure 3.6. For each block, 6 1-hour simulations are needed to average the short-term fatigue damage in case of the statistical uncertainty. The results obtained from FAST are time history with corresponding axial forces, flapwise and edgewise bending moments, shown in Figure 3.7. Then the stress of tower base can be calculated by equation (3.1) and stress ranges with cycles are achieved through Rainflow counting method. Due to the large amount of load cases, a batch file command was made up with Matlab. This file combines Rainflow counting method with S-N curves based approach to calculate fatigue damage for each sea state and this can keep the computation until all the fatigue lives come out.

The unit damage for those sea states under mean wind speed 18 m/s whose probability of occurrence is more than 0.1 ‰ are determined in Table 3.7. Afterwards, the actual damage for each combination can be obtained by simple scaling up of the unit damage and corresponding probability, which is shown in Table 3.8. Finally, all actual damage under different mean wind speeds are summed to achieve the total fatigue damage.

Main input parameters of spar-type wind turbine for FAST	
Total run time (s)	3660s (including transient time)
Recommended time step (s)	0.02
Time step for output	0.2
InflowWind input	
Wind type	Binary TurbSim
Reference height (m)	10
Power law exponent	0.14
Reference wind speed (m/s)	Depends on each sea state
HydroDyn input	
Water depth (m)	200
Wave model	JONSWAP/Pierson-Moskowitz spectrum
Wave analysis time (s)	3660
Wave time step (s)	0.02
Wave height (m)	Depends on each sea state
Wave period (s)	Depends on each sea state
Wave direction (degree)	0
Wave random seeds	Six random seeds for each sea state
TurbSim input	
Random seeds	Six random seeds for each wind speed
Vertical grid-point matrix	33
Horizontal grid-point matrix	33
Time step (s)	0.02
Analysis time (s)	3660
Usable time (s)	3600
Grid height (m)	170
Grid width (m)	170
Spectrum model	IEC Kaimal
Turbulence type	Normal
Wind profile type	Power law

Figure 3.6 Input file of FAST for the spar-type FWT
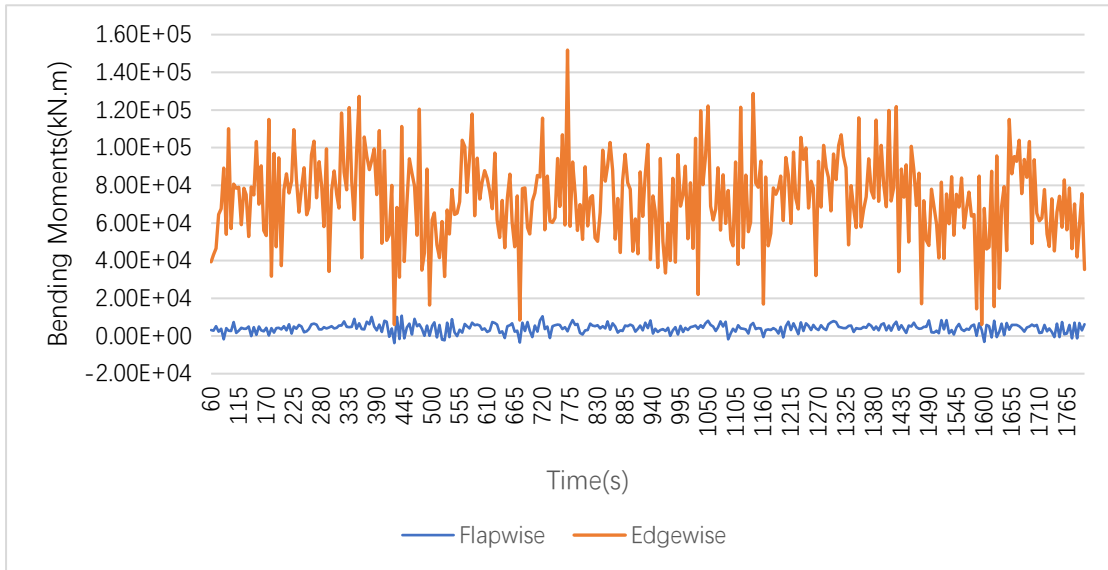
(a)
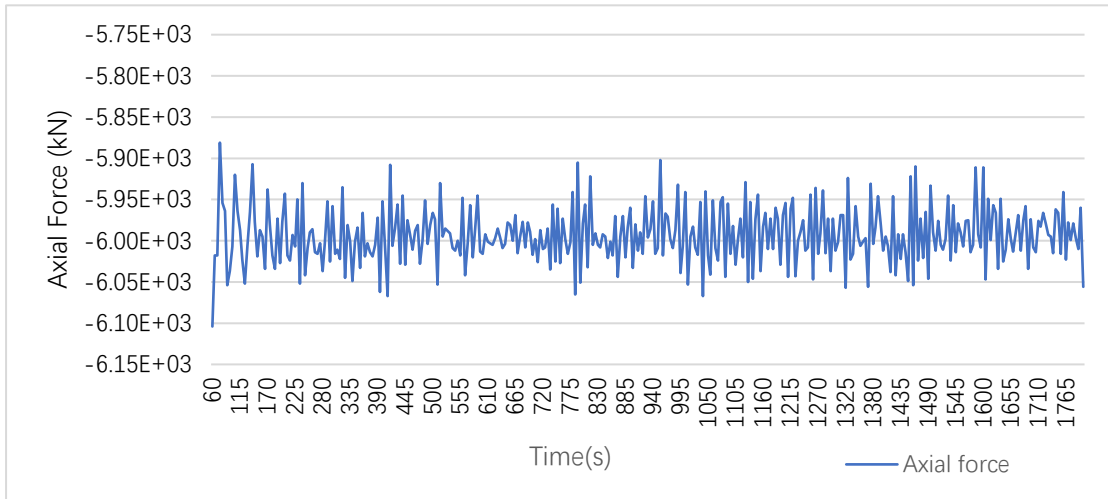
(b)

Figure 3.7 Time history of (a) flapwise and edgewise bending moments (b) axial force

Table 3.7 Unit fatigue damage of each sea state for mean wind speed 18m/s

	Hs[m]	0-1	1-2	2-3	3-4	4-5	5-6	6-7	7-8	8-9	9-10
	Hs,i[m]	0.5	1.5	2.5	3.5	4.5	5.5	6.5	7.5	8.5	9.5
Tp[s]	Tp,j[s]										
0-1	0.5										
1-2	1.5										
2-3	2.5										
3-4	3.5										
4-5	4.5										
5-6	5.5		1.41E-5	1.86E-5							
6-7	6.5		1.46E-5	2.36E-5	4.26E-5						
7-8	7.5			2.28E-5	4.17E-5	8.27E-5					
8-9	8.5			2.32E-5	4.15E-5	7.93E-5	1.47E-4				
9-10	9.5			2.46E-5	4.50E-5	7.97E-5	1.35E-4	2.16E-4			
10-11	10.5			2.58E-5	4.80E-5	8.90E-5	1.64E-4	2.91E-4	4.94E-4		
11-12	11.5				4.85E-5	8.90E-5	1.63E-4	3.02E-4	5.34E-4		
12-13	12.5				4.66E-5	8.48E-5	1.50E-4	2.61E-4	4.61E-4	7.87E-4	
13-14	13.5				4.30E-5	7.75E-5	1.36E-4	2.29E-4	3.73E-4	5.82E-4	
14-15	14.5					6.92E-5	1.20E-4	2.00E-4	3.22E-4	5.00E-4	
15-16	15.5						1.05E-4	1.75E-4	2.80E-4		
16-17	16.5										
17-18	17.5										

Table 3.8 Actual fatigue damage of each sea state for mean wind speed 18 m/s

	Hs[m]	0-1	1-2	2-3	3-4	4-5	5-6	6-7	7-8	8-9	9-10
	Hs,i[m]	0.5	1.5	2.5	3.5	4.5	5.5	6.5	7.5	8.5	9.5
Tp[s]	Tp,j[s]										
0-1	0.5										
1-2	1.5										
2-3	2.5										
3-4	3.5										
4-5	4.5										
5-6	5.5		2.05E-9	2.93E-9							
6-7	6.5		1.81E-9	8.50E-9	9.45E-9						
7-8	7.5			1.07E-8	2.55E-8	2.30E-8					
8-9	8.5			9.68E-9	3.95E-8	6.69E-8	4.24E-8				
9-10	9.5			6.98E-9	4.43E-8	1.14E-7	1.25E-7	5.05E-8			
10-11	10.5			4.14E-9	3.63E-8	1.39E-7	2.64E-7	2.20E-7	6.61E-8		
11-12	11.5				2.25E-8	1.10E-7	2.84E-7	3.85E-7	2.22E-7		
12-13	12.5				1.13E-8	6.39E-8	1.98E-7	3.37E-7	2.95E-7	1.07E-7	
13-14	13.5				4.79E-9	2.94E-8	1.02E-7	2.00E-7	2.09E-7	1.02E-7	
14-15	14.5					1.13E-8	4.06E-8	8.50E-8	1.01E-7	6.10E-8	
15-16	15.5						1.34E-8	2.79E-8	3.37E-8		
16-17	16.5										
17-18	17.5										

The results calculated using this joint probability lumping approach has been compared with the results calculated by Erin et al., (2014) as shown in Figure 3.8. The fatigue damage is calculated for 12 locations on the tower base and the results show a good agreement with Erin's results.

Figure 3.8 1-hour fatigue damage calculated by Erin et al., (2014) and joint lumping approach under 18 m/s of wind speed, 5 m of significant wave height and 14 s of peak period

An obvious trend can be observed from Table 3.7: a higher wave causes increase of fatigue damage. However, from the perspective of wave periods, significant changes of fatigue damage distribution are found and highest fatigue damage appears when Tp is close to the 11 s for each wave height. The reason is that NREL 5-MW wind turbine uses a conventional variable-speed, variable blade-pitch-to-feather control system which can reduce the rotor thrust when the continuously increasing wind speed goes above the rated. Nevertheless, this might introduce negative damping in the system and caused large resonant motions of the FWT. Hence a modification was proposed to reduce the gains in the blade-pitch control system. Hansen et al. (2015) stated that the rotor azimuth responded as a second-order system with a natural frequency and discussed a damping ratio in an idealized blade-pitch control system. To keep a feasible relationship between the proportional and integral gains, a smaller controller-response natural frequency was selected while preserving the recommended controller damping ratio and Jonkman et al. (2009) recommended the value of 0.6 rad/s (11 s) which was above the platform-pitch natural frequency of about 0.21 rad/s (29.7 s).

Furthermore, on one hand the decreased peak period leads to an increased number of load cycles per time which linearly increases the fatigue damage (Passon, 2015). On the other hand, the high fatigue damage appears when Tp is approaching the period of the structure's first eigenmode due to resonance. However, the tower natural frequency is about 2 s with relatively smaller joint probabilities of the sea states, and in this case it can be ignored in the simplified calculation.

This simplified lumping method also reduces the large amount of computational time. All the computers used in the simulations have same configurations. The Figure 3.9 shows a comparison of computational time among spar-type, tension-leg and semi-submersible FWTs. It can be seen from the Figure that the simplified lumping approach with 498 load cases has much shorter computational time compared to 1386 cases. For complicated structures like spar-type and semi-submersible type FWTs, it saves more time in simulation.
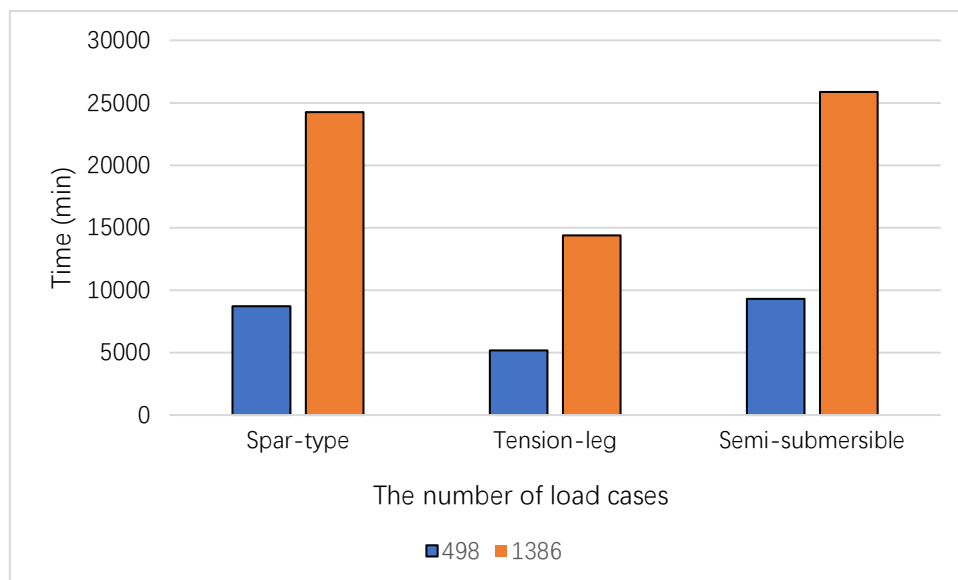
Figure 3.9 Computational time of three types of FWTs

The total fatigue damage of Location 1 on the tower base section is 6.967×10^{-6} (16.48

years) calculated by 498 load cases with 1-hour simulation while the total fatigue damage calculated

by 1386 load cases is 7.031×10^{-6} (16.23 years). The discrepancy between these two results is

only 0.91%. Thus, it can be concluded that the simplified lumping approach can largely reduce

computational time but it has sound accuracy.

Fatigue damage is accumulated from numerous sea states described by joint probability of

wind and waves. An example application to conduct fatigue analysis for a 5-MW spar-type wind

turbine is given to demonstrate the capability of this approach. A three-dimensional scatter diagram

is built to illustrate this simplified lumping approach with class widths of 1m for the significant

wave height, 1s for the wave period and 2m/s for the wind speed. The sea states with the minimum

probability of 0.1 ‰ are considered. Of the theoretically possible 1386 combinations of the 11 wave

heights, 14 wave periods and 9 wind speed classes, only 498 load cases have a probability of 0.1 ‰

and higher, which makes the time-domain analysis more efficient and accurate. The total probability

of occurrence is 98.2% and it is feasible to use these load cases to conduct fatigue calculation. The

computational time of 498 load cases is about 8715 min which significantly reduced the total

simulation time by about 65%. The results calculated by simplified lumping approach show a good

agreement with only 0.91% discrepancy compared to the fatigue damage calculated by all load cases.

However, this approach does not take wind and wave misalignment into consideration, with which

a more conservative result is obtained.

3.6 Narrow-band Solution

The bandwidth of the aerodynamic response is so wide that frequency-domain analysis provides a

more conservative result (Yeter et al., 2016). To overcome this disadvantage, various methods have

been proposed for this purpose. Some researchers added a correction factor (Wirsching, 1980; Benasciutti and Tovo; 2004; Kim et al., 2007), while some others derived equivalent stress in a closed form (Chaudhury and Dover, 1985) or proposed more complicated models to estimate the long-term stress distributions (Tunna, 1986). Moreover, Benasciutti and Tovo (2006) gave a review on wide-band Gaussian stochastic process and a comparison of these methods was given by Halfpenny (1999). The narrow-band solution was developed by Rice (1954) and it is generally conservative and roughly overestimating the fatigue damage when Palmgren-Miner's rule and S-N curves are used to predict the fatigue life (Bishop and Sherratt, 1989).

The objective of this section is to provide a basis for the evaluation and selection of fatigue prediction models on the fatigue assessment of tower base of FWT. Various possible models are tested to determine the type of long-term stress distributions, and both narrow-band and wide-band solutions are reviewed and investigated.

Bendat (1964) proposed a method to predict fatigue damage by using the power spectral density of stress. The method assumed that the distribution of stress peaks followed a Rayleigh distribution, thus the narrow-band solution for the number of cycles for each stress range value can be calculated as follows:

$$n_i(\Delta S) = f_p T_d \left\{ \frac{\Delta S}{4m_0} e^{-\frac{\Delta S^2}{8m_0}} \right\} \tag{3.36}$$

where $n_i(\Delta S)$ is the number of cycles at a specific stress range value, T_d is the time length that the stress occurs, f_p is the peak occurrence frequency and m_0 is the 0th spectral moment of power spectral density. For ith spectral moment, m_i can be expressed as:

$$m_i = \int_0^\infty f^i S(f) df \tag{3.37}$$

where $S(f)$ is the single-sided power spectral density.

Following Palmgren-Miner's rule, the accumulated fatigue damage for one sea state can be estimated as below:

$$D_{Narrow} = \sum_i \frac{n_i}{N_i} = \frac{f_p T_d}{A} \int \Delta S^m p(\Delta S) d\Delta S = \frac{f_p T_d}{A} \int \Delta S^m \left\{ \frac{\Delta S}{4m_0} e^{-\frac{\Delta S^2}{8m_0}} \right\} d\Delta S \qquad (3.38)$$

where A and m are material constants of the S-N curve.

In this narrow-band solution, the structural dynamic response was obtained from FAST code in time-domain analysis. The stress ranges were achieved via Rainflow counting method with related cycles. FFT was used to transform the stress from time-domain to frequency-domain to get power spectral density and finally narrow-band fatigue damage was integrated using equation (3.38). Normally, the structural dynamic response can be achieved from frequency-domain software, like Orcflex directly, which makes frequency-domain method much easier.

This method is established by assuming that the variation of stresses is a narrow-band random Gaussian process. The total fatigue damage should encompass all sea states with the joint probability of wind and waves, which is explained in Chapter 2.

3.7 Wide-band Solution

The wide-band solution is defined as smaller waves riding on a low frequency carrier. Wide-band solutions are generally less conservative than narrow-band solutions that are widely used in offshore industries. However, many of these solutions are semi-empirical derived from narrow-band solutions or even completely empirical. Several wide-band solutions are introduced in this section.

3.7.1 Wirsching-Light Method

Wirsching and Light (1980) added a correction factor to the narrow-band approximation and this factor is obtained from large amount of Monte Carlo simulations. The factor is empirical and defined as:

$$D = \alpha_{WL} D_{narrow} \tag{3.39}$$

where α_{WL} stands for wide-band correction factor and D_{narrow} represents the fatigue damage calculated by narrow-band solution.

$$\alpha_{WL} = a_{WL} + (1 - a_{WL})\left(1 - \sqrt{1 - \alpha^2}\right)^{b_{WL}} \tag{3.40}$$

$$a_{WL} = 0.926 - 0.033m \tag{3.41}$$

$$b_{WL} = 1.587m - 2.323 \tag{3.42}$$

$$\alpha = \frac{m_2}{\sqrt{m_0 m_4}} \tag{3.43}$$

3.7.2 Dirlik Method

Dirlik (1985) proposed a method to Figure out the conservatism of narrow-band method. The stress ranges were fitted by one exponential and two Rayleigh probability density functions and given as:

$$p(\Delta S) = \frac{\frac{D_1}{Q} e^{-\frac{Z}{Q}} + \frac{D_2 Z}{R^2} e^{-\frac{Z^2}{2R^2}} + D_3 Z e^{-\frac{Z^2}{2}}}{2\sqrt{m_0}} \tag{3.44}$$

$$Z = \frac{\Delta S}{2\sqrt{m_0}} \tag{3.45}$$

$$X_m = \frac{m_1}{m_0}\sqrt{\frac{m_2}{m_4}} \tag{3.46}$$

$$\alpha = \frac{m_2}{\sqrt{m_0 m_4}} \tag{3.47}$$

$$R = \frac{\alpha - X_m - D_1^2}{1 - \alpha - D_1 + D_1^2} \tag{3.48}$$

$$D_1 = \frac{2(X_m - \alpha^2)}{1 + \alpha^2} \tag{3.49}$$

$$D_2 = \frac{1 - \alpha - D_1 + D_1^2}{1 - R} \tag{3.50}$$

$$D_3 = 1 - D_1 - D_2 \tag{3.51}$$

$$Q = \frac{1.25(\alpha - D_3 - D_2 R)}{D_1} \tag{3.52}$$

Therefore, the closed-form expression of fatigue damage estimated by Dirlik can be derived

as:

$$D = \frac{f_p T_d}{A} \left(2\sqrt{m_0}\right)^m \left[D_1 Q^m \Gamma(1 + m) + \left(\sqrt{2}\right)^m \Gamma\left(1 + \frac{m}{2}\right) (D_2 |R|^m + D_3) \right] \tag{3.53}$$

3.7.3 Rice Method

Another correction factor based on Rice (1944) is formulated as:

$$\alpha_{Rice} = \frac{1 + \beta}{2} \left[1 + \frac{\sqrt{1 - \beta^2}}{2\sqrt{\pi}\beta} (1 - \beta^2)^{\frac{m+1}{2}} \frac{\Gamma\left(\frac{1 + m}{2}\right)}{\Gamma\left(1 + \frac{m}{2}\right)} \right] \tag{3.54}$$

where the factor β is calculated by:

$$\beta = \sqrt{1 - v^2} \tag{3.55}$$

$$v = \sqrt{\frac{m_0 m_2}{m_1^2} - 1} \tag{3.56}$$

3.7.4 Tovo and Benasciutti Method

Tovo and Benasciutti (2005) proposed a method to modify the narrow-band solution, the fatigue damage is expressed as follow:

$$D = [c + (1 - c)\alpha^{m-1}]\alpha D_{narrow} \tag{3.57}$$

where c is the weighting factor and can be estimated by:

$$c = \frac{(\alpha_1 - \alpha)[1.112(1 + \alpha\alpha_1 - (\alpha + \alpha_1))e^{2.11\alpha} + (\alpha_1 - \alpha)]}{(\alpha - 1)^2} \tag{3.58}$$

$$\alpha_1 = \frac{m_1}{\sqrt{m_0 m_2}} \tag{3.59}$$

where D_{narrow} is estimated by equation (3.38).

3.7.5 Tunna Method

Tunna (1986) method is similar to the narrow-band solution and the bandwidth parameter is added into the probability density function, expressed as below:

$$p(\Delta S) = \frac{\Delta S}{4\alpha m_0} e^{-\frac{\Delta S^2}{8\alpha m_0}} \tag{3.60}$$

3.7.6 Zhao-Baker Method

Zhao and Baker (1992) combined theoretical assumptions with numerical simulations and deemed stress distribution a unified expression. The formula consists of Weibull and Rayleigh probability density functions with weighting factor.

$$p(\Delta S) = \omega \frac{\alpha\beta}{2\sqrt{m_0}} \left(\frac{\Delta S}{2\sqrt{m_0}}\right)^{\beta-1} e^{-\alpha\left(\frac{\Delta S}{2\sqrt{m_0}}\right)^{\beta}} + \frac{(1-\omega)}{2\sqrt{m_0}} \left(\frac{\Delta S}{2\sqrt{m_0}}\right) e^{-\frac{1}{2}\left(\frac{\Delta S}{2\sqrt{m_0}}\right)^2} \tag{3.61}$$

where α and β are the parameters of Weibull distribution, ω is weighting factor, and all are

defined as below:

$$\omega = \frac{1 - \alpha}{1 - \sqrt{\frac{2}{\pi}} \Gamma\left(1 + \frac{1}{\beta}\right) \alpha_1^{-1/\beta}} \tag{3.62}$$

$$\alpha_1 = 8 - 7\alpha \tag{3.63}$$

$$\beta = \begin{cases} 1.1, & \alpha < 0.9 \\ 1.1 + 9(\alpha - 0.9), & \alpha \geq 0.9 \end{cases} \tag{3.64}$$

3.8 Comparison Between Narrow-band and Wide-band Solutions

In this section, three types of FWTs introduced before are deployed to conduct fatigue assessment. 12 locations on the tower base section are examined with both narrow-band solution and wide-band solutions. The axial stresses are estimated by equation (3.1) and axial force and bending moment are obtained through the non-linear aero-hydro-servo-elastic analysis tool, FAST. The spectral density functions of axial stress are achieved by applying FFT method. 6 1-hour simulation sessionsare performed for each sea state to ensure the accuracy of results. The wind turbines are assumed to be located at site No.14 in North Sea where joint probabilities of wind and waves were calculated in Section 3.5. It should be noted that only aligned wind and wave conditions are considered in this study and global X(surge) direction is aligned with the wind and waves which leads to a more conservative fatigue life. Moreover, an additional 60 s is added in the simulation time length since the start-up transient behavior may have impacts on the prediction results of structure response. The time-domain solution based on the simplified lumping approach is assumed to be the reference data. The results of estimated fatigue damage based on various models for three concepts of FWTs have shown in Figures 3.10-3.12.
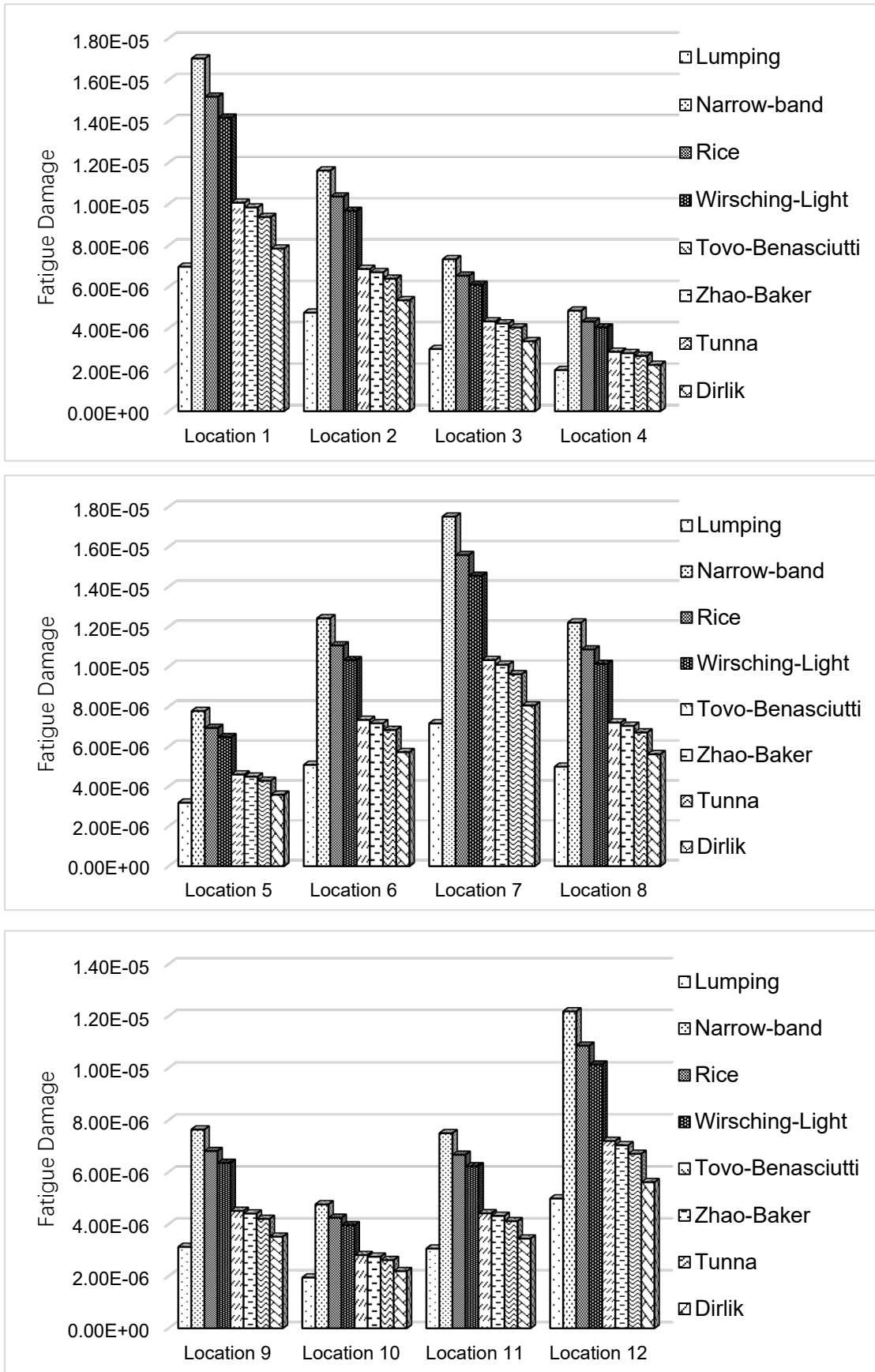
Figure 3.10 Estimated fatigue damage of various wide-band models for spar-type wind turbine
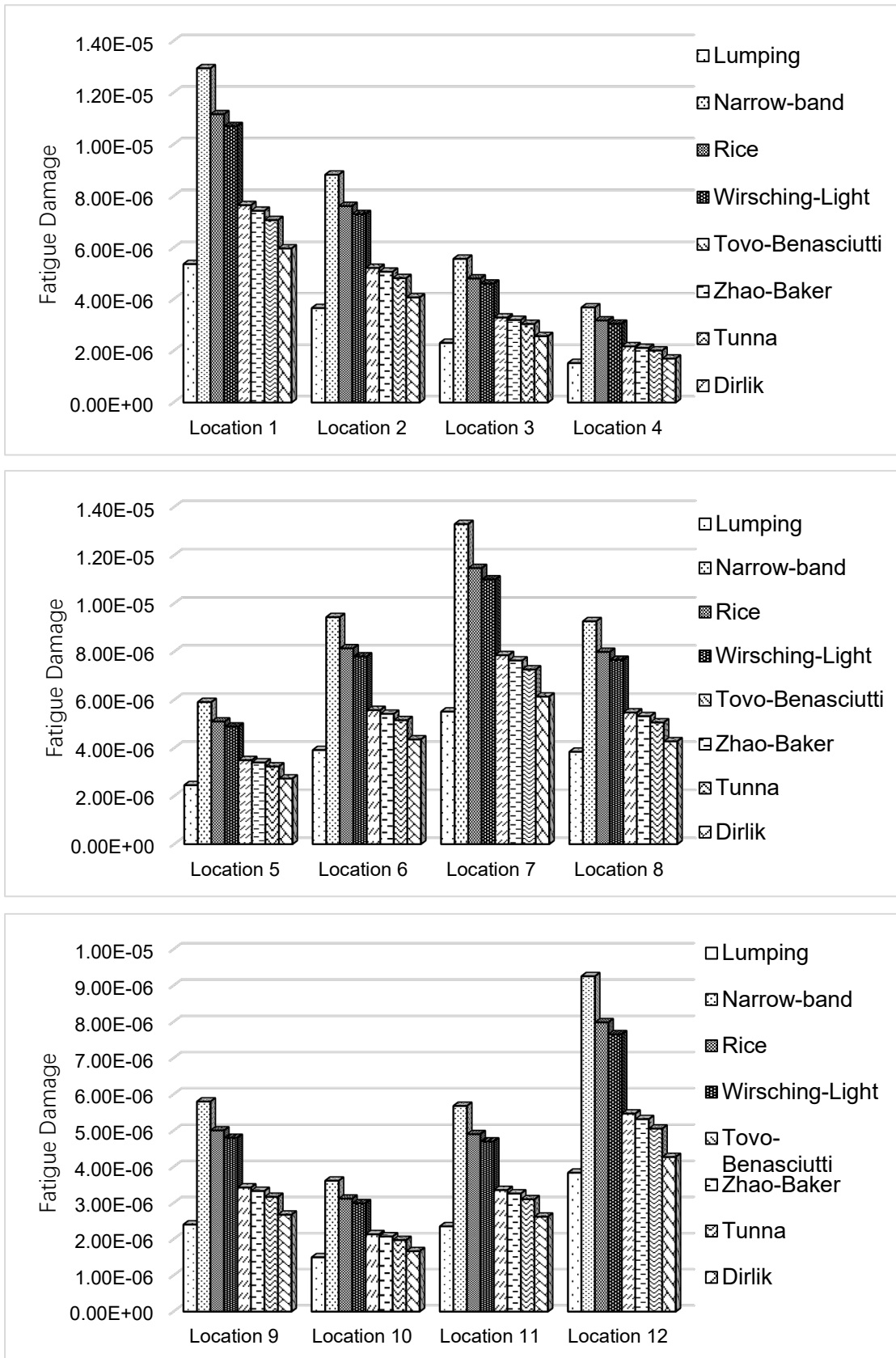
Figure 3.11 Estimated fatigue damage of various wide-band models for tension-leg wind turbine
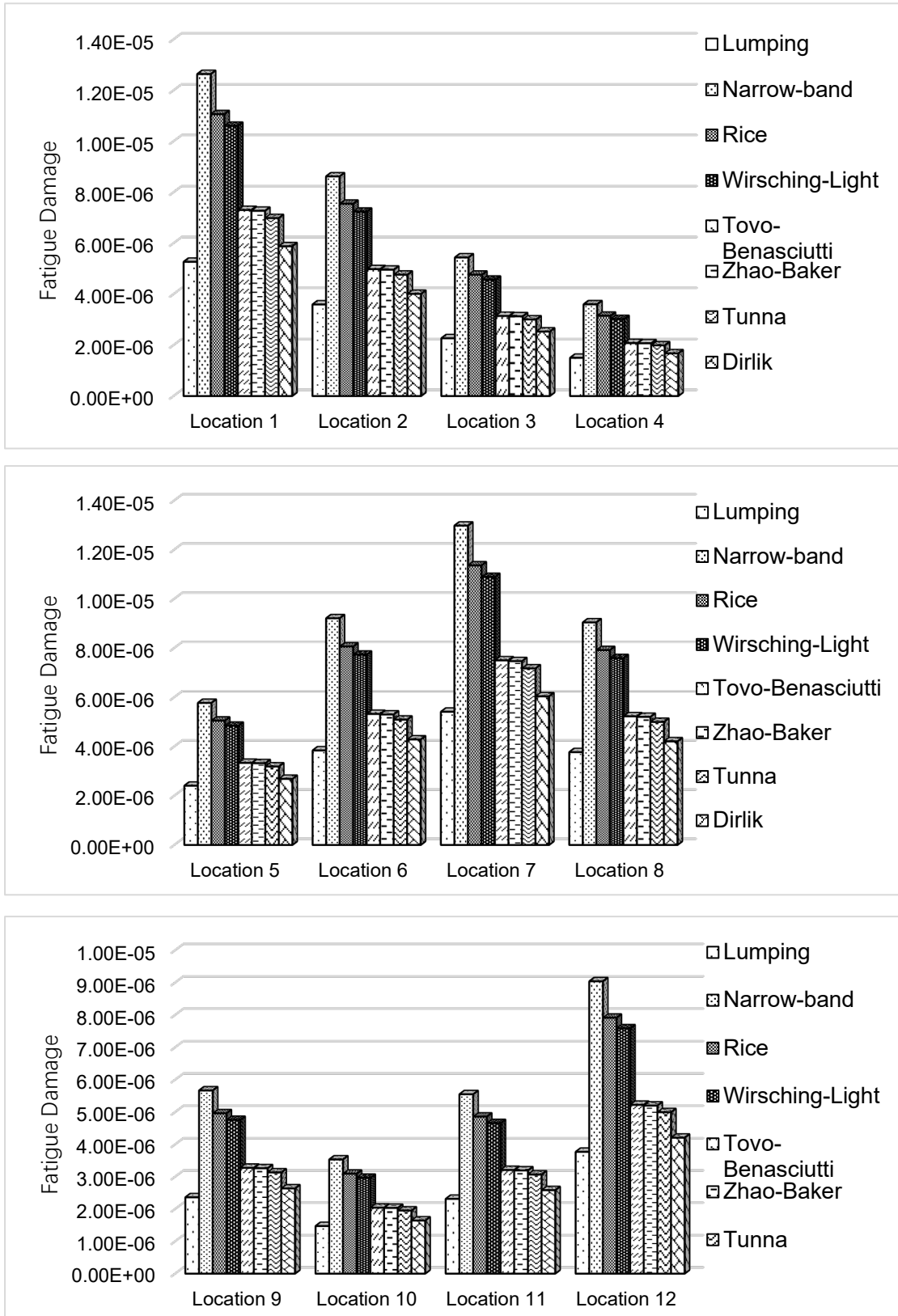
Figure 3.12 Estimated fatigue damage of various wide-band models for semi-submersible wind turbine
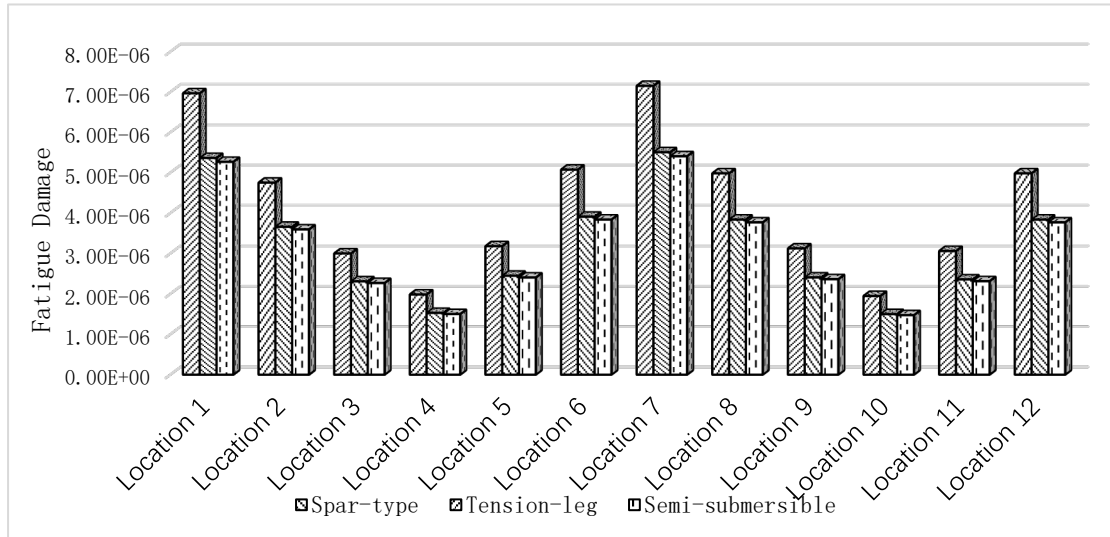
Figure 3.13 Estimated fatigue damage calculated by simplified lumping approach for spar-type, tension-leg and semi-submersible wind turbines

3.8.1 Discussion

The Figures 3.10-3.12 show the comparisons of estimated fatigue damage of various wide-band models for spar-type, tension-leg and semi-submersible wind turbines. For the tower bases, the distributions of fatigue damage have two approximately equal peaks separated by 180 degree, aligned with wind and wave directions for all types of FWTs. Location 1 and Location 7 suffers more severe fatigue damage which indicates that these two locations are critical points while the points in the direction perpendicular to wind and wave (Location 4 and 10) experienced minimum fatigue damage. A narrow-band solution and six wide-band solutions are used to assess fatigue damage compared with simplified lumping approach. These fatigue damage models bring their own multi-variable probability density functions or the correction factors to describe the short-term distributions of stress to improve the accuracy of the narrow-band solution. It can be found:

- The narrow-band solution gives a generally conservative result compared to wide-band solutions.

- The prediction model proposed by Dirlik demonstrates a better estimation in this case since more parameters make the prediction model more flexible. However, the change of these parameters may bring more uncertainties as well.

- Models proposed by Tovo-Benasciutti, Tunna and Zhao-Baker have similar results which are slightly higher than that of the lumping approach.

- The solution proposed by Tunna has only two parameters which makes the model more simplified, though the result is not superior.

Therefore, among the wide-band models, the Tunna solution seems to be the best choice to perform the fatigue damage prediction of FWTs here and this solution overestimates the 'Lumping' fatigue damage estimation by 34.4% while the narrow-band solution compared to 'Lumping' brings a difference about 143.9%.

As seen from Figure 3.13, the spar-type generally suffers the most damage and it is seen to be significantly sensitive to the wave height. This also can be observed from Table 3.7: the largest wave heights cause the most damage for the spar-type wind turbine. The fatigue damage of tension-leg wind turbine is similar to that of semi-submersible wind turbine and approximately 25% less than that of spar-type wind turbine.

3.9 Summary

This chapter presents several fatigue prediction methods to investigate 1-hour short-term fatigue damage of spar-type, tension-leg and semi-submersible FWTs which are assumed to be located in North Sea. A simplified lumping approach has been used with consideration of joint probability of wind and waves based on the traditional wave scatter diagram. The results predicted by this method

are used as references for the comparisons between narrow-band solutions and wide-band solutions.

The narrow-band solution and wide-band solutions are introduced and fatigue assessment is performed to investigate the difference between these solutions. This research can serve as a general basis for the fatigue assessment of FWTs with S-N curves based approaches.

Chapter 4. Fracture Mechanics Based Fatigue Analysis of FWTs

4.1 Introduction

FM based approaches are advanced compared to S-N curves based approaches since the former give the detailed crack growth description (Ziegler and Muskulus, 2016). However, features like model complexity and determination of material constants limit the application of FM based model for the design of offshore structures, thus very few researches based on FM theory have been applied on offshore FWTs. Therefore, this chapter aims to discuss the applicability of the linear elastic FM model to evaluate the fatigue life of offshore FWTs.

Parametric studies of initial crack sizes, critical crack depths, SCFs, mathematical load sequences effect with use of Paris' equation and also the physical load sequence effect are investigated. The stress history of the tower base is obtained from FAST code and then proceeded to Rainflow counting method to get stress ranges and cycles. Then the stress ranges with related cycles are applied in Paris' equation as one cycle of a CA load. Crack growth increments Δa and Δc can be calculated for each stress cycles. Repeat this step for crack height $a + \Delta a$ and continue until the limit to crack growth or the specified design life is reached.

A comparison between fatigue lives predicted by S-N curves and FM based approaches is made. The results show that fatigue lives predicted by S-N curves are longer than those predicted by FM based approaches. It is also found that FWTs are more prone to physical load sequence effect due to the noticeable increases and decreases in mean stress. Therefore, two overload (OL) retardation models are explained and compared based on experimental data. Afterwards, a modified Space-state model is proposed with consideration of threshold intensity factor range and fracture toughness

which has been applied in the fatigue assessment of a spar-type FWT successfully.

4.2 Linear Elastic Fracture Mechanics

As to normal fatigue crack propagation, it can be divided into three stages. The crack starts from 'stage 1', which is usually known as the 'initiation' phase, mainly being 'a short crack', and then continues to 'stage 2', called 'sTable propagation'. Finally, the crack enters into the 'stage 3', 'fast propagation', being 'a long crack' until the structure fails. As mentioned in Chapter 2, linear elastic FM analysis has been widely applied in critical assessment for offshore structures to determine the remaining fatigue life with Paris' law. Thus, it generally reaches a concordance that linear elastic FM can provide a reasonable prediction of crack growth rate for stage 2. The procedure for estimating remaining service life is combined with Paris' law (Paris and Erdogan, 1963), which is expressed as:

$$\frac{da}{dN} = \begin{cases} C(\Delta K)^m & \Delta K > \Delta K_{th} \\ 0 & \Delta K \leq \Delta K_{th} \end{cases} \qquad (4.1)$$

where C is the crack growth rate coefficient and m is material constant, a is crack length, N is number of load cycles, ΔK is the stress intensity factor range in terms of a stress cycle and ΔK_{th} is threshold stress intensity factor range.

The traditional fatigue prediction is performed by S-N curves and the relationship between S-N curves and Paris' law can be established. Paris' law was obtained under CA stress ranges so the equation (4.1) can be expressed as:

$$N\Delta S^m = \int_{a_0}^{a_f} \frac{da}{C(\Delta K)^m} \qquad (4.2)$$

where a_0 is initial crack size and a_f is critical crack size. It can be seen from the equation that the right side is a constant after integration which is same with the parameter A and A_r in

equation(2.1) and (2.2). Thus, the fatigue problem can be solved by linear elastic FM based approaches. However, the linear elastic FM based approaches are only used with CA loadings and as for the VA loadings, it regards each stress range as a one-cycle CA loading. Therefore, it largely ignores the load sequence effects during fatigue assessment.

4.3 Parametric Study

A parametric study to investigate the impact of the variations of initial crack sizes, critical crack depths, stress concentration factors and mathematical load sequences on the fatigue life prediction of the FM analysis is performed. Five different initial crack sizes(crack length and crack depth) ((0.1 mm, 0.1 mm), (0.2 mm, 0.2 mm), (0.3 mm, 0.3 mm), (0.4 mm, 0.4 mm), (0.5 mm, 0.5 mm)) and five different critical crack depths (15% t, 30% t, 45% t, 60% t, 75% t) where t is the thickness of the tower base), five stress concentration factors (2, 2.5, 3, 3.5, 4), three different mathematical load sequences (high to low, low to high, and random process) are selected for this parametric study. Baniotopoulos (2007) pointed out that welds in a wind turbine tower were normally designed as full penetration butt welds of high quality. In this FM analysis, initial surface cracks are assumed to propagate at the surface of full penetration butt welds at the tower base, as shown in Figure 4.1. The related parameters for FM model are listed in Table 4.1.
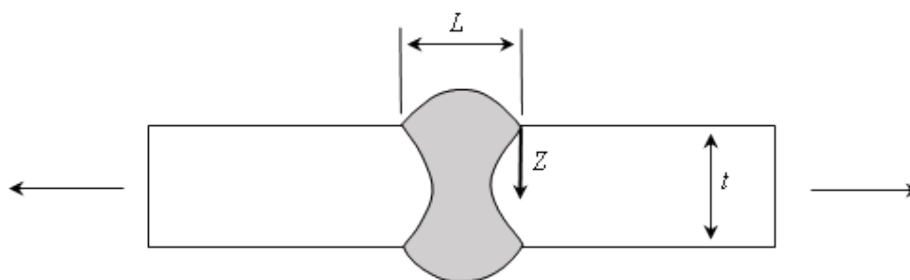
Figure 4.1 Initial surface crack at the surface of full penetration butt welds

Table 4.1 The applied parameters for FM model

Parameter	Value
Initial crack depth a_0	0.39 mm
Initial crack half length c_0	0.39 mm
Critical crack depth a_c	75% t mm
Exponent in flaw growth law m	3.0
Material constant	5.2×10^{-13}
Stress concentration factor (SCF)	2.0

4.3.1 Effect of Initial Crack Size

One problem in the FM based fatigue prediction is to determine initial crack size for crack growth

analysis. A report of initial flaw sizes based on experimental observations was provided by Hudak

et al. (1990), relating to surface flaws present in Inconel 718 weldments. The report shown that: (1)

the initial flaw depth is found to follow a lognormal distribution with a median = 0.0153 in. (≈ 0.39

mm); (2) the predominant flaw shape is semicircular, namely the ratio of the depth over the length

of an initial crack $a_0/2c_0 = 0.5$ where a_0 and c_0 are the initial depth and half-length of crack,

respectively.

The most often used materials in ship and offshore structures are ordinary-strength or higher-

strength structural steels. The mechanism of crack propagation and initiation in such steel

weldments is generally different from that in Inconel weldments. However, Inconel and structural

steels are both metals and the welding procedures for them are usually similar. It is thus expected

that the initial crack sizes of Inconel and steels are similar. Accordingly, as suggested by Chen et al.

(2011), the initial crack sizes observed by Hudak et al. (1990) are used in the present study. In

addition, other studies (Liu and Mahadevan, 2008; DNV, 2014) show the initial crack depth might

be assumed to be from 0.1 mm to 1.0 mm. Fatigue lives of location 1 on the tower base section

calculated on the basis of different initial crack depths are plotted in Figure 4.2(a).

Figure 4.2(a) indicates that estimated fatigue lives drop with the increase of initial crack size

as (0.1 mm, 0.1 mm) are about 19.5% longer than those predicted with initial crack size as (0.5 mm,

0.5 mm) with $\ln(C) = -29.84$. Moreover, fatigue lives decrease quickly with the increase of

$\ln(C)$ as $\ln(C) = -29.84$ are approximately four times longer than $\ln(C) = -28.28$ where the

initial crack size is (0.1 mm, 0.1 mm). It illustrates that the fatigue lives of tower base are generally

sensitive to the assumed initial crack sizes and very sensitive to the material constant C. Ratios of

fatigue lives predicted by the FM and S-N curves based approaches with varying initial crack sizes

are shown in Figure 4.2(b). It again shows that the ratio of fatigue lives calculated by two approaches

decreases slightly with the increase of the initial crack size. In addition, the selection of initial crack

size and $\ln(C)$ have significant impacts on the estimated fatigue lives, which may cause huge

differences in fatigue lives compared to those predicted by S-N-based approaches.
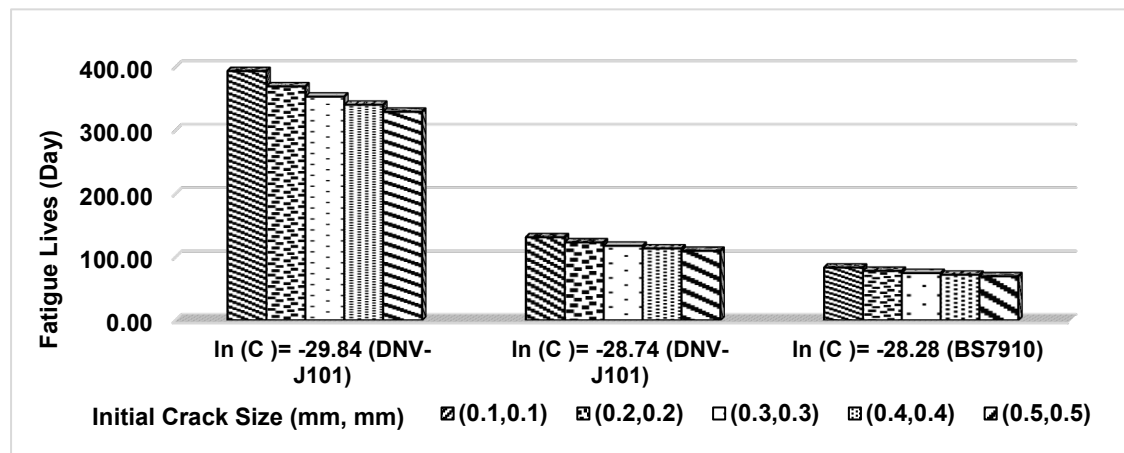
(a)
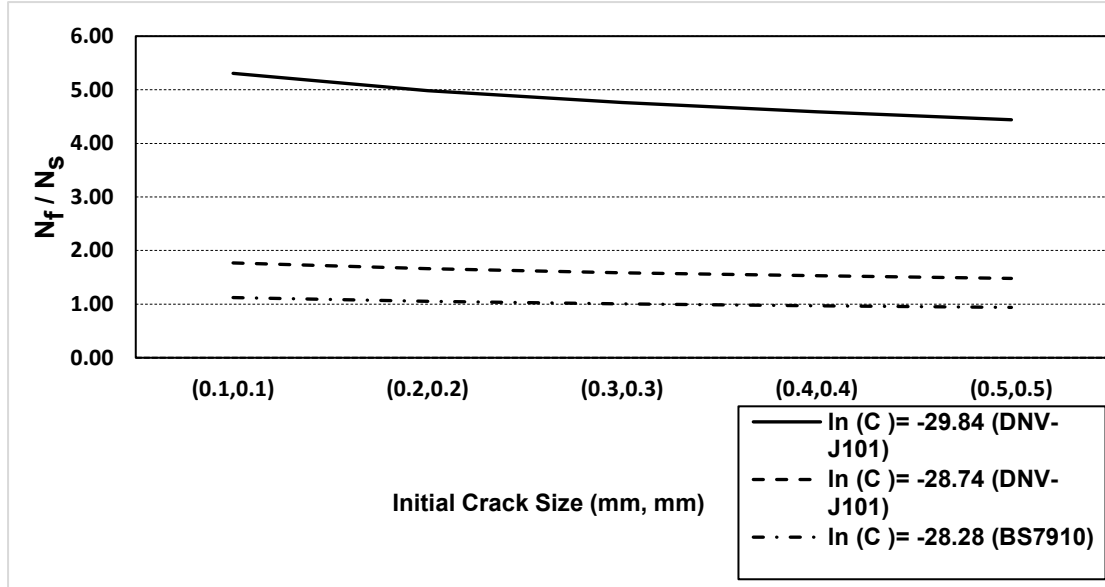
(b)

Figure 4.2 Comparison between S-N curve based approach and FM based approach with different initial crack depth and material constant C at 0 degree of the tower base ($k_t = 2$, critical crack depth = 0.75t): (a) Fatigue lives; (b) Ratios of fatigue lives predicted by the FM based approach to those predicted by S-N curves based approach ($\frac{N_f}{N_s}$)

4.3.2 Effect of Critical Crack Size

Few articles recommended any specific critical crack depth, a_c, of wind turbine tower base. The critical crack size used in previous studies are wall thickness t, $t/2$, or a function of fracture toughness, geometry function and average stress range (Li et al., 2010). Moreover, DnV-GL (2014) recommends through-thickness crack corresponding to the failure criteria of the S-N curve. Thus, a parametric study to investigate the effect of critical crack depths is conducted in this section.

The comparison of fatigue lives predicted based on different critical crack depths are performed and the results are shown in Figure 4.3(a), in which the critical crack depths selected as 15%, 30%, 45%, 60% and 75% of tower thickness are utilized for the parametric study.

Figure 4.3(a) demonstrates that fatigue lives calculated based on the critical crack depth selected as 75% of tower thickness are 18.2% longer than those calculated on the basis of a critical crack depth chosen as 15% of tower thickness with $\ln(C) = -29.84$. It shows the ratio changs very slightly when the critical crack depth is more than 50% of wall thickness from Figure 4.3(b). It also can be seen that when the critical crack depth is selected as 75% of tower thickness and $\ln(C) = -28.28$, similar fatigue lives to those predicted by S-N curves based approach can be achieved. Therefore, it proves that the selection of initial parameters in FM analysis is indeed important. It also indicated that FM analysis is insensitive to the critical crack depth when the depth is more than 50% of tower thickness.

(a)
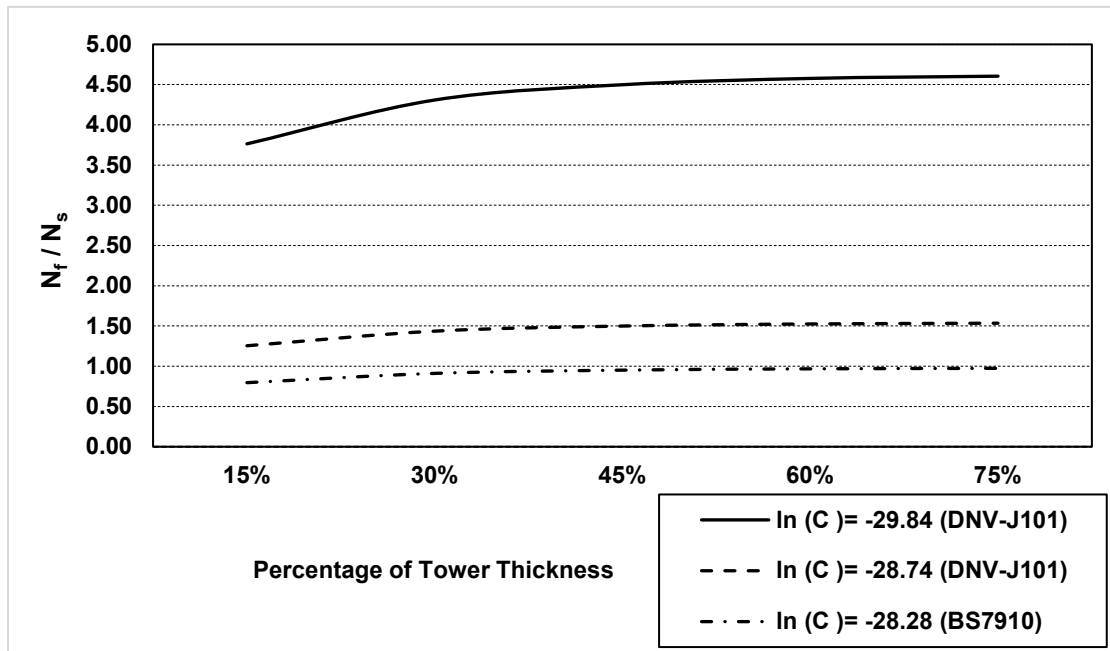
(b)

Figure 4.3 Comparison between S-N curve based approach and FM based approach with different

critical crack depth and material constant C at 0 degree of the tower base ($k_t = 2$, initial crack

depth = 0.39 mm): (a) Fatigue lives; (b) Ratios of fatigue lives predicted by the FM based approach

to those predicted by S-N curves based approach ($\frac{N_f}{N_s}$)

4.3.3 Effect of SCF

The ratio of fatigue life predicted by the FM and S-N curves based approaches under different stress

concentration factors is shown in Figure 4.4. The results show that fatigue lives drop quickly with

the growth of stress concentration factors. Fatigue lives calculated on the basis of a stress

concentration factor at 4 are much shorter than those calculated on the basis of a factor at 2 with

$\ln(C) = -29.84$. As expected, Figure 4.4(b) indicates that the ratio of the fatigue life is changed

significantly with the variation of stress concentration factors and also the $\ln(C)$, which indicates

that the ratio is highly sensitive to the variation of stress concentration factors and $\ln(C)$. It is thus

important to select proper stress concentration factors and C for crack propagation prediction when the FM based approach is used for fatigue life prediction for a FWT. However, it should also be noted that the value of a stress concentration factor at welding often depends on the welding quality.
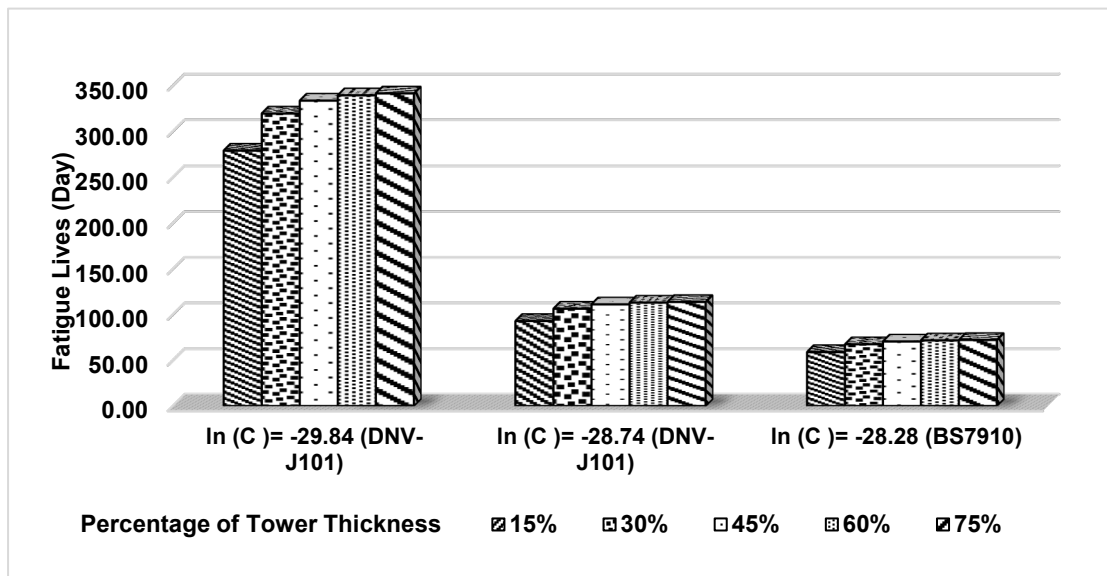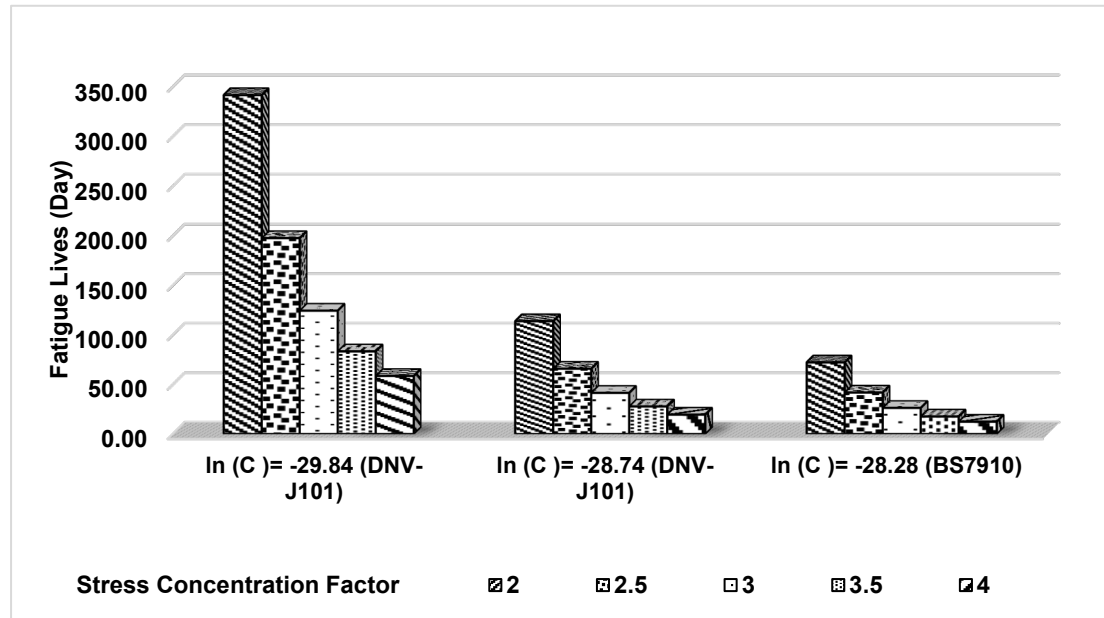

(a)
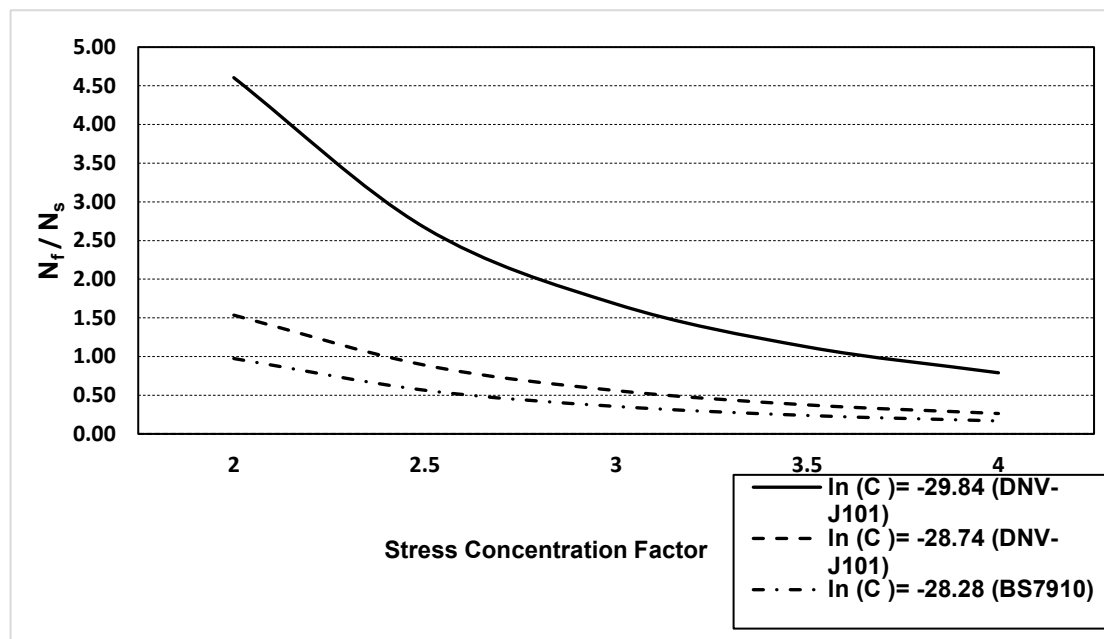
(b)

Figure 4.4 Comparison between S-N curve based approach and FM based approach with different stress concentration factors and material constant C at 0 degree of the tower base (initial crack

depth = 0.39 mm, critical crack depth = 0.75t): (a) Fatigue lives; (b) Ratios of fatigue lives predicted by the FM based approach to those predicted by S-N curves based approach $(\frac{N_f}{N_s})$

4.3.4 Effect of Mathmatical Load Sequence

The mathematical load sequence is discussed from three scenarios: low-to-high, high-to-low and a random sequence.

The comparison of fatigue lives predicted by three load sequence is made in Figure 4.5. It indicates that fatigue lives are shorter when the loads act on the tower base from low to high. When the load sequence is a random one, it has a longer fatigue life than other two load sequence. With the $\ln(C) = -29.84$, fatigue lives predicted from a random sequence are only 8% longer than those fatigue lives predicted by the load sequence from low to high. That may indicate that the impact of mathematical load sequence is negligible in the FM analysis.
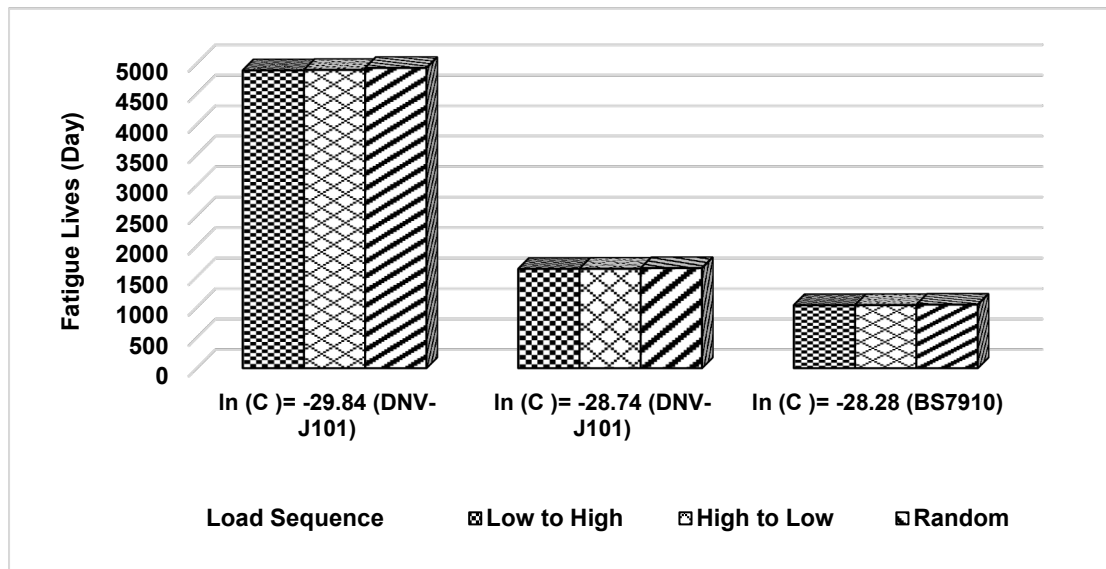
Figure 4.5 Comparison of fatigue lives predicted by different load sequence and material constant C at 90 degree of the tower base (initial crack depth = 0.39 mm, critical crack depth = 0.75t)

However, for offshore FWTs, there are noticeable increases and decreases in mean stress,

which may be exerted by the changing directions of wind and waves and its unique structure. Figure 4.6 shows the comparison of fatigue lives predicted by three mathematical load sequences and physical load sequence. Unlike effects caused by mathematical load sequences, the physical load sequences have more impacts on the FWT fatigue lives. The fatigue lives predicated with physical load sequence effects are about 12% longer than those with mathematical load sequence effects. Thus, it is essential to take UL and OL effects into consideration when performing the fatigue assessment of offshore FWTs.
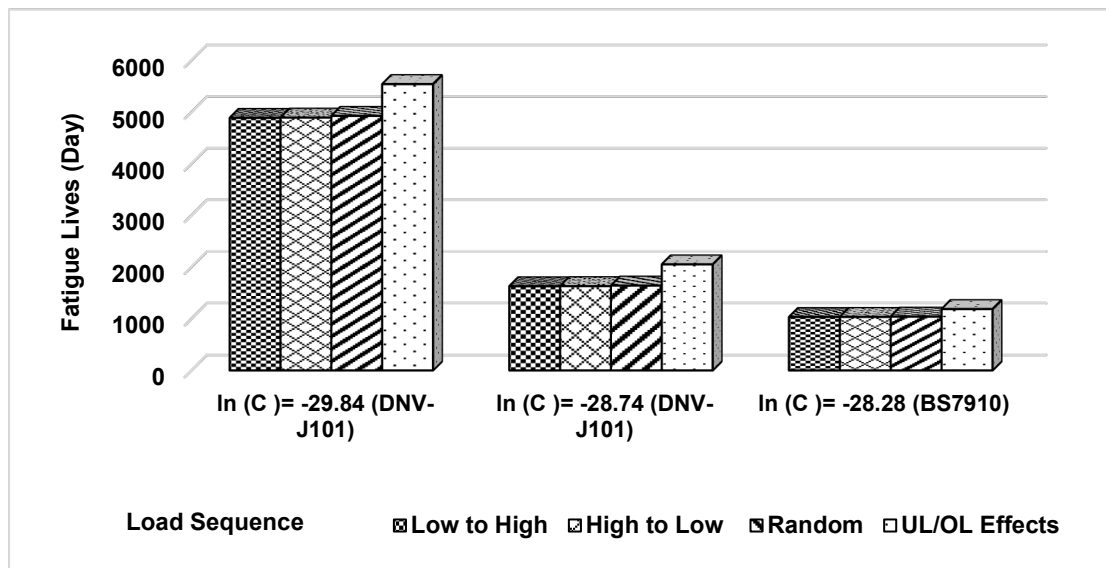
Figure 4.6 Comparison of fatigue lives predicted by three mathematical load sequences and physical load sequence

4.4 Comparison Between S-N Curves and FM Based Fatigue Analysis

12 locations at the tower base section, as shown in Figure 4.7, are selected for the S-N curves and FM based fatigue assessment in this study. The locations are introduced in Section 3.2.4. The maximum stress occurs around the Locations 1 (0 degree) and 7 (180 degree), which indicates that these locations are two critical points of the FWTs for fatigue assessment. In FM analysis, a semi-

elliptical shape surface crack with initial sizes of (0.39 mm, 0.39 mm) is assumed to propagate at the welding seam at the tower base. The critical crack depth is set as 75% of the tower thickness. The material constants are 1.46×10^{12} and 3, respectively. The equation 4.1 is used to perform FM analysis without considering other factors.

Fatigue lives of 12 locations at the tower base predicted by the FM approach and the S-N curves based approach are plotted in Figure 4.7. Figure 4.7 shows that fatigue lives predicted by S-N curves based approach and FM based approach are quite different. The fatigue lives based on S-N cures are much longer than those calculated by FM based approach, which indicates that FM based approach provides significantly conservative fatigue life prediction for the tower base.

However, fatigue lives become longer when FM based approach considers the load sequence effects. It indicates that load sequence has a non-negligible impact in the fatigue assessment of FWTs. In other words, S-N curves based approaches can be applied in the design phase of FTWs with consideration of SCFs. But it is not reliable for the reassessment after some years in operation e.g. due to corrosion effect, change of geometry or variation of material constant. FM based approach with Paris' equation gives the details of crack propagation but does not take load sequence effect into account which results in a more conservative fatigue life. Thus, the fatigue analysis using FM based approaches with consideration of load sequence effects is essential.
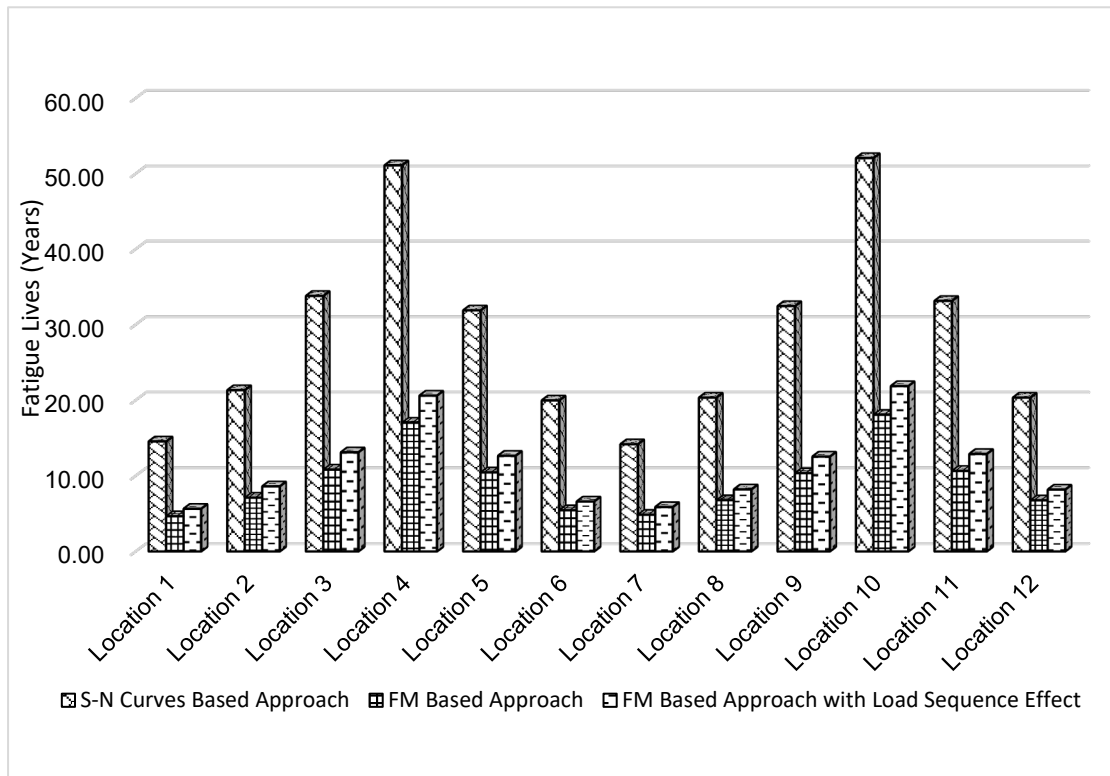
Figure 4.7 Fatigue lives of 12 points around tower base section predicted by FM based approach and the S-N curves based approach

4.5 Description of Two OL Retardation Models

There are two effects of the load sequence on the crack growth rate. One is mathematical effect which is discussed in Section 4.4 in three scenarios: low-to-high, high-to-low and a random sequence. However, the results show limited effect on the estimated fatigue lives. Another one is physical effect, as OLs cause retardation and ULs cause acceleration. But the accelerating effect is generally smaller than the retardation, thus only retardation effect is considered in this section. Three retardation concepts are already illustrated in Chapter 2; however, most researchers believe that the first and second concepts are more reasonable. In the reminder of this thesis, more efforts are focused on these two concepts.

4.5.1 Plastic Zone Ahead of Crack (Space-state Model)

Ray and Patankar (2001) developed a code based on the concept of crack closure in the wake of the crack. The crack opening stress S^o is a function of the current cycle, which is representing the stress history that affects the crack growth rate in the current cycle. The maximum stress S_k^{max} and minimum stress S_k^{min} are the inputs for kth cycle, and preceded by minimum stress S_{k-1}^{min}, to determine the range of effective stress intensity factor, ΔK_{eff}^k.

$$\Delta K_{eff}^k = \sqrt{\pi a_{k-1}} F(a_{k-1}, \omega) \left(S_k^{max} - max(S_k^{min}, S_{k-1}^o) U(S_k^{max} - S_{k-1}^o) \right) \tag{4.3}$$

where a_{k-1} and S_{k-1}^o are the crack size and crack opening stress for $k-1$ cycle, respectively. F is a crack-length-dependent correction factor compensating for finite geometry of the specimen with the width parameter ω. $U(x)$ is the Heaviside unit step function equals to 0 if $x < 0$ or 1 for $x \geq 0$.

Before generating the equation of crack opening stress for VA loads, a function was derived for steady-state crack opening stress S_k^{oss} under different levels of CA loads from the empirical relation (Newman, 1984) that is valid for non-zero peak stress:

$$S_k^{oss} = (A_k^0 + A_k^1 R_k + A_k^1 (R_k)^2 + A_k^3 (R_k)^3) S_k^{max} \tag{4.4}$$

where

$$R_k = \frac{S_k^{min}}{S_k^{max}} U(S_k^{max}), \quad k \geq 0 \tag{4.5}$$

$$A_k^0 = (0.825 - 0.34\alpha_k + 0.05(\alpha_k)^2) \left[cos \left(\frac{\pi}{2} \frac{S_k^{max}}{S^{flow}} \right) F(a_{k-1}, \omega) \right]^{\frac{1}{\alpha_k}} \tag{4.6}$$

$$A_k^1 = (0.415 - 0.071\alpha_k) \left(\frac{S_k^{max}}{S^{flow}} \right) F(a_{k-1}, \omega) \tag{4.7}$$

$$A_k^2 = (1 - A_k^0 - A_k^1 - A_k^3) U(R_k) \tag{4.8}$$

$$A_k^3 = (2A_k^0 + A_k^1 - 1) U(R_k) \tag{4.9}$$

The constraint factor α_k is obtained from crack length increment and S^{flow} is calculated by ultimate tensile strength and yield stress. Then the opening stress in the kth cycle, S_{op}^k, is determined using semi-empirical relationship based on the plastic zone in the wake of the crack:

$$S_{op}^k = \left(\frac{1}{1+\eta}\right)S_{k-1}^o + \left(\frac{1}{1+\eta}\right)S_k^{oss} + \left(\frac{1}{1+\eta}\right)(S_k^{oss} - S_{k-1}^o)U(S_k^{oss} - S_{k-1}^o) + \left(\frac{1}{1+\eta}\right)\left(S_k^{oss} - \right.$$

$$\left. S_k^{oss\_old}\right)U\left(S_{k-1}^{min} - S_k^{min}\right)[1 - U(S_k^{oss} - S_{k-1}^o)] \tag{4.10}$$

for center crack with finite width

$$\eta = \frac{tS_y}{2\omega EP} \tag{4.11}$$

where E is the modulus of elasticity, t is the thickness of specimen. It should be pointed out that a precise relationship of η is unknown due to lack of adequate experiment data. So η could be estimated through a single OL test and can be applied to the specimen made of the same material.

4.5.2 Plastic Zone at Crack Flanks (Generalized Willenborg Model)

Willenborg et al. (1971) proposed a crack growth model based on the concept of a plastic zone in front of crack tip. The OL causes the residual compressive stress, which decreases the effective stress range of the crack until the subsequent crack extension and the second plastic zone has passed the primary plastic zone. However, it cannot capture the acceleration effect due to UL. This model is widely applied because of its simplicity despite of the inherent shortcomings. The effective stress intensity factor of kth cycle is calculated by

$$\Delta K_{eff}^k = \left(K_{max}^k - K_{min}^k\right)U^k \tag{4.12}$$

In this case, U^k is evaluated for CA loading using

$$U^k = \frac{1-f}{1-R_f} \tag{4.13}$$

The crack opening ratio, f, is defined as:

$$f = \frac{S_{op}}{S_{max}} = \begin{cases} max(R_k, A_k^0 + A_k^1 R_k + A_k^1 (R_k)^2 + A_k^3 (R_k)^3) & R_k \geq 0 \\ A_k^0 + A_k^1 R_k & -2 \leq R_k < 0 \end{cases} \tag{4.14}$$

The stress ratio, R_f, can be calculated by

$$R_f = \frac{K_{min}^k - K_r^k}{K_{max}^k - K_r^k} \tag{4.15}$$

$$K_r^k = \emptyset \left(\sqrt{\frac{y_p^k - a^k}{2r_y^k}} - 1 \right) H(y_p^k - y^k) \tag{4.16}$$

$$y_p^k = max(y^1, y^2 \dots y^{k-1}) \tag{4.17}$$

$$y^x = a^x + 2r_y^x \tag{4.18}$$

$$r_y^x = \frac{\varphi}{2\pi} \left(\frac{K_{max}^x}{S_y} \right)^2 \tag{4.19}$$

where S_y is yield stress for the material, y is the distance between the specimen surface and the theoretical extent of the plastic zone, y_p is the maximum value of y of all previous stress cycles, $\emptyset$ is the factor considering crack arrest by Gallagher(1974), $2r_y$ is the plastic zone size and φ depends on stress condition.

4.5.3 Validation and Comparison of Models
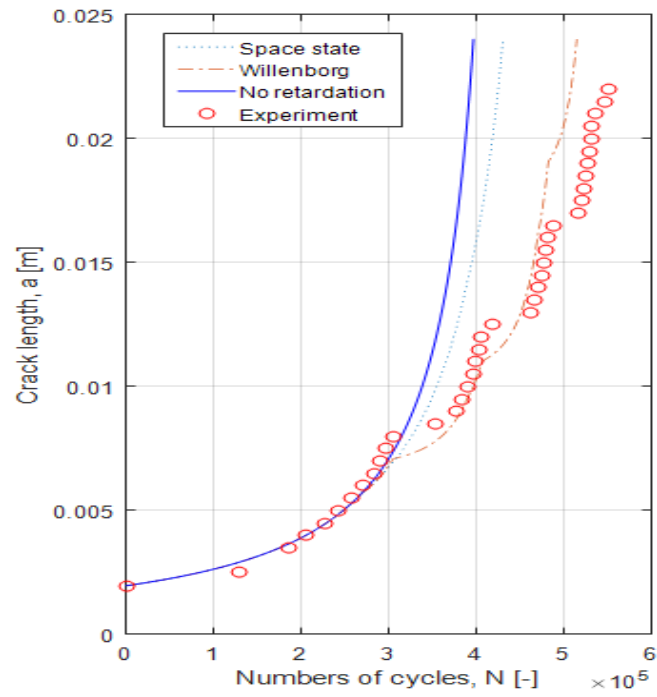
(a)
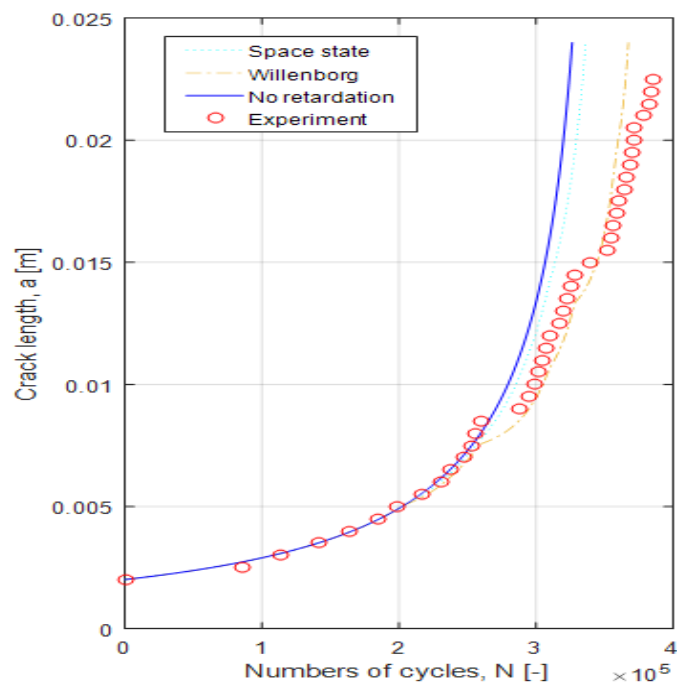
(b)

Figure 4.8 Crack length with numbers of cycles for experiments and simulations of two specimens

(a)SR4 (b) AW9
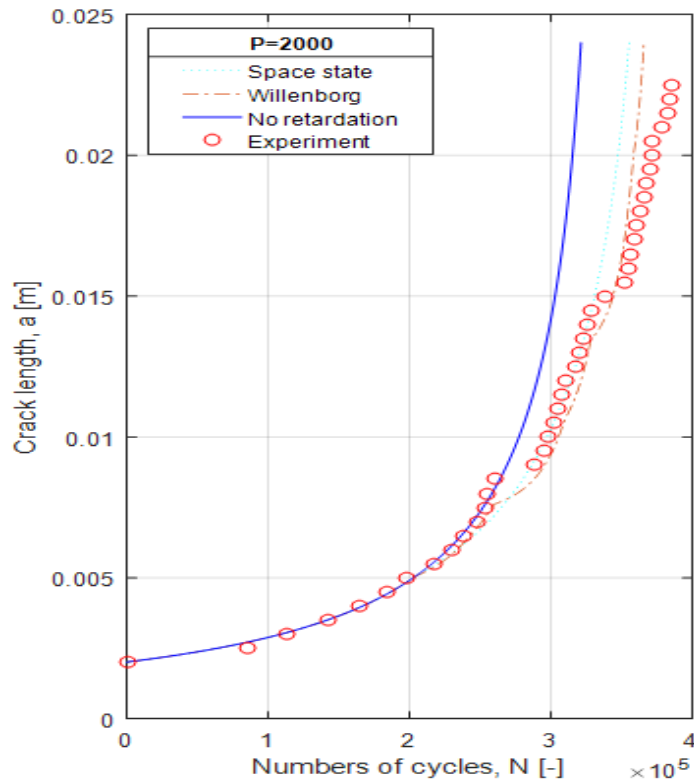
Figure 4.9 Crack length with numbers of cycles for Space-state model (P=2000) of specimen AW9

Maljaars et al. (2015) conducted some experiments to examine OLs' retardation impacts on a C-Mn steel specimen with various types of OLs and different stress ratio. In this thesis, the raw data for specimen number SR4 and AW9 with different initial crack lengths, 1.95 mm and 2.01 mm, are provided by the author and used in the model validation and comparison. Table 4.2 provides the chemical composition and the mechanical properties of the specimen are provided in Table 4.3.

Table 4.2 Chemical properties of specimen (weight%)

C	Si	Mn	Ni	P	S	N
0.065	0.28	1.46	0.23	0.012	0.0006	0.003

Cu	Mo	Cr	V	Nb	Ti	B	Al
0.16	0.038	0.044	0.001	0.02	0.002	0.0002	0.039

Table 4.3 Mechanical properties of specimen

S_u (MPa)	S_y (MPa)	w (mm)	t (mm)
508	391	70.4	35.0

Three types of OLs are provided in Table 4.4. and the applications of OLs at number of cycles are given in Table 4.5.

Table 4.4 Three types of OLs

OL	S_{min}	S_{max}	S_{OL}	ΔS_{OL}	R
	(MPa)	(MPa)	(MPa)	(MPa)	(-)
1	67	220	290	223	0.23
2	67	220	334	267	0.20
3	67	220	372	305	0.18

Table 4.5 OL applied at the number of cycles

Specimen	OL type (Number of cycles)				
SR4	1(269415)	3(304883)	1(389149)	3(406275)	1(469853)
	3(481960)	1(522718)	3(530567)	1(550820)	
AW9	1(204706)	2(259845)	1(310060)	2(328208)	1(358599)
	2(371645)				
AW5	1(263882)	1(305241)	3(320976)	1(376532)	3(390426)
	1(426289)	3(443671)	1(482332)	3(490675)	

Figure 4.8 gives the comparisons between Space-state model and Generalized Willenborg model and also compares with the sTable crack growth that predicted by Paris' Law for specimens of SR4

and AW9. Some conclusions can be obtained from these simulations:

- Paris' Law gives a good prediction when only constant loads apply on the specimen.

- Both Space-state model and Generalized Willenborg model could capture the OL retardation phenomenon.

- Huge retardation effects are observed from experiments data and crack length predicted by Paris' Law significantly fail to show this phenomenon.

- Specimen AW9 indicates a more significant retardation effect due to the larger OLs.

- Generalized Willenborg models provide more accurate predictions than Space-state models for these two specimens, and Space-state models underestimate the retardation effects for the specimens.

The reason for the mismatch could be the decay rate factor, η, in equation (4.11). The decay rate factor has been investigated by some researchers (Porter, 1972; Ray and Patankar, 2001). The ratio $\frac{t}{\omega P}$ in the decay rate factor is 0.013 for Porter's experiments, and 0.025, 0.1 and 0.5 for Malijaars' experiments (Malijaars et al., 2015), respectively. Figure 4.9 illustrates the example of artificial modification of P value for specimen AW9. It can be seen that the Space-state model achieves a more accurate result than that without modification. However, this value is highly dependent on different materials and geometries and single OL test can determine this value.

4.6 Parametric Study of Paramters Affecting Retardation

A parametric study to investigate the retardation impact of the variations of stress ratios with/without same stress ranges and OL ratios on the fatigue life prediction with the Space-state model, Generalized Willenborg model and no retardation model is performed. Four different stress ratios

(0.1, 0.3, 0.5, 0.7) with same stress range (50MPa) and with different stress ranges (90MPa, 70MPa, 50MPa, 30MPa), two different OL ratios (2, 2.5) with different stress ranges (50MPa, 40MPa) are selected for this parametric study. Only one OL is applied for each simulation.

4.6.1 Stress Ratio with Same Stress Range

Numbers of cycles to failure with various stress ratios

	0.1	0.3	0.5	0.7
☐ No retardation	431018	257234	176697	131265
⊠ Space state	437102	263385	183636	134832
⊡ Willenborg	717479	305258	195788	138866

Stress ratio, R [-]

(a)
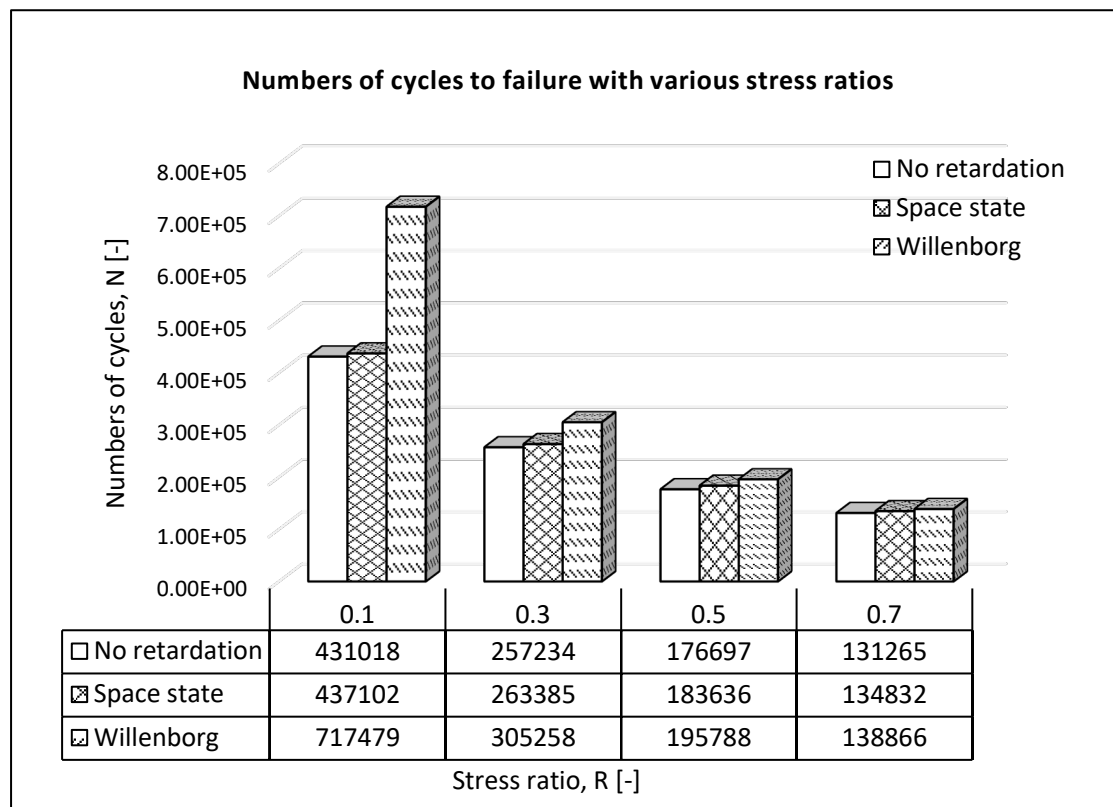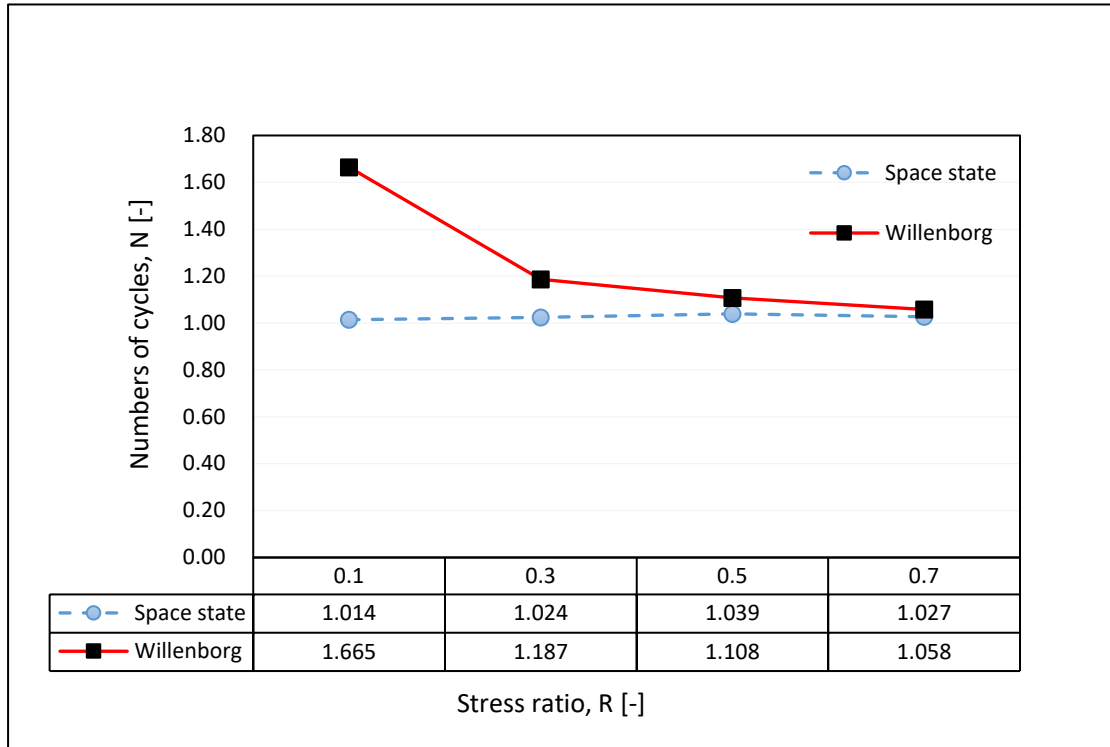
Figure 4.10 Comparison between Space-state model, Generalized Willenborg model and no retardation model with various stress ratios (stress range =50MPa, OL ratio=2): (a) Numbers of cycles to failure; (b) Ratios of cycles to failure predicted by Space-state model to those predicted by Generalized Willenborg model compared with no retardation model

The comparison between Space-state model, Generalized Willenborg model and no retardation model with various stress ratios and same stress range is shown in Figure 4.9. In Figure 4.9(a), the results show the cycles to failure predicted by Generalized Willenborg model drop quickly from 717,479 to 138,866 with the increase of stress ratios from 0.1 to 0.7 while the cycles to failure predicted by Space-state model are from 437,102 to 134,832, slightly higher than those predicted by no retardation model. Therefore, a conclusion can be reached that the retardation effect decreases with an increase of stress ratio. The cycles to failure predicted by Generalized Willenborg model

has a significant difference from other two models at R=0.1 and R=0.3, approximately 1.66 and

1.18 times longer than the no retardation model, respectively. The cycles to failure predicted by

Space-state model is slightly higher than those predicted by no retardation model and the range of

difference is from 1.4% to 3.9%. Figure 4.9(b) illustrates that a downward trend of ratios of cycles

to failure comparing with no retardation model becomes mild when the stress ratio is more than 0.3.

It also shows that the change of ratios predicted by Space-state model is negligible. Thus, it can be

summarized that compared with Space-state model with the same stress range the Generalized

Willenborg model is more sensitive to the change of stress ratio.

4.6.2 Stress Ratio with Different Stress Range

Numbers of cycles to failure with various stress ratio (different stress ranges)

	0.1	0.3	0.5	0.7
☐ No retardation	48824	74246	176695	905279
☒ Space state	55458	81393	183635	912460
☐ Willenborg	85930	95360	195788	932392

Stress ratio, R [-]

(a)

	0.1	0.3	0.5	0.7
Space state	1.136	1.096	1.039	1.008
Willenborg	1.760	1.284	1.108	1.030
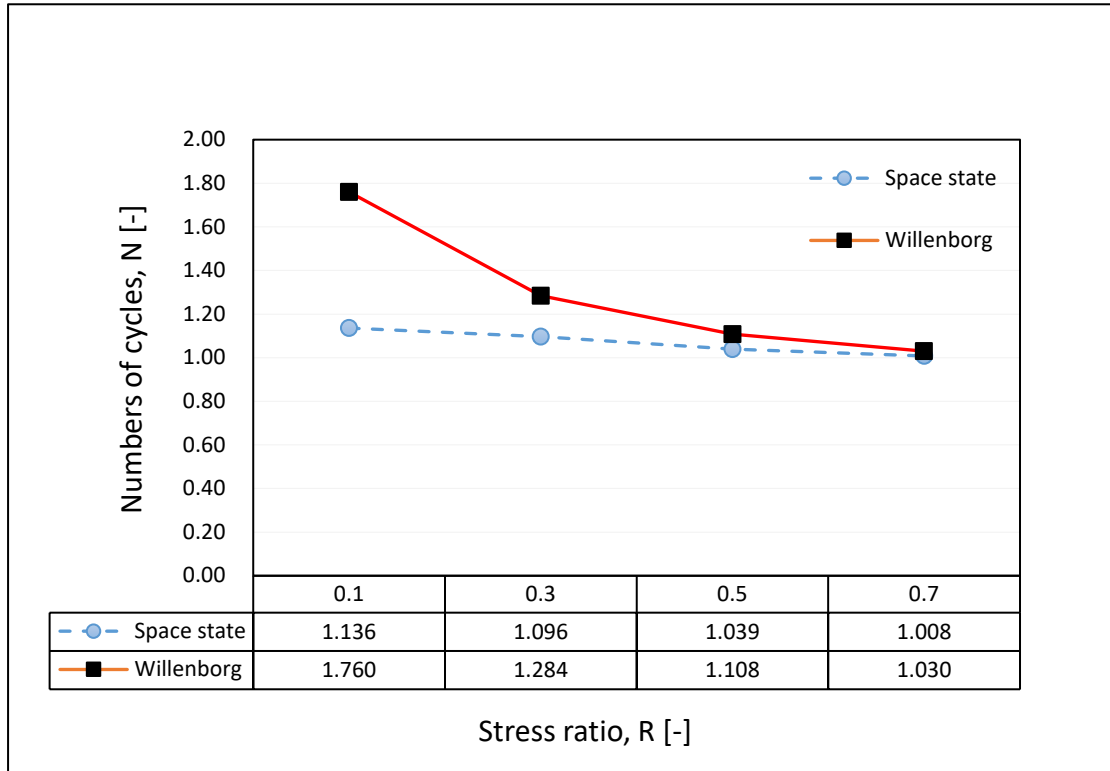
Stress ratio, R [-]

(b)

Figure 4.11 Comparison between Space-state model, Generalized Willenborg model and no retardation model with various stress ratios (stress range =90MPa, 70MPa, 50MPa, 30MPa, OL ratio=2): (a) Numbers of cycles to failure; (b) Ratios of cycles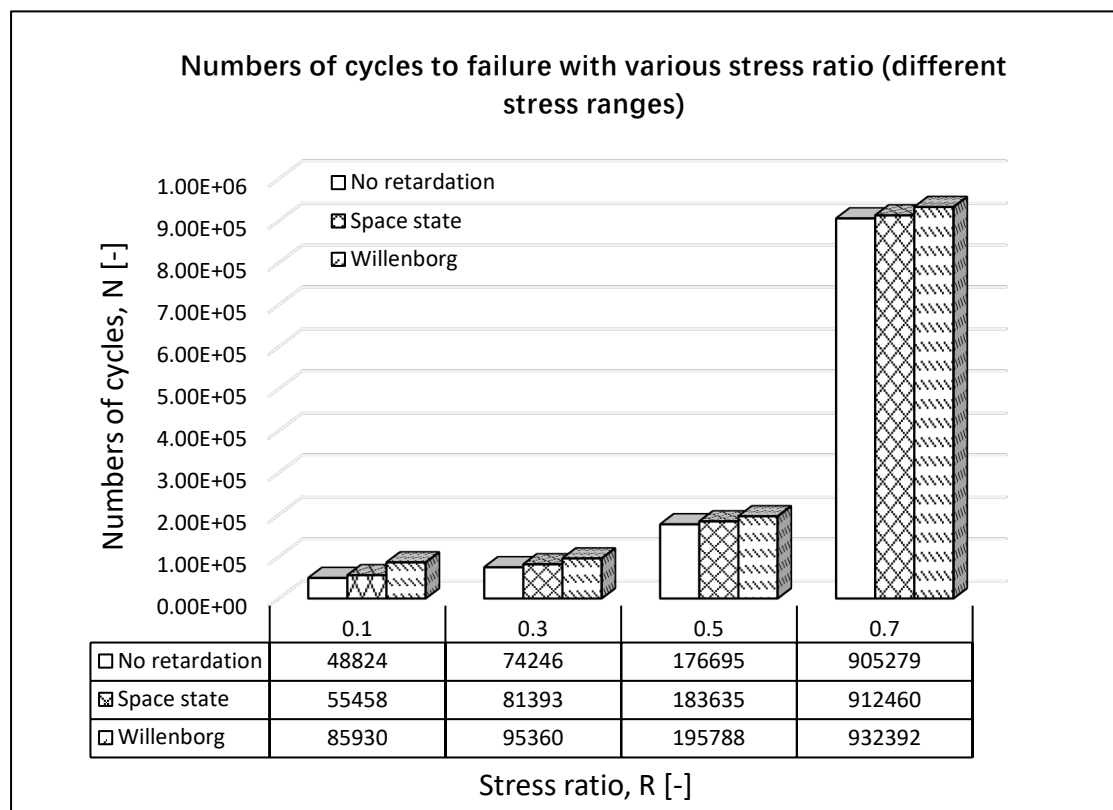 to failure predicted by Space-state model to those predicted by Generalized Willenborg model comparing with no retardation model

The comparison between Space-state model, Generalized Willenborg model and no retardation model with various stress ratios and different stress ranges (90MPa, 70MPa, 50MPa and 30MPa) is shown in Figure 4.10. The Figure 4.10(a) shows a general upward trend in the change of stress ratios and it is can be found that the cycles to failure predicted by all the models increase dramatically with the change of stress ratios from 0.1 to 0.7. Apparent from Figure4.10(a), there is a considerable increase from R=0.5 to R=0.7 and the cycles to failure predicted by Generalized Willenborg model reach a peak of 932,392 when the stress ratio R equals to 0.7. Similar trends have been achieved for

Space-state model and no retardation model. It is opposite to what is suggested in Section 4.6.1. The main reason is that the stress ranges have a gradual decline from 90 MPa to 30 MPa rather than being a fixed value. Figure 4.10(b) indicates that there is a big discrepancy of 76% and 55% when stress ratio equals to 0.1 and stress range equals to 90MPa compared to Space-state model and no retardation model. Moreover, the ratios predicted at R=0.7 are approximately the same with all three models. Therefore, according to Figure 4.10, it may be summarized that the stress range has a huge impact on the prediction of fatigue lives and especially for those predicted by Generalized Willenborg model at a lower stress ratio. Again, it reveals Generalized Willenborg model is highly sensitive to the change of stress ratio since there is a significant drop from 1.76 to 1.03. Meanwhile, it shows Space-state model is generally sensitive to the variation of stress ratio.

4.6.3 OL Ratio

Numbers of cycles to failure with various overload ratios (same stress ratios, differen stress ranges)

	2	2.5	2	2.5
☐ No retardation	176695	176349	406266	405917
☒ Space state	183635	184910	412667	414785
☒ Willenborg	195788	389328	436395	805368

Overload ratio, OLR [-]
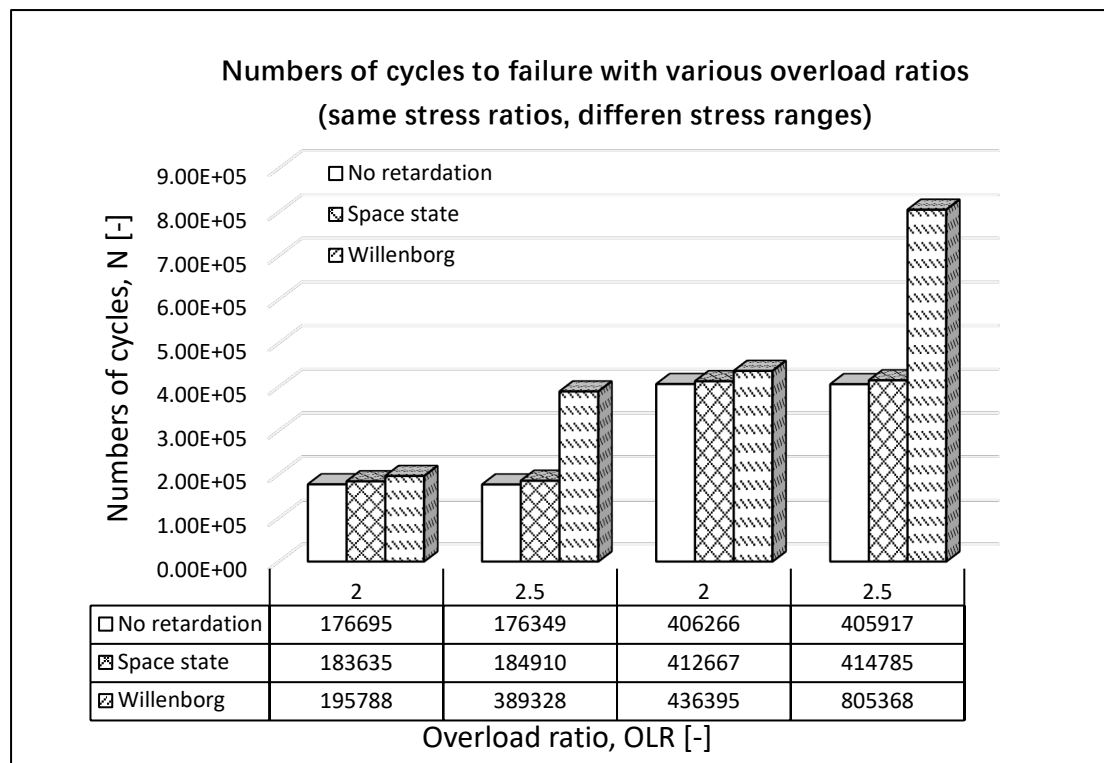
Figure 4.12 Numbers of cycles to failure predicted by Space-state model, Generalized Willenborg

model and no retardation model with various OL ratios (stress range = 50MPa and 40MPa, stress

ratio=0.5)

Figure 4.11 shows the OL ratios affecting the numbers of cycles to failure predicted by Space-state

model, Generalized Willenborg model and no retardation model with stress ranges of 50MPa and

40MPa. It is again found that the stress range has a huge impact on the prediction of fatigue lives.

The numbers of cycles to failure extend from 195788 to 436395 with stress range reduced from

50MPa to 40MPa at OL ratio of 2 predicted by Generalized Willenborg model while the numbers

of cycles to failure predicted by Space-state model increase from 183635 to 412667. Similar

tendency is seen from no retardation model. When the OL ratio rises from 2 to 2.5, obvious growth

of the numbers of cycles to failure has been observed for both Space-state model and Generalized

Willenborg model. The Figure also indicates that there is no significant difference from the numbers

of cycles to failure predicted by all models at a low OL ratio. However, in contrast, dramatic

difference is observed when the OL ratio is in a high range. The number of cycles to failure predicted

by Generalized Willenborg model (OL ratio=2, stress range =50MPa) is 6.6% and 10.8% longer

than Space-state model and no retardation model, respectively. When the OL ratio reaches to 2.5,

the difference of the cycles to failure increases to 111% and 121%, respectively. Moreover, this

difference also becomes larger with the increase of the stress range since only 98.4% and 94.2% at

stress range of 40MPa have been used. In summary, the results suggest that Generalized Willenborg

model is strongly sensitive to the variation of OL ratio, especially in high stress ranges.

4.6.4 Summary

The retardation effect of the variations of stress ratios with/without same stress ranges and OL ratios on the fatigue life prediction with Space-state model, Generalized Willenborg model and no retardation model is investigated. The results show that:

- The retardation effect decreases with the increase of stress ratio at the same stress range. However, it is highly dependent on the variations of the stress range when the stress range is different.

- Space-state model and Generalized Willenborg model demonstrate the different results on the numbers of cycles to failure caused by OLs. All Figures indicate that both models provide the longer fatigue lives than those predicted by no retardation model. Moreover, Generalized Willenborg model provides longer fatigue lives than those predicted by Space-state model.

- The OL ratio is the key influencing factor for the retardation effect which is subject to the OL. It can be concluded that compared with Space-state model Generalized Willenborg model is more sensitive to the variation of the OL ratio and stress ratio.

4.7 Modified Space-state Model

The concept of crack closure has been widely investigated and many empirical models can be found in many literatures (Iwasaki, 1982; Kurihara et al., 1987; Booth and Maddox, 1988; Ding et al., 2017). The stress ratio, R, is usually the dominated parameter in the prediction. With crack closure model, researchersproposed an effective stress intensity factor range, ΔK, which is related to the contact of crack flanks behind crack tip. This phenomenon has been used to explain not only the mean stress effect in both regimes 1 and 2 of crack propagation, but also the transient crack growth

behavior following OLs, the growth rate of short cracks and effect of thickness (Antunes et al., 2015).

However, Antunes et al., (2015) indicate a significant impact of ΔK and K_{max}. The results were in line with the experimental data. Therefore, researchers realized that a single parameter, R, is not enough for a proper modeling of crack closure concept. Since crack closure is greatly dependent on ΔK and K_{max}, it seems the model based on threshold stress intensity factor range ΔK_{th} and fracture toughness K_{IC} may be a more physically based than being a R-based model. Thus, a modified model is proposed based on Space-state model.

The below equation recommended by BS7910(2013) is adopted herein as the basic formulation for establishing the crack growth rate model under fatigue.

$$\frac{da}{dN} = A\left(\Delta K_{eff}\right)^m \tag{4.20}$$

$$\Delta K_{eff} = \frac{\Delta K - \Delta K_{th}}{1 - R} \tag{4.21}$$

where R is the stress ratio and ΔK_{th} is the threshold stress intensity factor range. This formula can replace can replace equation (4.3) in Space-state model.

Based on the equation proposed by Davenport and Brook(1979), the threshold stress intensity factor range is given by:

$$\Delta K_{th} = \Delta K_0 \left(\frac{(K_{IC} - K_{max})(1 - R)}{K_{IC} - \Delta K_0}\right)^{\frac{1}{3}} \tag{4.22}$$

where ΔK_0 stands for the threshold value at R=0 and K_{max} is the maximum of stress intensity factor. ΔK_0 can be expressed based on the Vosikovsky(1978) in general form:

$$\Delta K_{th} = \Delta K_0 - BR \tag{4.23}$$

where B is a material constant and ΔK_0 is usually obtained from experimental data.

When the maximum stress intensity factor in a cycle, K_{max}, approaches the critical level for failure under static load, K_{IC}, the crack enters the period of unstable propagation. K_{IC} is normally based on the experimental measurement, and it can be expressed in any one of equations below:

$$K_{IC} = \left(\frac{J_{IN}E}{1 - \gamma^2}\right)^{\frac{1}{2}} \qquad (4.24)$$

or

$$CTOD = \frac{4}{\pi}\frac{K_{IC}^2}{E\sigma_{ys}} \qquad (4.25)$$

where E and γ are the Young's Modulus and Poisson's ratio of material, respectively.

This proposed model takes the threshold stress intensity factor range ΔK_{th} and fracture toughness K_{IC} into consideration when calculating the opening stress intensity factor through Space-state model.

Figure 4.13 shows the comparison between Space-state model and other models to predict numbers of cycles of specimen AW9 and AW5. The results indicate that modified Space-state model provides a more accurate prediction than those predicted by Space-state model, even though Space-state model has artificially modified P value. However, modified Space-state model still underestimates the retardation effect of OLs. The Table 4.6 shows the standard deviations for four models compared with the experimental data. It again shows Willenborg model has a smaller standard deviation values than other models and has a better agreement with experimental data. The results predicted by modified Space-state model have less priorities than those predicted by Generalized Willenborg model, but the modified Space-state model can predict both OL and UL effects and it has the ability of modelling three-dimensional cracks, which is quite important for full

scale offshore structures.
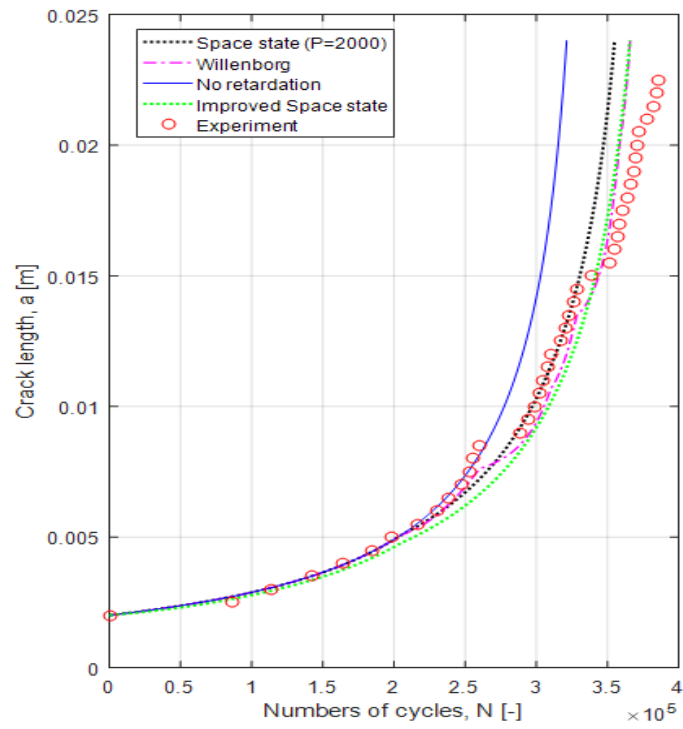
(a)
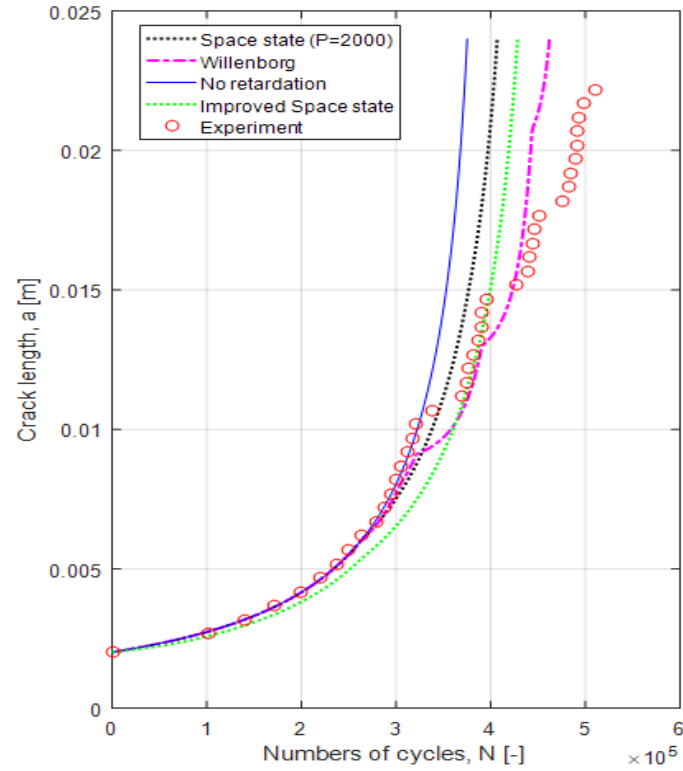
(b)

Figure 4.13 The comparison of crack length with numbers of cycles predicted by modified Space-

state model and other models of specimen (a) AW9 and (b) AW5

Table 4.6 Standard deviations for four models

Standard Deviation	Space-state	Willenborg	No retardation	Modified Space-state
AW9	25402.15	23586.43	44936.17	24942.26
AW5	75129.34	38165.95	104964.70	56463.31

4.7.1 Application to Spar-type FWT

In offshore FWT systems, there are always noticeable changes in mean stress because of changing wind and wave directions. Due to the large changes of mean stress, the offshore wind turbines are prone to load sequence effects. Dragt et al. (2016) gave a simplified method to address the large numbers of stress signals of offshore wind turbines. To reduce the number of stress signals, several blocks were used to divide the stress signal into many segments. Three patterns were defined based on the trend of increase, decrease and remaining constant of the stress signal in each block. This largely reduced the number of VA cycles and converted them into CA cycles. Finally, FM based prediction models could be used to estimate the fatigue lives.

Figure 4.14 shows the crack length over numbers of cycles for the tower base of a spar-type wind turbine with the method proposed by Dragt et al. (2016). The environmental condition is conFigured as follows: 4.5 m for significant wave height, 12 s for peak period and 7 m/s for mean wind speed at the hub height for a 3-hour simulation. The initial crack of the tower base is set as 2 mm and material constants are set as specimen of AW9 since the retardation factor for this specimen is already examined. The stress history is achieved through FAST code and then applied to four FM models. The Figure 4.14 gives the results predicted by four models on real wind turbine data. It can

be seen from the Figure that there is no obvious difference between Space-state model and no retardation model. Generalized Willenborg provides the most unconservative result comparing to other models and the result predicted by the modified Space-state model is in the range of other three models. This difference is attributed to the following reasons:

- As far as the load conditions of real offshore wind turbine are concerned, OLs and ULs are continuously followed up by researchers. Suppose there is an OL that is followed by an UL, the retardation effect may decrease or even be offset by the UL, which causes little impact on the fatigue life.

- A single OL is applied between two CA loads in section 4.5.3, and it gives enough time to develop the retardation effect. However, in real load conditions, new OLs or ULs will appear before the full development of retardation effects, which may reduce the retardation effect as well.

- Generalized Willenborg model provides the most unconservative result since it can only predict OL retardation effects, making the fatigue life longer than other models.

The fatigue life predicted by modified Space-state model is between the fatigue lives predicted by Generalized Willenborg model and that by Space-state model, which looks like more reasonable. The reason is that the opening stress calculated by Space-state model is empirical only and it does not take the range of threshold stress intensity factor and fracture toughness into consideration, and this may lead tolarger range and shorter fatigue lives. However, more experiments are needed to validate the modified Space-state model with more realistic offshore wind turbine loads.

In summary, there are still many challenges to predict fatigue lives of offshore FWTs accurately. Some factors will affect the prediction of fatigue lives, for instance, the algorithm used to deal with

the stress signal, the determination of decay factor in prediction models for different material and the impacts on the combination of OL/UL or UL/OL. Thus, more studies should be carried out in the future.
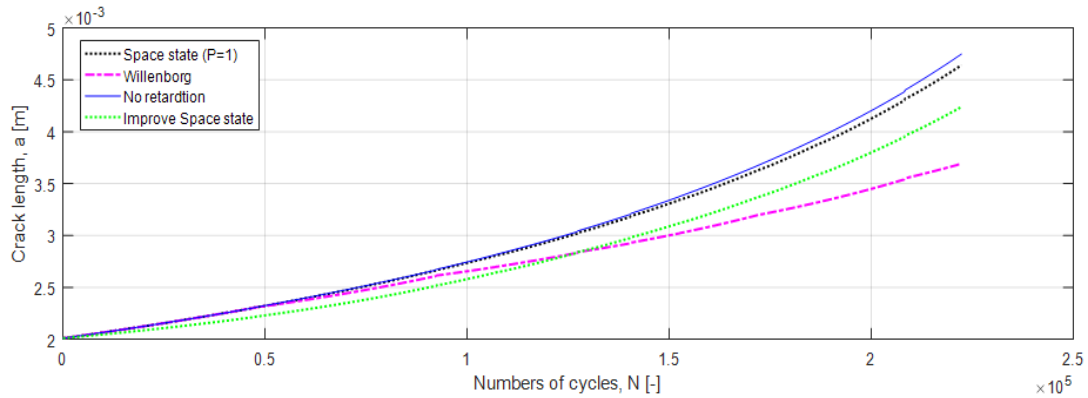
Figure 4.14 Crack length versus numbers of cycles use Space-state, Generalized Willenborg, no retardation and modified Space-state model

4.8 Summary

In this chapter, a comparison between fatigue lives predicted by S-N curves and FM based approaches is performed. Also, a parametric study to investigate the impact of initial crack sizes, critical crack depths, stress concentration factors and mathematical effect of load sequence on fatigue life of the tower base is conducted. Moreover, physical effects of load sequence are considered with three OL retardation models. A parametric study is also conducted to investigate the impact of retardation with Space-state model, Generalized Willenborg model and no retardation model. Finally, a modified Space-state model has been proposed with consideration of the threshold stress intensity factor range and fracture toughness and these parameters are applied to a real offshore wind turbine for fatigue calculation. Some important results are obtained below:

- Fatigue lives predicted by the FM based approach are generally more conservative than those predicted by S-N curves based approach and are highly sensitive to stress concentration factors.

- The OL ratio is the key influencing factor for the retardation effect that is subject to the OL. It can be concluded that Generalized Willenborg model is more sensitive to the variation of the OL ratio and stress ratio compared with Space-state model.

- The decay rate factor, η, in the Space-state model significantly underestimates the effects of retardation. Therefore, a corresponding modification is recommended through single OL test.

- More experiments are required to validate the modified Space-state model with more real offshore wind turbine loads.

Chapter 5. Conclusions and Future Work

5.1 Conclusions

The traditional S-N curves based methods and FM based methods are widely used in offshore fixed wind turbine systems. However, hydro-elastic loads and coupled loads between floating platform and mooring system cannot be ignored in FWT system. The wave and wind induced loads are highly related to the structural motions and responses and the instantaneous position should be updated with the changes of hydrodynamic and aerodynamic forces all the time. Moreover, the structure response amplitude increases at the nature frequency and nature eigen-frequency. These factors bring a lot of challenges in the fatigue assessment of offshore FWTs. Thus, this thesis aims to present several methods to perform fatigue assessment of offshore FWTs because there are only immature fatigue analysis procedures for this kind of structures and this thesis also tries to develop models to improve the efficiency and accuracy in the such assessment.

On the basis of wave scatter diagrams, a simplified lumping approach is used with joint probability of wind and waves for the environmental conditions of FWTs. The stress history for each sea state lump with the minimum probability of 0.1 ‰ is achieved through time-domain simulations executed by FAST software and then proceeding to Rainflow counting algorithm to convert into stress ranges. Finally, fatigue lives are calculated using a two-segment S-N curve combined with Palmgren-Miner's rule.

1386 load cases are simulated to examine the total fatigue damage and computational time. It is found that 498 load cases with the minimum probability of 0.1 ‰ are enough to represent the whole load cases with only 0.91% discrepancy and the simulation time is significantly shorter than

performing simulations with a total of 1386 load cases. Also, the results obtained by this method is nicely in line with other publications. Therefore, the result obtained by the simplified lumping approach is treated as a reference for the remaining researches.

The spectral fatigue analysis has been a common practice for offshore structures, and it is also based on S-N curves and Palmgren-Miner's rule. However, the prediction based on spectral fatigue analysis in the field of offshore FWTs does not go a long way. To fill the gap, fatigue lives of the tower base sections for spar-type, tension-leg, semi-submersible FWTs are calculated and compared by the author. The long-term stress distribution is fitted by various probabilistic models, accounting for both narrow-band and wide-band loading processes. It can be seen that the distribution of fatigue damage has two approximately equal peaks separately by 180 degree, aligned with wind and wave directions for all types of FWTs. Location 1 and Location 7 suffer more severe fatigue damage, which indicates that these two locations are critical points while the points in the direction perpendicular to wind and wave (Location 4 and Location 10) experience minimum fatigue damage.

The results also indicate that the narrow-band solution gives a generally conservative result compared with wide-band solutions. Models proposed by Tovo-Benasciutti, Tunna and Zhao-Baker have similar results which are slightly higher than that of the lumping approach. The prediction model proposed by Dirlik demonstrates a better estimation in this case since more parameters make the prediction model more flexible. However, the change of these parameters may bring more uncertainties as well. The solution proposed by Tunna has only two parameters which makes the model more simplified, though the result is not superior. This work is not only to quantify the difference among these prediction models but also provide a basis for the evaluating and quickly selecting fatigue prediction models with spectral fatigue method.

FM approaches are normally advanced than S-N curves approaches since the former give a detailed crack propagation description. However, Paris' law is only suiTable for CA loadings without considering the effects of stress ratio, the change of threshold intensity factor range and fracture toughness; especially it ignores the impacts on the physical load sequences. Nevertheless, FWTs are very complicated structures which are very sensitive to the changing wind and waves. This leads to noticeable increases and decreases in the mean stress. Thus, the OL and UL impacts should be taken into consideration during the fatigue assessment of FWTs. Chapter 4 investigates parametric impacts from four aspects, e.g. initial crack size, critical crack size, stress concentration factor and mathematical load sequence in FM analysis. It aims to quantify which parameters have more significant impact on the fatigue lives under Paris' equation. Based on the parametric studies, it is found that fatigue life of the wind turbine tower is generally sensitive to the assumed initial crack sizes. The ratio of fatigue lives predicted by two approaches is changed negligibly when the critical crack depths are more than 50% of tower thickness. It is also highly sensitive to the variation of SCFs which is dependent on the welding quality.

A comparison between fatigue lives predicted by S-N curves and FM based approaches is made. The results show that fatigue lives predicted by S-N curves are longer than those predicted by FM based approaches but it is not reliable for the reassessment after some years in operation e.g. due to corrosion effect, change of geometry or variation of material constant. Thus, fatigue assessment with use of Paris' equation seems more feasible. However, it is also found that FWTs are more prone to physical load sequence effect due to the noticeable increases and decreases in mean stress which is not considered in Paris' equation.

As a consequence, due to the limitations of Paris' equation, a study regarding to three concepts

of OL is performed. A parametric research is carried out based on the variations of stress ratios with/without same stress ranges and OL ratios using three FM based models. The results suggest that the OL ratio is the key influencing factor for the retardation effect that is subject to the OL. The retardation effect decreases with the increase of stress ratio at the same stress range. However, it is highly dependent on the variations of the stress range when the stress range is different.

Nevertheless, all of these models have their disadvantages. Thus, on the basis of Space-state model, a modified Space-state model has been proposed with considerations of the threshold stress intensity factor range and fracture toughness. The modified Space-state model is validated by experimental data and a good agreement has been achieved. Finally, this modified Space-state model is applied to a real spar-type wind turbine to investigate how load sequence affects the fatigue lives of FWTs.

Several fatigue assessment methods are presented in this thesis. For the unique structure of offshore FWTs, S-N curves based approaches are not suiTable for reassessment during the service life due to some uncertainty factors, e.g. corrosion effect and the change of structure geometries which are not considered in S-N curves based approaches. FM based approach with use of Paris's equation largely underestimates the load sequence impact of FWTs which is quite important to these kinds of structures. Thus, the modified Space-state model with consideration of threshold stress intensity factor range and fracture toughness is recommended herein to perform fatigue assessment for offshore FWTs.

5.2 Futuer Work

The present research work has been undertaken during the last several years to fulfill the

requirements of a PhD. A more integrated summary of fatigue assessment methods of FWTs is performed in this thesis. The detailed fatigue assessment procedure for FWTs is presented. The current methods can be developed in several parts:

- The joint probability of wind and waves for each block still needs to be divided into several parts, such as wind and wave misalignments. The probability calculated in the simplified lumping approach assumed that wind and waves are always coming from the same directions, which leads to a conservative result. However, more computational time is needed as the number of cases increase.

- Only normal operation load cases have been considered in the thesis. However, based on the recommendation of IEC regulations, the conditions of parked, parked and fault, transport, assembly, maintenance and repair should be considered in the fatigue assessment, which would further increase the number of simulations as well.

- The initial crack size assumed in parametric study is empirically based. More scientific measures should be adopted, such as Non-destructive testing.

- The stress concentration factor is highly dependent on the welding quality. It may be obtained by direct measurement of a proper physical model or through FEA.

- The retardation effect is really sensitive to the decay factor or arrest factor in prediction models. Thus, a more scientific procedure should be developed to determine such values.

- In the analysis of data from real wind turbines, load combination is also quite essential. For instance, ULs followed by OLs or OLs followed by ULs.

Reference

A. A. Aguilar Espinosa, N.A. Fellows, & J.F. Durodola. (2013). Experimental measurement of crack opening and closure loads for 6082-t6 aluminium subjected to periodic single and block overloads and underloads. International Journal of Fatigue, 47(FEB.), 71-82.

ABS. (2014). Guide for Fatigue Assessment of Offshore Structures.

Alawi, H, & Shaban, M. (1989). Fatigue crack growth under random loading. Engineering Fracture Mechanics, 32(5), 845-854.

Anderson, TL. (2005). Fracture mechanics: fundamentals and applications, third edition, CRC press.

Asok Ray, & Ravindra Patankar. (2001). Fatigue crack growth under variable -amplitude loading: part Ⅰ-model formulation in state-space setting. Applied Mathematical Modelling, 25(11), p.979-994.

ASTM, A.E. (2005). 1049–Standard practices for cycle counting in fatigue analysis. West Conshohocken (PA).

Aubault, A., Cermelli, C. and Roddier, D., 2009, May. Windfloat: A floating foundation for offshore wind turbines. Part III: Structural analysis. In Proceedings of 28th International Conference on Ocean, Offshore and Arctic Engineering, Honolulu, HI, Paper No. OMAE2009-79232.

Bachynski, E.E., Kvittem, M.I., Luan, C. and Moan, T. (2014). Wind-wave misalignment effects on floating wind turbines: motions and tower load effects. Journal of Offshore Mechanics and Arctic Engineering, 136(4), p.041902.

Baniotopoulos, C.C. (2007). Design of wind-sensitive structures. In Wind Effects on Buildings and Design of Wind-Sensitive Structures (p. 201-227). Springer Vienna.

Bendat JS. (1964). Probability functions for random responses. NASA Report on Contract NASA, 5-4590.

Bernard, & Michael, C. (1970). Fatigue damage under wide-band random stress. The Journal of the Acoustical Society of America, 47(1B), 390.

Benasciutti, & R. Tovo. (2004). Cycle distribution and fatigue damage assessment in broad-band non-gaussian random processes., 20(2), 115-127.

Benasciutti D. (2004). Fatigue analysis of random loadings, Ph.D. thesis. University of Ferrara.

Bishop NWM, Sherratt F. (1989). Fatigue life prediction from power spectral density data. Part 1: traditional approaches and part 2: recent developments. EnvironEng; 2:11–9.

Booth GS, Maddox SJ. (1988). Correlation of fatigue crack growth data obtained at different stress ratios. In: Mechanics of fatigue crack closure, ASTM STP 982; p. 516–27.

BS7910, B.S. (2015). Guide on methods for assessing the acceptability of flaws in fusion welded structures. British Standards Institutions, London.

Conti, J. and Holtberg, P. (2011). International Energy Outlook 2011. Available from: http://www.eia.gov/forecasts/ieo/pdf/0484(2011).pdf

Chaudhury, G. K., & Dover, W. D. (1985). Fatigue analysis of offshore platforms subject to sea wave loadings. International Journal of Fatigue, 7(1), 13-19.

Chen, N.Z., Wang, G. and Soares, C.G. (2011). Palmgren–Miner's rule and fracture mechanics-based inspection planning. Engineering Fracture Mechanics, 78(18), p.3166-3182.

Davenport, R. T., & Brook, R. (1979). The threshold stress intensity range in fatigue. Fatigue & Fracture of Engineering Materials & Structures, 1(2).

Ding, Z, Wang, X, Gao, Z, Bao, S. (2017). An experimental investigation and prediction of fatigue crack growth under overload/underload in Q345R steel. International Journal of Fatigue, 98, 155-166

Dong, W., Moan, T. and Gao, Z. (2012). Fatigue reliability analysis of the jacket support structure for offshore wind turbine considering the effect of corrosion and inspection. Reliability Engineering & System Safety, 106, p.11-27.

Dong, W., Moan, T. and Gao, Z., 2011. Long-term fatigue analysis of multi-planar tubular joints for jacket-type offshore wind turbine in time domain. Engineering Structures, 33(6), pp.2002-2014.

Downing, S.D. and Socie, D.F., 1982. Simple rainflow counting algorithms. International journal of fatigue, 4(1), pp.31-40.

Dragt, R., Allaix, D., Maljaars, J. J., Tuitman, J., Salman, Y., & Otheguy, M. (2017). Approach to include load sequence effects in the design of an offshore wind turbine substructure.

Eder, M. A., & Bitsche, R. D. (2015). Fracture analysis of adhesive joints in wind turbine blades. Wind Energy, 18(6), 1007-1022.

EWEA. (2012). Task Force 'Deep Offshore & New Foundation Concepts'

Gallagher, J., Hughes, T. (1974). Influence of yield strength on overload affected fatigue crack growth behaviour in 4340 steel. Wright-Patterson: Air Force Flight Dynamics Laboratory.

Halfpenny, A. (1999). A frequency domain approach for fatigue life estimation from finite element

analysis. Key Engineering Materials, 167-168, 401-410.

Henderson, A., Patel, M. H., Halliday, J., & Watson, G. (2000). Floating offshore wind farms—an option? Offshore Wind Energy in Mediterranean and Other European Seas (OWEMES). Italy.

Hudak Jr, S.J., McClung, R.C., Bartlett, M.L., Fitzgerald, J.H. and Russell, D.A. (1990). A comparison of single-cycle versus multiple-cycle proof testing strategies. Contractor report no. 4318. National Aeronautics and Space Administration, DC.

J.C. Marin, A. Barroso, F. Paris and J. Canas. (2009). Study of fatigue damage in wind turbine blades. Engineering Failure Analysis 16, p. 656–668.

Jiang, Z., Xing, Y., Guo, Y., Moan, T., & Gao, Z. (2015). Long-term contact fatigue analysis of a planetary bearing in a land-based wind turbine drivetrain. Wind Energy, 18(4), 591-611.

John, C, & Andrei, K. (2009). A crack closure model of fatigue crack growth in plates of finite thickness under small-scale yielding conditions. Mechanics of Materials, 41(2), 165-173.

Jonkman, J., Marshall, L. and Buhl, M. L. Jr. (2005). FAST user's guide. USA: NREL/EL-500-38230.

Jonkman, J. M. and M.L. Buhl, Jr. (2007). Load analysis of a floating offshore wind turbine using fully coupled simulation. WindPower 2007 Conference & Exhibition, Los Angeles, California

Jonkman, J., Butterfield, S., Musial, W. (2009). Definition of a 5-MW Reference Wind Turbine for Offshore System Development. Technical Report, NREL/TP-500e38060. NREL, Golden, Colorado, USA.

Jonkman, J. and Musial, W., (2010). Offshore code comparison collaboration (OC3) for IEA Wind Task 23 offshore wind technology and deployment (No. NREL/TP-5000-48191). National Renewable Energy Laboratory (NREL), Golden, CO..

Jonkman, J.M., Robertson, A.N., Hayman, G.J. (2014). HydroDyn User's Guide and Theory Manual. Technical Report. NREL, Golden, Colorado, USA.

Jonkman, B. J., & Buhl, M. L. J. (2006). Turbsim user's guide. (7), 58.

Johannessen, K., Meling, T.S. and Hayer, S. (2001), January. Joint distribution for wind and waves in the northern North Sea. In The 11th International Offshore and Polar Engineering Conference. International Society of Offshore and Polar Engineers.

Jr, J. C. N. (1984). A crack opening stress equation for fatigue crack growth. International Journal of Fracture, 24(4).

Kaldellis, J. K., & Zafirakis, D. P. (2012). Trends, prospects, and r&d directions in wind turbine technology. Comprehensive Renewable Energy, 671-724.

Karimirad, M. (2014). Design aspects. In: Karimirad, M. (ed.) Offshore Energy Structures. Springer International Publishing

Kensche, C. W. (2006). Fatigue of composites for wind turbines. International Journal of Fatigue, 28(10), p.1363-1374.

Kim B, Wang XZ, Shin YS. (2007). Extreme load and fatigue damage on FPSO in combined waves and swells. In: 10th International symposium on practical design of ships and other floating structures. Houston (TX, USA); p. 203–10.

Kvittem, M.I., Moan, T., Gao, Z. and Luan, C. (2011). Short-term fatigue analysis of semi-submersible wind turbine tower. Surge, 108, p.0-058.

Kurihara M, Katoh A, Kawahara M. (1987). Effects of stress ratio and step loading on fatigue crack propagation rate. In: Current research on fatigue cracks (Current Japanese Materials Research). London: Elsevier.

Kvittem, M.I. and Moan, T. (2015). Time domain analysis procedures for fatigue assessment of a semi-submersible wind turbine. Marine Structures, 40, p.38-59.

Laino, D.J. and Hansen, A.C. (1997). An integrated approach to wind turbine fatigue analysis. Journal of Solar Energy Engineering, 119, p.242-247.

Laino, D.J. and Hansen, A.C. (2004). Current efforts toward improved aerodynamic modelling using the Aerodyn Subroutines. In A Collection of the 2004 ASME Wind Energy Symposium (p. 329-338).

Li, L., Gao, Z. and Moan, T. (2013). Joint environmental data at five European offshore sites for design of combined wind and wave energy devices. In ASME 32nd International Conference on Ocean, Offshore and Arctic Engineering, Nantes, France, June, p. 9-14.

Li, Y., Lence, B.J., Shi-Liang, Z. and Wu, Q. (2010). Stochastic fatigue assessment for berthing monopiles in inland waterways. Journal of Waterway, Port, Coastal, and Ocean Engineering, 137(2), p.43-53.

Liu, Y. and Mahadevan, S. (2009). Probabilistic fatigue life prediction using an equivalent initial flaw size distribution. International Journal of Fatigue, 31(3), p.476-487.

Long, H. and Moe, G. (2012). Preliminary design of bottom-fixed lattice offshore wind turbine towers in the fatigue limit state by the frequency domain method. Journal of Offshore Mechanics and Arctic Engineering, 134(3), p.031902.

Lorc.dk. (2011). Roedsand-2. http://www.lorc.dk/offshore-wind-farms-map/roedsand-2. Accessed April 2014

Lorc-website. (2011). http://www.lorc.dk/. Accessed Feb 2014.

Lozano-Minguez, E.; Kolios, A.J. and Brennan, F.P. (2011) Multi-criteria assessment of offshore wind turbine support structures. Renewable Energy 36: 2831-2837.

Maljaars, J., Pijpers, R., & Slot, H. (2015). Load sequence effects in fatigue crack growth of thick-walled welded C–Mn steel members. International Journal of Fatigue, 79, 10-24.

Mandell, J. F., & Samborsky, D. D. (1997). Doe/msu composite material fatigue database: test methods, materials, and analysis.

Marino, E., Giusti, A., & Manuel, L. (2017). Offshore wind turbine fatigue loads: the influence of alternative wave modeling for different turbulent and mean winds. Renewable Energy, 102.

Martínez, I. and Pavn, C.L. (2011). Deliverable D3. 4: Recommended concepts for further documentation and analysis. Marine Renewable Integrated Application Platform.

Matsuishi, M. and Endo, T. (1968). Fatigue of metals subjected to varying stress. Japan Society of Mechanical Engineers, Fukuoka, Japan, 68(2), p.37-40.

Mehmanparast, A., Brennan, F., & Tavares, I. (2017). Fatigue crack growth rates for offshore wind monopile weldments in air and seawater: slic inter-laboratory test results. Materials & Design, S0264127516313776.

Miner, M.A. (1945). Cumulative Damage in Fatigue. Journal of Applied Mechanics 67: A159-A164.

Moriarty, P.J. and Hansen, A.C. (2005). AeroDyn theory manual (No. NREL/TP-500-36881). National Renewable Energy Lab., Golden, CO..

Muljadi, E. and Butterfield, C. P. (1999). Pitch-controlled variable-speed. Presented at the 1999 IEEE Industry Applications, Phoenix, Arizona. NREL/CP-500-27143.

Nejad, A.R., Bachynski, E.E., Gao, Z. and Moan, T. (2015). Fatigue damage comparison of mechanical components in a land-based and a spar floating wind turbine. Procedia Engineering, 101, p.330-338.

Nejad, A. R., Bachynski, E.E., Kvittem, M. I., Luan, C., Gao, Z. and Moan, T. (2015). Stochastic dynamic load effect and fatigue damage analysis of drivetrains in land-based and tlp, spar and semi-submersible floating wind turbines. Marine Structures, 42, p. 137-153.

Nejad, A.R, Gao, Z, Moan, T. (2014). On long-term fatigue damage and reliability analysis of gears

under wind loads in offshore wind turbine drivetrains. Int J Fatigue; 61:116-28.

Newman JC. (1992). Fastran II – a fatigue crack growth structural analysis program. NASA Technical Memorandum 104159.

Paris, P.C. and Erdogan, F. (1963). December. A critical analysis of crack propagation laws. ASME.

Passon, P. (2015). Damage equivalent wind-wave correlations on basis of damage contour lines for the fatigue design of offshore wind turbines. Renewable Energy, 81, p.723-736.

Passon, P and Branner, K. (2014). Load calculation methods for offshore wind turbine foundations. Ships Offshore Struct, 9(4):433-49.

Porter, T. R. (1972). Method of analysis and prediction for variable amplitude fatigue crack growth. Engineering Fracture Mechanics, 4(4), 717-736.

Ray A, Patankar R. (2001). Fatigue crack growth under variable amplitude loading: Part I – Model formulation in state-space setting. Appl Math Model; 25:979–94.

Rice, S. O. (1945). Mathematical analysis of random noise. Bell Labs Technical Journal, 24(1), 46-156.

Roald, L., Jonkman, J., Robertson, A., et al., (2013). The effect of second-order hydrodynamics on floating offshorewind turbines. Energy Proc 35, 253-264.

Robertson, A.N. and Jonkman, J.M. (2011). January. Loads analysis of several offshore floating wind turbine concepts. In the Twenty-first International Offshore and Polar Engineering Conference. International Society of Offshore and Polar Engineers.

Roddier, D., Peiffer, A., Aubault, A., and Weinstein, J. (2011). A Generic 5MW WindFloat for Numerical Tool Validation & Comparison Against a Generic Spar. 30th International Conference on Ocean, Offshore and Arctic Engineering, Rotterdam, The Netherlands.

Schijve J. (1988). Fatigue crack closure: observations and technical significance. In: Mechanics of fatigue crack closure, ASTM STP 982; pp. 5–34

Seidel, M. (2014). Wave induced fatigue loads on monopiles - new approaches for lumping of scatter Tables and site-specific interpolation of fatigue loads. In: Conference proceedings IWEC, Hannover.

Skaare, B., Hanson, T.D. and Nielsen, F.G. (2007). Importance of control strategies on fatigue life of floating wind turbines. In Proceedings of 26th International Conference on Offshore Mechanics and Arctic Engineering, p. 493-500.

Sharma, N. and Dean. R. (1981). Second-order directional seas and associated wave forces. Society of Petroleum Engineers Journal, 4:129-140.

Smith, K. R., Corvalán, Carlos F., & Kjellstr M, T. (1999). How much global ill health is attribuTable to environmental factors? Epidemiology, 10(5), 573-584.

Standard, I.E.C. (2009). Wind turbines-Part 3: Design requirements for offshore wind turbines.

Sutherland, H. J. & Mandell, J. F. (2004). Effect of mean stress on the damage of wind turbine blades. journal of solar energy engineering, 126(4), 1041-1049.

Tunna, J. M. (1986). Fatigue life prediction for gaussian random loads at the design stage. Fatigue & Fracture of Engineering Materials & Structures, 9(3), 169-184.

Van der Tempel J. (2006). Design of support structures for offshore wind turbines, Ph.D. thesis. Delft University of Technology.

Veritas, D.N. (2014). Design of offshore wind turbine structures. Offshore Standard DNV-OS-J101.

Veritas, D.N. (2015). Structural design of column stabilised units-LRFD method. Offshore Standard DNVGL-OS-C103.

Vosikovsky, O. (1975). Fatigue-crack growth in an x-65 line-pipe steel at low cyclic frequencies in aqueous environments. Journal of Engineering Materials & Technology, 97(4), 298.

Wenbin D., Torgeir M., & Zhen G. (2012). Fatigue reliability analysis of the jacket support structure for offshore wind turbine considering the effect of corrosion and inspection. Reliability Engineering & System Safety, 106, 11-27.

Wheeler OE. (1972). Spectrum loading and crack growth. J Basic Eng Trans ASME; 94:181–6.

Willenborg J, Engle RM, Wood HA. (1971). A crack growth retardation model using an effective stress concept. Wright-Patterson: Air Force Flight Dynamics Laboratory.

Wolf, E. (1970). Fatigue crack closure under cyclic tension. Engineering Fracture Mechanics, 2(1), 37-45.

Wu, Y. S., & Schijve, J. (1995). Fatigue-crack closure measurements on 2024-t3 sheet specimens. Fatigue & Fracture of Engineering Materials & Structures, 18(9), 917-921.

Yeter B, Garbatov Y, Guedes Soares C. (2014). Fatigue damage analysis of a fixed offshore wind turbine supporting structure. In: Guedes Soares C, Pena F, editors. Developments in maritime transportation and exploitation of sea resources. UK: Taylor & Francis Group; p. 415–24.

Yeter, B., Garbatov, Y. and Soares, C.G. (2015). Fatigue damage assessment of fixed offshore wind turbine tripod support structures. Engineering Structures, 101, p.518-528.

Yeter, B., Garbatov, Y., & Guedes Soares, C. (2016). Evaluation of fatigue damage model predictions for fixed offshore wind turbine support structures. International Journal of Fatigue, 87, S0142112316000086.

Yuen BKC, Taheri F. (2006). Proposed modifications to the Wheeler retardation model for multiple overloading fatigue life prediction. Int J Fatigue; 28:1803–19.

Zhenyu Ding, Xiaogui Wang, Zengliang Gao, & Shiyi Bao. (2017). An experimental investigation and prediction of fatigue crack growth under overload/underload in q345r steel. International Journal of Fatigue, 98(May), 155-166.

Zhao T, Zhang J, Jiang Y. (2008). A study of fatigue crack growth of 7075–T651 aluminum alloy. Int J Fatigue; 30:1169–80.

Ziegler, L. and Muskulus, M., (2016). Comparing a fracture mechanics model to the SN-curve approach for jacket-supported offshore wind turbines: Challenges and opportunities for lifetime prediction. In ASME 2016 35th International Conference on Ocean, Offshore and Arctic Engineering, pp. V006T09A054-V006T09A054. American Society of Mechanical Engineers.

Zwick, D., & Muskulus, M. (2016). Simplified fatigue load assessment in offshore wind turbine structural analysis. Wind Energy, 19(2), 265-278.